Distribution Agreement

In presenting this thesis or dissertation as a partial fulfillment of the requirements for an advanced degree from Emory University, I hereby grant to Emory University and its agents the non-exclusive license to archive, make accessible, and display my thesis or dissertation in whole or in part in all forms of media, now or hereafter known, including display on the world wide web. I understand that I may select some access restrictions as part of the online submission of this thesis or dissertation. I retain all ownership rights to the copyright of the thesis or dissertation. I also retain the right to use in future works (such as articles or books) all or part of this thesis or dissertation.

Signature:

_____	_____
Rakieb Andargachew	Date

CD4 T cell affinity evolution under acute and chronic antigen exposure

By

Rakieb Andargachew
Doctor of Philosophy

Graduate Division of Biological and Biomedical Sciences
Immunology and Molecular Pathogenesis

_____

Brian D. Evavold
Advisor

_____

John D. Altman
Committee Member

_____

Mandy L. Ford
Committee Member

_____

Jacob E. Kohlmeier
Committee Member

_____

Jyothi Rengarajan
Committee Member

Accepted:

_____

Lisa A. Tedesco, Ph.D.
Dean of the James T. Laney School of Graduate Studies

_____

Date

CD4 T cell affinity evolution under acute and chronic antigen exposure

By

Rakieb Andargachew
M.S. Georgia State University, 2008

Advisor: Brian D. Evavold Ph.D.

An abstract of
A dissertation submitted to the Faculty of the
James T. Laney School of Graduate Studies of Emory University
in partial fulfillment of the requirements for the degree of
Doctor of Philosophy
in
Graduate Division of Biological and Biomedical Sciences
Immunology and Molecular Pathogenesis
2018

Abstract

CD4 T cell affinity evolution under acute and chronic antigen exposure
By Rakieb Andargachew

T cell receptor (TCR) interaction with pMHC on the respective cell surfaces of a T cell and an antigen-presenting cell can elicit a multitude of functional differentiation pathways or transpire without an outcome. The result hinges on affinity and other biophysical interaction parameters that govern TCR:pMHC binding and consequently modulate the degree of the T cell response. It is unclear what TCR affinities are represented within an antigen-specific polyclonal CD4 T cell population, and if TCR affinity diversity differs in the context of acute and chronic infections. Relative to in-solution measurements with recombinant proteins, single cell in-situ analysis of TCR affinity for membrane-anchored pMHC provides a more relevant assessment of this interaction and better correlates with a T cells' functional response. Here, using the 2-dimensional micropipette adhesion frequency assay (2D-MP), we measured the range and average TCR affinity of polyclonal IA^b GP_{66-77} specific CD4 T cells in the B6 acute (Armstrong) and chronic (CL13) models of LCMV infection. In both responses, the presence of antigen maintained an effector population with a high average TCR affinity that later declined at memory with antigen clearance. Greater than 1000-fold affinity ranges were measured in both responses and population average 2D affinity at peak and late time points were equivalent between the two infections. These results indicate that intrinsic and extrinsic factors regulate T cell function in chronic infections without altering TCR affinity diversity. To further elucidate the effects of antigen stimulation on 2D affinity and TCR:pMHC bond lifetime, we used a reductionist approach, tracking activation-induced changes in IA^b GP_{66-77} specific SMARTA transgenic CD4 T cells. In vitro, peptide-stimulated cells exhibited dynamic TCR:pMHC 2D affinities and bond lifetimes that decreased from naïve levels within the first 24 hours of antigen encounter but recovered at the 48-hour mark with the start of cell division. This occurred independently of antigen dose and degree of activation-induced TCR downregulation. Hence, 2D analysis of monoclonal and polyclonal T cells' affinities can represent the sum total of single cell TCR:pMHC interaction dynamics within the respective cellular environments.

CD4 T cell affinity evolution under acute and chronic antigen exposure

By

Rakieb Andargachew
M.S. Georgia State University, 2008

Advisor: Brian D. Evavold Ph.D.

A dissertation submitted to the Faculty of the
James T. Laney School of Graduate Studies of Emory University
in partial fulfillment of the requirements for the degree of
Doctor of Philosophy
in
Graduate Division of Biological and Biomedical Sciences
Immunology and Molecular Pathogenesis
2018

Table of Contents

Chapter 1. Introduction

As part of the adaptive branch of the immune system, CD4 T cells play a critical role in fighting foreign intruders and eliminating cancerous cells from the host. The first step towards carrying out this vital task is the clear recognition and discrimination between foreign and self-encounters (1, 2). Achieved through a specific interaction between pMHCs and self-educated TCRs, this interplay determines the activation status, functional properties, and survival fates of the receptor carrying T cells. The use of transgenic monoclonal TCRs and altered peptide ligands (APLs) has informed our understanding of TCR:pMHC affinity, binding kinetic rates and other biophysical parameters that play a role in the T cell's response to infection, and in the thymic selection of immature T cells (3-8). Such models are critical for highlighting the impact of these binding conditions on T cell responses, a task that may be complicated and obscured by a system with polyclonal TCRs. However, identifying TCR:pMHC interaction parameters that predict and correlate with efficacious polyclonal T cell responses inform T cell vaccine designs and cell therapies aimed at rescuing T cell functionality in chronic infections that pose a health challenge. With the advent of new technologies, TCR affinity ranges, the role of high and low-affinity cells and other biophysical frameworks are further explored and highlighted in the natural polyclonal T cell population and during ongoing immune responses (9, 10). Coupled with such technological advancements and our understanding of the TCR within its cellular context as well as T cell activation and differentiation conditions, the exploration of cell surface TCR:pMHC biophysical interaction measures are revolutionizing T cell therapies. Targeted towards boosting protection against infection and cancer, some of these

therapeutic advancements include the isolation and adoptive transfer of antigen-specific T cells into patients with chronic infections and the use of T cells with high-affinity engineered TCRs as a treatment for cancer (11-14). In this work, we review and examine how TCR:pMHC interaction parameters and functional responses evolve under acute and chronic antigen exposure of monoclonal and polyclonal CD4 T cells.

TCR:pMHC interaction-relevant structures

Alpha (α) beta (β) T cells carry unique T cell receptors (TCRs) that are generated through genetic recombination of variable (V), diversity (D – only β gene) and joining (J) gene segments to create a T cell repertoire which, post-thymic selection, represents 10^8 and 10^{12} distinct TCRs in mice and humans respectively (15, 16). Structurally, the TCR resembles the Fab fragment of an immunoglobulin (Ig) molecule with a single variable (V) and constant (C) region that each possesses distinct disulfide-linked β sheet structures. Cysteine residues in the C regions of α and β form disulfide bonds that link the two chains and form the heterodimeric TCR (17). Attached to their non-polymorphic membrane proximal Cα and Cβ domains, VJ(α) and VDJ(β) segments make up the Vα and Vβ parts of the TCR. Each segment contains three complementary determining regions (CDRs) responsible for antigen recognition. The TCR hypervariable CDR3 loop, located at the V(D)J junction, interacts with the presented peptide while MHC restriction of T cells is attributed to the germline encoded CDR1 and CDR2 loops that originate from the V gene segment (18). Even though certain exceptions that fall outside this specified interaction exist, most TCR-MHC alignments show this conserved orientation (18-20).

T cell recognition of antigen is limited to the combined molecular structure of processed 8-24 amino acid long linear peptides bound to major histocompatibility molecules (pMHC) displayed on the surface of antigen-presenting cells (APCs) (1, 21). The two classes of MHC molecules, MHC I and II, have similar non-polymorphic immunoglobulin (Ig) like membrane proximal domains in addition to a highly polymorphic distal β sheet flanked by two alpha helices that form the peptide binding groove. MHC I has an α chain with three domains non-covalently linked to a β microglobulin which lacks a transmembrane domain whereas MHC II is formed by an α and a β chain that each contain transmembrane domains. The $\alpha_1\alpha_2$ from MHC I and $\alpha_1\beta_1$ from MHC II form the peptide-binding groove that faces the TCR. MHC I molecules have a peptide-binding groove with closed ends that restrict the presented peptides to a length of 8-10 residues while the more open MHC II peptide-binding groove accommodates much longer peptides. Regardless, both MHC I and MHC II presented peptides contain core nonamer (P1-P9) residues with some serving as MHC anchors while others provide side chains that form TCR contacts (22).

The T cell receptor lacks signaling components but exists in a complex with CD3 chains that carry immunoreceptor tyrosine-based activation motifs (ITAM) that, post phosphorylation, act as scaffolds for the recruitment of other signaling proteins. CD3δε, CD3γδ, and CD3ζζ constitute the CD3 signaling modules and with the exception of the ζ chain which has a short nine amino acid long ectodomain and three cytoplasmic ITAMs, the other three chains contain single extracellular Ig-like domains that sit on a short stalk and a single cytoplasmic ITAM motif (23, 24). Hydrophobic and hydrogen bonds facilitate the interactions with Cα and Cβ domains of the TCR and aid in the dimerization

of the external Ig-like CD3 domains with further dimerization of the different CD3 chains occurring through conserved cysteines in the stalk regions (25). In the case of the ζ chain which lacks a large external domain, disulfide linkage in its transmembrane region results in homodimer formation (26). The TCR-CD3 complex is formed through electrostatic interactions between acidic residues in the transmembrane region of the CD3 chains and basic residues from the conserved antigen receptor transmembrane (CART) motif of the TCR subunits (26). A highly conserved arginine (R) in the TCRα chain interacts with aspartic residues (D) from each CD3ζ ζ chain while a lysine residue contacts an aspartic residue from each CD3δε unit. Similarly, a lysine residue in TCRβ brings CD3γε into the complex through the aspartic(ε) and glutamic acid (γ) residues (27). In the more favored model, the sum of all these interactions cluster the CD3 heterodimers to the intersection between the TCR α and β chains on one side of the TCR instead of on opposite ends and at a one to one TCR to CD3-complex stoichiometry (24).

In close proximity to the TCR and aiding in the recognition of pMHC is the co-receptor CD4 or CD8. The single chain CD4 glycoprotein has four Ig-like domains (D1D2-hinge-D3D4) and binds to a non-polymorphic region of the MHC class II molecule. This is through the insertion of the membrane distal D1 domain into the hydrophobic pocket between the membrane-proximal α2 and β2 chains of MHC II (23). While this interaction has been shown to have a low-affinity with minimal to no contribution in TCR:pMHC binding, its role is critical during CD4 T cell activation (28, 29). In contrast to CD4, the CD8 co-receptor has an α and β chain that each contain single Ig domains. This receptor can exist as a CD8αα homodimer on certain T cells, but the majority of peripheral cells express the CD8αβ heterodimeric form which binds to a

conserved region of the MHC class I membrane proximal α3 domain (23). This interaction has a much higher affinity than that observed with the CD4 co-receptor, and thus TCR:pMHC binding studies mutate a portion of the α3 pMHC region to abrogate CD8 binding or otherwise account for CD8's contribution in TCR:pMHC interactions (30). Both CD4 and CD8α chains contain two cysteine residues in their cytoplasmic tails that coordinate a zinc molecule with two other cysteines found in the Src family tyrosine kinase Lck, resulting in a zinc clasp that tethers Lck to the co-receptors (31). Required for TCR signaling and thus for the transition from the CD4 CD8 double positive to the single positive stage in the thymus, co-receptor sequestered Lck transmits survival signals in T cells that carry MHC specific TCRs (32, 33).

The general binding polarity between TCR and pMHC results in the alignment of the TCR Vα domain with the MHC I α_2 or MHC II β_1 chains and the N-terminus of the MHC bound peptide. On the opposite end, the TCR Vβ domain aligns with the α_1 of MHC I or II and the C-terminus of the antigenic peptide (17-19, 23). Although some exceptions exist (34), most interactions follow this alignment between the receptor and ligand and a general diagonal docking angle is observed with some variations on the actual binding angle (35). This specific manner of interaction progresses in a 'two-step' binding sequence, with the more rigid TCR αβ CDR1 and CDR2 loops binding their respective MHC I and II chains first followed by their more flexible CDR3 loops engaging the presented peptide with some conformational rearrangement (36, 37). In this 'induced fit' model, the flexibility of the CDR3 loops allows for the recognition of distinct peptides that are presented on the same MHC molecule with co-receptors and the CD3 chains also contributing to the resulting binding angle (36, 37). This conserved

pMHC-TCR docking orientation or binding is the first step in TCR triggering events and mutations that alter this polarity have been shown to result in a defective T cell activation status (38).

Measuring TCR:pMHC interaction : 3D and 2D analysis

Receptor-ligand studies have made use of recombinant protein technology and examined binding relationships between soluble forms of interacting proteins. In instances where one of the species is anchored to a substrate or within the cell membrane, such assays measure the interaction in a 3-dimensional (3D) context as one or both reactants are free to move in all three dimensions (39, 40). Although such methods are commonly used in TCR:pMHC binding studies, the requirement for recombinant TCRs has imposed limitations on their use in the analysis of polyclonal T cells. Hence, studies that examine the effects of TCR:pMHC interaction on the T cell's response have relied on monoclonal TCR transgenic T cells and the ex-vivo functional analysis of polyclonal populations to gauge pMHC potency and infer the quality of interaction with polyclonal TCRs. More recently the importance of understanding the biophysical dynamics between TCR and pMHC within their respective cellular contexts, i.e., in situ 2-dimensional restrictions (2D), has been highlighted due to its increased correlation with TCR ligand discrimination and T cell function (41, 42). The TCR and structural modules such as the associated CD3-complex, the co-receptor (CD4/CD8), the cellular environment inclusive of the T cell membrane, other receptors, the cell cytoskeleton and intracellular signaling components all play a role in carrying out the highly specific T cell response. Consequently, these factors have implications in the cell surface interaction between

membrane-anchored TCRs and pMHCs. Discussed here are the most common methods of 3D and 2D analysis of TCR:pMHC binding. Although the strengths and weaknesses of each assay may prevent definitive conclusions on the relationship between TCR:pMHC binding kinetics and the associated T cell response, combinatorial analysis can provide better insights.

3D: Surface Plasmon Resonance (SPR)

Traditional receptor-ligand affinity and interaction kinetic rate measurements are performed using surface plasmon resonance spectroscopy. The introduction of the first BIACORE instrument transformed receptor-ligand binding studies allowing the use of label-free reactants compared to radioactive or fluorescent label dependent binding assays (43). In this optical technique, one of the interacting molecules is immobilized on a biochemically modified metal-based biosensor chip and exposed to a ligand that is in a fluid phase. The interaction between the receptor-ligand pair results in changes to the optical properties of the sensor allowing real-time detection of kinetic on and off rates (k_{on} (M^{-1} s^{-1}), k_{off} s^{-1}) which are defined by concentration and time respectively. The binding affinity between the reactants is described by the equilibrium dissociation constant K_D (M) which is measured as the concentration of unbound ligand at the equilibrium point of when bound and unbound immobilized receptor concentrations are equivalent. K_D [M] can also be derived from the kinetic rates (K_D [M] = k_{off}/k_{on} = $1/K_a$ (inverse of the association constant or affinity)) (44, 45) and low K_D values portray a high-affinity interaction given its inverse relationship with the association constant which defines affinity (46). The interaction half-life can also be derived from the off rate by the

equation $t_{(1/2)} = \ln 2 / k_{off.}$ (3). Initial SPR measurements that described TCR:pMHC interaction with these parameters used the well-characterized CD4 2B4 TCR specific for IE^k moth and pigeon cytochrome c peptides (MCC, PCC) (47) and the CD8 2C TCR specific for the L^d p2Ca antigen (48). Conclusions from these SPR measurements demonstrated that TCR:pMHC interactions were marked by a slow association rate (k_{on}), fast off rates, and a low-affinity ((25°C) 2B4 K_D~50-60 μM, 2C K_D~0.1μM). This was comparable to previously measured affinities that used live T cells, soluble pMHCs and radiolabeled anti-TCR antibodies in competitive binding assays with the 2B4 TCR (K_D~40-60 μM), 5C.C7 which is of similar specificity (47, 49), and the 2C CD8 T cell (L^d p2Ca -K_D~2 μM) (50). Since then, SPR K_D measurements for several TCR transgenic systems have confirmed this interaction to be of lower affinity (K_D 1-100μM) compared to high-affinity antibody-antigen interactions that have K_D values of <1nM (51). SPR characterized affinities for some of the well-studied transgenic TCR-cognate pMHC systems include 5C.C7 (IE^k MCC - K_D~22.9-43.5μM) (42, 52), 3.L2 (IE^k Hb - K_D~12μM) (5) CD4 T cells and OTI (K^b Ova K_D~5.9 μM) (53), P14 (K_D~2.4μM) (54) CD8 T cells. With the use of these and other transgenic TCR models, all three parameters of TCR:pMHC interaction (affinity, half-life/off-rate and on rate) have been correlated to T cell function complicating attempts to identify a single predictive measure (3, 55). Furthermore, the requirements of soluble TCRs has restricted the use of this assay to monoclonal systems leaving polyclonal TCR:pMHC interaction studies largely relying on functional assessments.

3D: pMHC Tetramers (avidity)

Fluorescently labeled soluble pMHC tetramers that bind TCR on the T cell surface have now become the most common reagent for the identification and enumeration of antigen-specific polyclonal T cells using flow cytometry (9, 29, 56). This technology utilizes the interaction between soluble biotinylated recombinant pMHC molecules and the four biotin binding sites on a single fluorescently labeled streptavidin to generate pMHC tetramers that now bind TCR with increased avidity solving the lack of stable binding between soluble pMHC monomers and cell surface TCRs (57). Tetramers are now available for several human and mouse MHC class I and class II antigens through the National Institute of Health tetramer core facility, or commercially by Beckman Coulter, ProImmune and Immudex. In addition to its other applications, this reagent is now widely used in SPR and ex-vivo analysis of TCR:pMHC interaction characteristics of monoclonal and polyclonal T cells isolated from mouse and human hosts under infection or diseased conditions. Although not a measure of monomeric TCR:pMHC affinity and kinetic rates, its correlation to SPR analysis has contributed to its wide use in the estimation of these parameters (8, 29). Such applications include the titration of tetramer staining concentrations to determine on-rates, K_D values and derive half-life from tetramer decay assays that use blocking anti-MHC antibodies or streptamer technology (7, 8, 56, 58-60). Tetramer K_D values have defined thresholds for positive and negative selection in the OT-I system (8), whereas in polyclonal studies, increased tetramer avidity was noted in polyclonal CD4 T cells responding to a secondary infection as compared to the primary response (56). Tetramer $t_{1/2}$ and not K_D has also been identified as the selection factor correlating to the survival of memory CD4 T cells (60) and the efficacy

of CD8 T cells that can clear CMV infection post an adoptive transfer into infected hosts (13, 59). However, as an avidity interaction, tetramer based TCR:pMHC affinity and kinetic rate analysis may not always reflect monomeric TCR:pMHC interaction and can be affected by several factors. These include fluctuations in cell surface TCR numbers, changes in the T cell's activation status, modifications in cytoskeletal and cell membrane components, and assay dependent confounding factors (3, 29, 61-65).

2D: Forster resonance energy transfer (FRET)

FRET technology has also been used in a single-molecule microscopy-based receptor-ligand interaction analysis to determine TCR:pMHC affinity and kinetic rates (42). In this assay, the receptor and ligand are labeled with either a donor or acceptor fluorophore and the specific interaction quantified through the photo-bleaching and recovery of FRET donor signal. The affinity and kinetic rates for the 5C.C7 TCR was measured in synapses and TCR microclusters using this technique (42). A FRET donor fluorophore was introduced in the single-chain variable fragment (scFv) of the anti-TCRβ clone H57 monoclonal antibody. The modified antibody labeled the TCR near the region found in close proximity to the MHC presented peptide which carries the acceptor fluorophore. To mimic the in-situ 2D restriction of the interaction, planar lipid bilayers with GPI anchored pMHC, ICAM-1, and B7-1 molecules were used to present antigen to the T cell. Conversion of surface receptor and ligand density (per area) to volume-based concentrations [M] showed 2D TCR affinity to be higher than previous SPR in solution measurements (37°C - 2D-K_D 4.8 μM, SPR 3D- K_D 39.8μM). Close to a 100-fold higher on-rate contributed to the increased affinity, which was hypothesized to occur due to the

2D context resulting in a favorable alignment between TCR and pMHC. Interaction half-life was significantly reduced (2D – 0.109s, 3D – 1.24s)) and the decrease attributed to cell cytoskeletal changes that destabilize the interaction. Thus, inhibition of actin polymerization by latrunculin A and cytochalasin D restored interaction half-life to SPR measured levels. Such differences underscored the value of 2D in-situ studies over 3D solution measurements (42, 55). Although a highly useful assay, this method has yet to be adapted for ex-vivo polyclonal T cell affinity analysis.

2D: Micropipette adhesion Frequency assay (2D-MP)

Utilizing concepts of cell-cell adhesion through receptor-ligand specific interactions, the microscopy-based micropipette adhesion frequency assay measures the TCR:pMHC interaction between a single T cell and a surrogate antigen-presenting cell (40, 41). An initial biotinylation of human red blood cells (hRBC) followed by a sequential addition of streptavidin and biotinylated pMHC monomers serves to anchor pMHCs on to the RBC membrane, converting the cell into an APC. Micromanipulators are used to pick up individual cells on opposed glass micropipettes, one of which is motorized and controlled through a computer software. This allows the programming of a repeated contact and separation cycles between the micropipette held cells with the contact set to a predetermined duration. Integral to the assay is the highly elastic RBC membrane which acts as a force sensor sensitive to as low as single bond generated stretching-force that occurs when the two cells are mechanically separated (40, 66). The visible change in the RBC shape is used to identify receptor-ligand specific binding events that are given a binary designation (adhesion (1) versus no adhesion (0)). Averaging multiple

independent contacts per tested T cell:hRBC pair generates an adhesion frequency value which describes the probability of adhesion (Pa) at the equilibrium contact time. This value can be used to derive the relative 2D affinity (in μm^4) of the cell in a mathematical model that also takes into account the TCR and pMHC densities per surface area (kept constant at approximately 3 μm^2) (66). Off-rates can also be derived from the adhesion curves generated by varying interaction contact time and taking an inverse of the duration required to reach a half-maximal adhesion (Pa) (66, 67). TCR transgenic systems with previously reported SPR and/or 2D affinities for their cognate antigens include the OT-I (41, 68), P14 (69, 70), and 2C (71) CD8 T cells as well as the 3.L2 (72), SMARTA and 2D2 (73) CD4 T cells. Similar to FRET-based observations, comparisons of 2D and 3D measurements for the OT-1 system and the 5C.C7 TCR demonstrated that on and off-rates were faster in this 2D assessment while both 3D and 2D measurements of half-life and affinity predicted antigen potency (39). However, unlike 3D measurements, 2D affinity and on-rates showed a wider range allowing a more sensitive detection and better correlation to T cell function and ligand potency than SPR based measurements (39, 41, 42, 72, 74). 2D-MP measures affinity and kinetic rates of TCRs anchored in their natural in-situ membrane environment with the associated CD3-complex, the co-receptor, other receptors and the underlying cell cytoskeleton. Inhibitors of actin polymerization (latrunculin A) and cholesterol depletion (methyl-beta-cyclodextrin, cholesterol oxidase) reduced 2D affinity and kinetic rates while a comparison of naïve and in vitro activated cells showed the latter to have a higher affinity (41). These findings further confirmed the need for in-situ assessments of TCR affinity which on the T cell is the sum of all the events and changes within and on the surface of the cell which allows the cell to tune its

response to antigen through the TCR. In contrast, 3D analysis relays context independent information. 2D affinity assessment is now being applied to ex vivo studies of polyclonal TCRs isolated from infected and diseased hosts providing single-cell measurements and immune response specific information of T cell affinity in relation to functional responses (10, 68, 75-79).

2D: Biomembrane force probe (BFP)

A variation on the 2D-MP assay, BFP allows TCR affinity and on and off-rate (bond lifetime) analysis by evaluating single bond formation and dissociation events with and without tensile force applied to the TCR:pMHC bond (55, 66). The increased sensitivity of the assay depends on the use of low-density pMHC coated beads attached to a hRBC membrane that acts as a force sensor/transducer sensitive to piconewton force. Thermal fluctuations in the bead that can be imaged in real-time by a high-speed camera and an image analysis software that can track the position of the bead with accuracy are also integral factors in this assay. The high spatial and temporal resolution allows for more accurate determination of kinetic rates which are derived from multiple bond-lifetime measurements (>500) for a given T cell. Attached to a hRBC, pMHC coated beads are held near the T cell to allow bond formation as a result of the random thermal fluctuation events of the bead that brings the two molecules in contact resulting in bond formation. This leads to a reduction in the thermal fluctuation of the bead and causes bead displacement both of which can be tracked by the high-speed camera and the image analysis software. Dissociation of the bond resets both parameters and tracking of the bead position over time identifies bond formation and dissociation events with the time

span between the two events identified as the bond-lifetime (39, 55, 66). These measurements can either be done under zero force (thermal fluctuation assay) or with specified force applied to the formed bond (force-clamp and force-ramp assays) (72, 80). In the force-clamp assay, the retracting T cell is clamped at a predetermined force until the bond ruptures and the bond lifetime is measured during the clamp phase. In the force-ramp assay the T cell is continuously retracted until the bond ruptures. This force dependent analysis of TCR:pMHC bonds makes this assay more relevant as recent studies using optical tweezers (81), DNA force sensors (82), as well as the BFP assay (72, 80) have all demonstrated TCR ligand discrimination is influenced by forces applied to the bond as a result of T cell motility, protein diffusion in the cell membrane, active protein transport within the cell and cytoskeletal rearrangement.

2D: Functional avidity (potency)

The requirements, availability, and suitability of other affinity analysis methods can preclude their use in the assessment of affinity largely with ex vivo polyclonal T cell samples. In the absence of such direct monomeric TCR affinity analysis methods but primarily as a predictive readout of in vivo response potential, EC_{50} peptide concentrations are derived for a given T cell function. As a relative measure, EC_{50} values gauge the quality of TCR:pMHC binding, an interaction occurring in 2D between the APC of choice and the T cell. Although this parameter shows a direct correlation with affinity/half-life (increased $1/EC_{50}$ = higher functional avidity/potency = high-affinity) (4-6, 47, 53, 72, 83, 84), several exceptions have been noted (85). One observation is functional avidity changes within a monoclonal T cell population expressing a fixed TCR

(86-89). Antigen dose-dependent tuning of avidity as well as changes in TCR signaling components such as activated Lck and the CD8 co-receptor have also explained these changes. Affinity for self during thymic-education, as read out by CD5 expression, has direct effects on peripheral responses to foreign pMHC. As noted in one study, differences in CD5 expression correlated to functional avidity variations between cells expressing TCRs of similar affinity (90). Likewise, intrinsic and extrinsic regulation through co-stimulatory and inhibitory receptors can also modulate T cell responses independent of TCR affinity (91-93).

TCR:pMHC interactions and T cell triggering

Once TCR engages pMHC, TCR triggering refers to the set of events that result in the transmission of this binding event into the intracellular ITAMs leading to their phosphorylation and the initiation of subsequent signaling cascades. Several studies have proposed varying TCR triggering models with some aimed at reconciling different TCR:pMHC interaction kinetics and biophysical parameters to the initiation and gradation of the T cell response. In the kinetic proofreading model, an interaction with a longer half-life (slower off rate) has a higher potential to complete the required triggering/signaling events for T cell activation while faster dissociation before necessary triggering/signaling events are completed resets the system (55, 94, 95). Observations that challenge this model include minor interaction half-life differences that lead to differing T cell responses, the cumulative nature of TCR signaling events, and the presence of TCRs that complete late signaling events but have altered early T cell signaling (30, 41, 96). As an amendment, the idea of a confinement time that occurs

through multiple binding and rebinding cycles between TCR and pMHC, before signaling is reset, was proposed to accommodate activation events observed in T cells with fast dissociation rates (97, 98). The number of engaged/triggered TCRs equating to the degree of the T cell response is described in the TCR occupancy and serial triggering models. Given that agonist pMHCs on the APC surface are outnumbered by self pMHCs, serial triggering describes the requirement of a fast dissociation rate for a single agonist pMHC to trigger multiple TCRs on a cell (99, 100). In a related concept, the TCR occupancy model equates the number of pMHC bound TCRs to the T cell response. A high dose antigen can compensate for a lower quality/affinity pMHC:TCR interaction by triggering several TCRs to reach a similar threshold signal that is needed to elicit a response (96, 101, 102). The difficulties in accurately quantifying pMHC occupied TCRs and studies that have shown bystander TCR downregulation during T cell activation have been the caveats to this model (103). The optimal dwell time model proposes an ideal TCR:pMHC interaction half-life range with a short or overly long half-life leading to diminished T cell responses (104), similar to the decreased response by T cells with either a too high or too low-affinity for pMHC. To define what occurs endogenously during T cell-dendritic cell encounters, several experiments that employed intravital imaging have supported the serial encounter model (105). T cell triggering occurs from signals accumulated during short-lived encounters with one or multiple APCs in the initial phase followed by a stable contact and motility resuming post initiation of IL-2 production and the start of T cell proliferation (101, 106, 107). Motility differed based on the affinity/kinetic properties of the interaction with high-affinity cells making stable and long-lasting conjugates

(synapse) while lower affinity interactions resulted in short-lived multiple contacts (kinapse) (108).

The above models address interaction parameters that lead to productive TCR triggering events. Other models describe how the spectrum of TCR:pMHC interactions translate to the chemical/physical changes that lead to ITAM phosphorylation. These include TCR aggregation, kinetic segregation and conformational changes (109). A proposed self:cognate pMHC pseudodimer aggregation model indicates self pMHC brings CD4 and the associated Lck to aid TCR triggering by agonist pMHC (110-112). Kinetic segregation describes changes in the localization of the TCR:CD3-complex relative to receptor tyrosine phosphatases (CD45, CD148) that dephosphorylate the steady-state constitutively phosphorylated ITAMs (113). Concurrent localization of the TCR:CD3 complex in lipid rafts enriched with constitutively active Lck (114) leads to optimal ITAM phosphorylation and TCR triggering. Physical exclusion of CD45 from the zones of TCR:pMHC contact occurs due to its large ectodomain (115). The conformational change model combines multiple findings that indicate physical changes in the TCR and the CD3-complex as well as the accumulating evidence that highlights the role of mechanical effects in TCR-ligand recognition. One aspect indicates pMHC binding can lead to a conformational change in the AB loop of the TCR Cα domain, induced by cognate interactions and not an antagonist (22, 116, 117). These studies also showed the same region can lead to TCR dimerization as a secondary event to TCR triggering (118). In the CD3-complex, cysteine motifs from the stalk regions of CD3γε keep this heterodimer rigid (119) and are hypothesized to do the same in the CD3δε chains (24, 25). This keeps the TCR-CD3 complex rigid as a whole and more able to

transduce any pulling pressure exerted by pMHC binding and concurrent cytoskeletal changes in the T cell or APC. The FG loop from Cβ protrudes from the TCR and lies above the CD3γε external domains, where the movement created by TCR:pMHC binding forces the FG loop onto the CD3 and allows the transmembrane α helices to slide relative to each other, resulting in further conformational changes that lead to ITAM phosphorylation (24, 25). Several mutational studies of the TCR and CD3 molecules have highlighted the importance of the above-mentioned structures in TCR triggering (120). On the cytoplasmic side, CD3ε and ζ chains are thought to be associated with the acidic phospholipids of the plasma membrane inner leaflets through certain basic residues (121, 122). This is hypothesized to keep the ITAMs inaccessible or "safe" from kinase phosphorylation at resting conditions while ligand-induced TCR-CD3 conformational changes and associated alterations in the acidic phosphatidylserine concentration in the plasma membrane frees the ITAMs, allowing Lck induced phosphorylation (123). Other support for the TCR-CD3 complex as a mechanosensor stems from studies that show enhancement of TCR triggering with the application of force (124) as seen with studies using optical tweezers (81), DNA force sensors (82), and the BFP assay (72, 80). This idea of the TCR as a mechanosensor is emerging as the favored TCR triggering model and can explain how different TCR:pMHC bonds can elicit a wide range of responses based on their ability to withstand pulling and shearing forces encountered as they engage an APC.

CD4 T cell response: multiple factors affecting outcome

TCR:pMHC affinity: Lessons from monoclonal CD4 and CD8 T cells

In vitro analysis of dose-response curves with altered peptide ligands (APLs) coupled with early SPR studies set the stage for defining the effects of TCR:pMHC affinity on a T cell's response (5, 6, 47, 53, 72, 83, 84). Several of these studies identified the linear relationship between TCR affinity and the degree of a T cell's functional response. An affinity-based thymic selection model for immature T cells was also defined using the same CD4 and CD8 monoclonal TCR systems with high-affinity agonist peptides leading to negative selection in comparison to weaker ligands that promoted positive thymocyte development (6, 53, 84). Several other studies have also identified characteristics of higher and lower affinity interactions, highlighting the role of affinity on a T cell's response and further identifying mechanisms that result in these differences.

In early T cell activation events, TCR signaling was found to be inherently different in agonistic higher affinity interactions that lead to increased CD3ζ ITAM phosphorylation, Ca2+ signaling, and ERK phosphorylation (2, 8). However, weak interactions have also been shown to accumulate similar signals albeit in a delayed time frame (73, 96, 125). Functionally, T cells recognizing high-affinity ligands also exhibit increased proliferation, cytokine production or targeted lysis of cells in vitro (5, 6, 47, 53, 72, 83, 84, 126). Extending the use of these models to study peripheral in vivo responses have also shown a correlation between TCR affinity and the extent of T cell activation, clonal expansion, functional responses and memory differentiation. In the 5C.C7 transgenic CD4 T cell APL model, peptide/LPS immunization with the higher affinity cognate antigen (MCC:IE^k) led to increased proliferation, IL-2 and, IFNγ production, and memory response compared to intermediate (K3 MCC:IE^k) and lower affinity ligands (102S MCC:IE^k) (42, 52). Intravital imaging also revealed decreased APC:T cell

conjugate formation in the low-affinity response but an increase in CD69 expression did indicate activation of the cells (101). Hence, both high and low-affinity interactions promote peripheral responses albeit to differing degrees.

Another preferred model providing several insights into affinity related peripheral T cell responses is the OT-1 TCR transgenic CD8 T cell and the spectrum of affinities represented by several APLs. Numerous notable affinity related observations have stemmed from this model. In an adoptive transfer setting, OT-1 T cells responding to high and low-affinity APL ligands in a Listeria Ova APL infection had a comparable phenotypic expression of activation markers, similarly differentiated into memory cells and expanded to a secondary challenge. However, OT-I T cells responding to lower affinity APLs exhibited decreased clonal expansion and entered the circulation at a faster rate than observed under higher affinity conditions (4). In a different study, asymmetric allocation of cell surface and internal components were noted in a higher affinity APL interaction compared to the symmetrical division induced with a lower affinity ligand. The asymmetric division generated $CD8^{hi}$, LFA-1^{hi} proximal daughter cells with the increased potential to form T cell:APC conjugates, proliferate, and generate VLA-4 expressing short-lived effector cells (SLECs) that migrated to tissues (127). A similar asymmetric division associated segregation of effector and central memory phenotype has also been identified in CD4 T cells (128). In a different study, OT-I T cells responding to recombinant Listeria that expressed Ova APLs upregulated IRF4 in a TCR affinity-dependent manner at five days post-infection. This transcription factor regulates the process of aerobic glycolysis in effector T cells and is critical in clonal expansion and sustained effector functions in CD4 as well as CD8 T cells (129, 130). These studies

further confirmed TCR affinities as low as ones that lead to positive thymic selection on self can lead to pMHC induced activation and memory formation in the periphery. However, lower affinity cells may expand to a lesser degree and differ in their migration kinetics while also exhibiting a lesser metabolic and cytokine production capacity.

Monoclonal TCR:APL interactions can span a spectrum of affinities and thus are useful in highlighting affinity related effects. However, as this analysis only examines a single TCR species, other TCR transgenic studies have also examined the role of TCR:pMHC interaction using multiple T cells of similar specificity but of differing or equivalent affinities. To determine the TCR:pMHC binding parameters that correlated with memory formation and survival, one study generated and examined the response of four different antigen-specific retrogenic T cells. In an LCMV Armstrong infection model, a comparison of tetramer K_D and $t_{1/2}$ assessment showed that a clone's entry into the memory pool correlated with sustained interactions with APCs ($t_{1/2}$) (60). Another study compared two CD4 TCR transgenic T cells and their response to infection with Listeria expressing the cognate MTB ESAT-6_{1-19} epitope. The higher avidity clone (with increased tetramer K_D and $t_{1/2}$) had a response magnitude similar to the lower affinity clone in the primary response. However, a secondary challenge resulted in a lower expansion due to the clone's decreased TCR expression observed in the primary response (131). A similar TCR downregulation effect was observed in a different Listeria model with two $LLO_{190-205}$ specific transgenic CD4 T cells of equivalent affinity exhibiting different expansion potential in a primary versus a secondary response (90, 132). In the NOD model of diabetes, eight distinct retrogenic TCRs with different 2D affinities for insulin were tested for their propensity to cause disease. Upregulation of pERK post in

vitro antigen stimulation of these cells occurred in an affinity-dependent manner aligning their 2D biophysical TCR:pMHC affinity measurements with the TCR's signaling capacity. A wide range of affinities led to insulitis however, the highest affinity cells were an exception as this increased affinity led to targeting by tolerance mechanisms (133) suggesting similar regulation can occur to prevent immunopathology during infection. Although these studies provide the advantage of addressing the role of affinity related and unrelated mechanisms on the immune response from a "multi-clonal" perspective, concurrent evaluations of a fully polyclonal response are needed.

TCR:pMHC affinity/polyclonal T cells

The diverse nature of the antigen-specific TCR repertoire proved challenging with respect to T cell frequency and affinity related evaluations. At the population level, accurate identification of antigen-specific cells is critical as this parameter is indicative of the magnitude and efficacy of the response. Furthermore, the relative abundance of high and low-affinity cells and their accurate quantification identifies the average affinity of the response. While necessary, this again differs from the critical nature of determining TCR affinity at the single cell level to highlight the diversity in the response. A limited number of assays can now identify antigen-specific cell frequency and single cell affinity post-induction of an immune response although each assay comes with its own degree of limitations. However, in mice, identifying the starting frequency and affinity of antigen-specific cells in the naïve repertoire is still a challenge. Limiting dilution assays (LDA) (134, 135), adoptive transfer models (136, 137), pMHC I and II tetramers (138, 139), and more recently, all three of these assays in combination with the Nur77GFP reporter

mouse have been employed to determine antigen-specific frequency in the naïve repertoire (78). The currently well-utilized tetramer pulldown assay identified the naïve precursor numbers for several epitopes allowing more direct assessment of T cell expansion and the relative magnitude of different responses (138, 139). However, binding to this reagent requires an affinity threshold that lower affinity CD4 T cells fail to reach. This is true both for foreign and self pMHC-specific T cells present during the response to an infection and in autoimmune diseases (10, 77, 140, 141). One work focused on tetramer-negative cells and applied an in vivo LDA assay with Nur77GFP mice to quantify high and low-affinity naïve antigen-specific precursor numbers for several IA^b restricted epitopes. Lower affinity (tetramer-negative) precursors were 3-10-fold greater in number than higher affinity cells (tetramer-positive) for all tested epitopes suggesting the immune response starts with a low-affinity bias (68).

Interestingly, despite this starting bias, several studies have identified a narrowing of the polyclonal affinity repertoire to enrich for higher affinity cells at memory (142, 143) and in recall responses (56, 58). As tetramer binding was used to discern these changes in the antigen-specific repertoire, it is unclear how the comprehensive population affinity is altered in primary and secondary responses. Using functional assays, other studies have also reported an increase in the functional avidity of polyclonal T cells at a memory time point and during a secondary challenge (58, 60, 144, 145). Although an increased functional response can occur independent of an affinity-based selection ((86, 87, 137), the functional maturation observed in some of these studies also corresponded to a higher avidity interaction with tetramer suggesting surface TCR:pMHC affinity-based selection. However, as this again examines a fraction of the antigen-specific

population, it is unclear how the contribution and selection of the lower affinity population proceeds.

To address these questions, an alternative assay, the 2D-MP, has been employed to re-examine overall T cell receptor affinity in T cells isolated from ongoing immune responses (10). This first polyclonal study compared the antigen-specific population affinity of CD4 T cells in a model of viral infection (LCMV Armstrong) and autoimmune disease (EAE). The T cell population specific to the foreign antigen was found to possess a >10-fold higher affinity compared to the autoimmune response. However, a high frequency of low-affinity (> 3 fold tetramer-negative) cells was identified in both models with a >100 fold affinity breadth detected from single cell affinity measurements (10). Since then, other autoimmune diseases (76, 77) and infection models (75) have been examined with this assay showing its applicability and sensitivity to polyclonal T cell studies that inherently possess a wider affinity range.

T cell repertoire analyses that have determined TCR$\alpha\beta$ gene usage at depths ranging from surface antibody staining to deep sequencing and paired $\alpha\beta$ single cell analysis have indicated a narrowing in the antigen-specific repertoire mainly using pMHC tetramers to isolate antigen-specific cells in the naïve and primary/secondary repertoire. Such studies have identified certain precursors are selected to proliferate and dominate over others leading to an antigen-specific repertoire with a restricted usage of TCR genes and CDR3 lengths that correlate with the enrichment of higher avidity TCRs (58, 60, 146-149). This is in contrast to other studies that have highlighted the importance of a diverse antigen-specific repertoire in providing protection against viral infections (150) and the contribution of tetramer undetected cells to overall antigen-specific TCR

genetic diversity (151). Modifications to the 2D-MP assay now include the ability to isolate antigen-specific single cells and perform gene sequencing, hence coupling single cell 2D affinity measurements to the analysis of TCR and other genes of interest (79).

Antigen dose

Several studies have identified the minimum number of pMHC required to activate CD4 and CD8 T cells. In general, 30-400 cognate pMHC per APC leads to naïve CD4 T cells activation, proliferation and IL-2 production (152, 153). More impressively, CD4 T cells were shown to flux calcium in response to a single pMHC while sustained calcium levels required the presence of 10-15 pMHC molecules within the contact area (5C.C7 and 2B4) (111). This sensitivity to antigen was significantly reduced in the absence of CD4 and such cells could only respond to APCs that presented greater than 25 cognate pMHCs at the APC: T cell synapse (110). In CD8 T cells, a single agonist pMHC was shown to induce T cell arrest, APC scanning, and some calcium flux, with 3 pMHC leading to cytotoxic activity and 10 being the minimum required for a stable synapse formation and maximal calcium flux (154, 155). Unlike the CD4 co-receptor which is necessary for T cell sensitivity to antigen levels, CD8 MHC interaction is required for full calcium flux and T cell function, independent of agonist pMHC concentration (OT-I and 2C) (156-158).

Despite this reported sensitivity, CD4 T cell clonal expansion and differentiation into memory require a sustained encounter with antigen (159) whereas the CD8 T cell response is programmed in the first 2-24hrs of stimulation (160). Nevertheless, clear correlations between antigen dose, duration of antigen encounter, and the magnitude of

the response have been demonstrated for both cell types (159, 161-164). Unlike these observations which fall within the limits of an acute antigen exposure, prolonged encounter as occurs with chronic infections has a different outcome (165). T cell proliferation, functional capacity, as well as memory formation is impaired in the presence of antigen that lingers past the T cell priming phase (≥10 days) (166-169). T cell differentiation is also altered with prolonged and high dose antigen encounter favoring T_{FH} formation while dampening T_{H1} and other helper type responses (135, 170-172). T_H differentiation pattern develops as a result of the combined effects of TCR affinity and antigen dose in the appropriate cytokine cues (172). A high TCR affinity favors T_{H1} differentiation while T_{FH} generation can occur with high to low-affinity ranges and with a high dose or prolonged antigen exposure (135, 170-172). Manipulation of antigen dose also results in the differential expansion of cells with a high and low functional avidity. Low dose antigen priming favors the formation of cells with a higher functional avidity (173). A similar relationship between antigen dose and the expansion of memory and secondary responders with a higher tetramer avidity has also been reported (174).

Inflammatory environment

Multiple aspects of the T cell response are influenced by the inflammatory environment which modulates the response through cytokines, chemokines, the activation and co-stimulatory receptor expression levels and nature of the elicited APCs, regulatory cells (T_{reg}, MDSCs, cytokines) and pathogen dependent mechanisms. Several studies have highlighted these effects indicating the need for evaluating T cell responses in context representative models. For instance, different adjuvants or vectors prime CD4 T cells

driving specific T_H differentiation patterns, TCR affinities/avidities and repertoire diversity (175-177). In vivo priming of T cells with peptide-loaded DCs and the LCMV inflammatory environment which has a dominant type I interferon signature favors a >10 fold expansion of CD8 T cells that have a significantly higher functional avidity than cells of the same specificity primed by Listeria which drives an IL-12 cytokine milieu (178). Differences in TCR proximal signaling with Lck, Zap70, pERK and other components accounted for the response differences highlighting the importance of cytokines in shaping the antigen-specific repertoire. CD4 T cells also demonstrate a similar environment dependent functionality in the two inflammatory environments (86, 164, 179, 180). Another cytokine with direct consequences in determining the magnitude and memory differentiation of CD4 and CD8 T cells is IL-2. Encountered cells also shape the response and the recruited antigen-specific population. For instance, antigen presentation by dendritic cells as compared to B cells and the combined presence exerts differential expansion and memory potential of CD4 T cells (181). Although DCs provide optimal priming of naïve T cells, B cells are necessary for the formation and maintenance of memory T cells (182-184). Furthermore, B cells promote low avidity cell expansion (185) and T cell responses to limiting antigen concentrations (186). Regulatory mechanisms in infection demonstrate a dual function both promoting and dampening the immune response as needed. For instance, T_{regs} promote the migration of antigen-specific cells from secondary lymphoid organs into infected tissues by orchestrating chemokine driven signals providing a timely response that resolves infection (187). The absence of T_{regs} in the priming phase was also found to severely impair CD4 T cell response in HSV-2 infection due a lack of T_{reg} aided DC migration to draining lymph nodes (188). T_{regs} that

normally reside in splenic white pulp limit pro-inflammatory cytokine signals on CD8 T cells through IL-10 and promote memory formation (189) and likely exert a similar influence on CD4 T cells. T_{reg} controlled antigen presentation by DCs has also been demonstrated to affect T cell functional avidity and set limits on expansion (190, 191). In the more canonical suppressive function, T_{regs} dampen T cell function and limit pathology especially in immune privileged sites and in persistent infections (192-194).

CD4 T cells in acute and chronic infections

CD4 T cells facilitate pathogen clearance through direct cytotoxic activity or more often by coordinating and licensing innate immune cells, B cells and CD8 T cells to carry out this task (191, 195). In the absence of CD4 T cells, the immune response to acute viral and bacterial infections is impaired. CD8 T cells primed without CD4 T cell help exhibit decreased proliferation and suboptimal memory formation and survival which leads to impaired secondary responses (190, 196-198). CD4 T cell produced IL-2 contributes to this efficient CD8 memory differentiation during primary T cell priming events (199). In humoral immunity, SAP sufficient CD4 T cells are critical in the formation of memory B cells and plasma cells, and T cell help enables class switching and maintenance of germinal centers which promote B cell affinity maturation (190, 200, 201).

In chronic infections, CD4 T cell functions have direct consequences on the containment or resolution of infection (202). For instance, CD4 T cell depletion in HIV infection has severe consequences leading to the progression to AIDS while in elite controllers active CD4 T cell responses with superior functional avidity contribute towards limiting viremia (203). Early and robust CD4 T cell functional responses which

can provide optimal CD8 help are also observed in patients that go on to clear HCV infection (204). CD4 depletion during HCV also leads to poor outcomes (205).

A highly utilized model that has provided several insights into the nuances of the immune response against acute and chronic viral infections is the LCMV mouse model. LCMV is part of the old-world arenaviruses, a group that includes Lassa hemorrhagic fever-causing virus. Rodents are the natural LCMV hosts but the virus can also infect immunocompromised individuals and lead to congenital infections (206). LCMV genome contains two ambisense RNA segments. The S (small – 3.5 kb) segment encodes for the viral nucleoprotein (NP) and the glycoprotein precursor (GPC) which gets cleaved into GP1 (extracellular – for attachment) and GP2 (transmembrane – for fusion) domains. The L (Large – 7.2 kb) segment codes for the Z (small zinc finger) matrix protein and the L/RNA-dependent RNA polymerase. Isolation of viral variants that led to acute and persistent infections and the single amino acid mutation in the glycoprotein that confers high-affinity interaction with the host receptor α-dystroglycan and the cell tropism leading to persistence were events that initially identified the tenets of this model (207-209). Although other variants exist, the widely used strains are the acute Armstrong (ARM) and chronic clone 13 (CL13) viruses. Although they lead to different infection outcomes, the two viruses share CD4 and CD8 T cell epitopes which have allowed a direct comparison of T cell responses across the two models (166). Several noteworthy discoveries from this model have informed our understanding of several aspects of the T cell response and acute and chronic infections leading to parallel observations in human infections (210). These include MHC restricted nature of the T cell response (211) and the generation, quantification and maintenance of effector and memory T cells (212-214)

in acute infections. In the chronic setting ideas of T cell exhaustion with hierarchal loss of polyfunctionality in CD8 and CD4 T cells (167, 215, 216), upregulation of inhibitory receptors (PD-1) (217) and the exhaustion signature of CD4 (169) and CD8(168) cells compared to memory T cells were all observed in this model. Furthermore, the ideas of rescuing immune responses against chronic infections through the PD-1(217) pathway and CD4 T cell help (218, 219) were first explored in this model. The clinical relevance of the abovementioned discoveries made in the LCMV infection models confirms its suitability for examining the co-evolution properties between polyclonal CD4 TCR affinities and functional responses under acute and chronic antigen exposure.

Chapter 2. CD4 T cell affinity diversity is equally maintained during acute and chronic infection

Originally published in *The Journal of Immunology*. Andargachew, R., R. J. Martinez, E. M. Kolawole, and B. D. Evavold. 2018. CD4 T Cell Affinity Diversity Is Equally Maintained during Acute and Chronic Infection. *J. Immunol*. 201: 19-30.

http://www.jimmunol.org/content/201/1/19

Abstract

T cell receptor (TCR) affinity for peptide-major histocompatibility complex (pMHC) dictates the functional efficiency of T cells and their propensity to differentiate into effectors and form memory. However, in the context of chronic infections it is unclear what the overall profile of TCR affinity for antigen is and if it differs from acute infections. Using the comprehensive affinity analysis provided by the 2-dimensional (2D) micropipette adhesion frequency assay (2D-MP) and the common indirect affinity evaluation methods of MHC class II tetramer and functional avidity, we tracked IA^b GP_{61-80} specific cells in the mouse model of acute (Armstrong) and chronic (clone 13) LCMV infection. In each response, we show CD4 T cell population affinity peaks at the effector phase and declines with memory. Of interest, the range and average relative 2D affinity was equivalent between acute and chronic infection, indicating chronic antigen exposure did not skew TCR affinity. In contrast, functional and tetramer avidity measurements revealed divergent results and lacked a consistent correlation with TCR affinity. Our findings highlight the immune system maintains a diverse range in TCR affinity even under the pressures of chronic antigen stimulation.

Introduction

One key parameter regulating T cell activation and functional differentiation in the CD4 T cell response is TCR affinity for antigen. The affinity between a receptor and ligand has often been determined using surface plasmon resonance (SPR) measurements (47, 48). However, the need for soluble forms of TCR and pMHC has made the use of this assay impractical for tracking the affinity of large numbers of antigen-specific polyclonal T cells in an ongoing immune response. As a result insights into TCR:pMHC affinity and how it instructs the T cell response during an infection have relied on the use of monoclonal TCRs and altered peptide ligands (APLs) with SPR defined affinities (3, 4, 8). Polyclonal TCR affinity analysis, on the other hand, has depended on ex vivo functional avidity and pMHC tetramer staining assays for indirect estimation of TCR affinity based on the positive correlation between these methods and SPR affinity measurements in monoclonal TCR systems (9, 56, 58, 92, 142). Hence in functional avidity assays, T cells able to mount functional responses by cytokine production, proliferation or cytotoxic activities in response to low dose antigen have generally possessed TCRs with high-affinity for antigen (4, 47, 101). Similarly, the increased staining or avidity of T cell clones for tetramerized pMHC has been correlated to the inherently high-affinity interaction between monomeric TCR and pMHC (29).

During an immune response, acute antigen exposure models that have examined both monoclonal and polyclonal populations have demonstrated T cell clones with increased avidity for tetramer and a high functional avidity are preferentially expanded in primary and secondary responses and are selected to become memory cells (56, 58, 86, 137, 142, 147). The observed narrowing of the affinity diversity of antigen-specific cells to

preferentially enrich for high-affinity T cell clones has been equated to a form of T cell affinity/avidity maturation (220). In contrast, experiments in chronic infections demonstrated the loss of high avidity clones and later enrichment of lower avidity cells suggesting a decrease in TCR affinity under continuous antigen experience and selection for a T cell affinity profile distinct from the one generated during an acute response (185, 221). As these observations stem from unrelated models that have yet to probe the same antigen-specificity and affinity evolution under acute and chronic antigen exposure, it is unclear if affinity skewing actually differs under these conditions. Furthermore, tetramer and functional avidity assays have shown bias towards sampling the highest affinity fraction of the antigen-specific repertoire potentially missing the full breadth and diversity in a full polyclonal response to infection (10, 141).

Re-evaluation of polyclonal T cell affinity profiles using the more comprehensive analysis of affinity provided by the 2D-MP assay has now shifted our understanding of TCR affinity breadth and the prevalence and contribution of high and low-affinity T cells during a polyclonal immune response (10, 76-78). This microscopy-based assay measures monomeric TCR:pMHC affinity at the single cell level with the TCR anchored in its natural T cell membrane context and pMHC coated on a surrogate antigen presenting cell hence providing a 2-dimensional affinity analysis highly predictive of T cell function (41, 67, 72, 79). Mounting data highlight low-affinity and tetramer-negative CD4 clones participate in the immune response, form functional memory and can comprise a larger portion of the antigen-specific compartment for a given epitope (4, 10, 46, 68, 78). Affinities ranging from 100-1000 fold have been shown for various antigens in differing immune responses, indicating the immune system maintains a wide breadth of affinities with all possessing the

capacity to undergo clonal expansion and form memory (10, 76-79). Although skewing towards high or low affinities has been noted in some models (10, 78), 2D affinity characterization of a polyclonal CD4 T cell response to chronic infection is lacking. In comparison to an acute infection, understanding how the chronic infection environment shifts and shapes the host's antigen-specific CD4 T cell populations' TCR affinity diversity can prove beneficial in CD4 T cell therapies aimed at rescuing immune responses in chronic infections (219, 222).

To understand the evolution of T cell affinity and functional responses during infection, we directly compared polyclonal CD4 TCR affinity to the same MHC II (IA^b) restricted GP_{61-80} epitope in the well-studied LCMV model of acute Armstrong (ARM) and chronic clone 13 (CL13) infections. Although they lead to different infection outcomes, the two viruses share CD4 and CD8 T cell epitopes allowing for a direct comparison of T cell responses across the two models (166). As the majority of the CD4 T cells target the GP_{61-80} peptide with a lower frequency of cells being specific to other minor epitopes, we focused our studies on this immunodominant response (223). 2D-MP, TCR tetramer avidity, tetramer half-life and functional avidity measurements were used to compare the biophysical TCR:pMHC binding and functional characteristics of CD4 T cells as they transitioned from peak effectors to memory cells. Our overall findings demonstrate CD4 TCR affinity diversity is equally maintained under acute and chronic infection with early effectors and late memory CD4 T cells in acute infection having 2D affinities identical to their chronic infection counterparts. Despite the dominance of high-affinity cells at the peak of the response, in both acute and chronic infection overall affinity decreased at memory paralleling antigen clearance. Functional and pMHCII tetramer avidity and half-

life measurements lacked a consistent correlation to 2D affinity measurements confirming TCR affinity contributes to but is not the sole parameter read out by tetramer and functional avidity assays. As affinity skewing of the CD4 T cell response is similar between acute and chronic infection, our data indicate other regulators modulate T cell function in chronic infection to limit immune pathology without altering affinity diversity in the CD4 T cell response. Hence therapeutic interventions may be able to recover CD4 T cell responses without the need to increase the breadth of TCR affinity.

Materials and Methods

Mice and virus infection

C57BL/6 (B6) mice were purchased from the National Cancer Institute (NCI) and Charles River. B-cell deficient (Ighm-/-) (224) mice on the B6 background were purchased from Jackson Laboratories. For acute and chronic LCMV infection, 6-10 week old female mice were i.p. injected with $2x10^5$pfu Armstrong or i.v. infected with $2x10^6$ pfu CL13 respectively (69, 166, 169, 216). Virus stocks were kindly provided by Dr. Rafi Ahmed's lab at Emory University, Atlanta, GA. All animals were housed at the Emory University Department of Animal Resources facility and all experiments were performed in accordance with the guidelines for the Care and Use of Laboratory animals under Emory University Institutional Animal Care and Use Committee approved protocols.

Intracellular cytokine staining: Functional avidity

Splenocytes isolated from infected mice were plated at $2x10^6$ cells per tested GP_{61-80} peptide concentration (GLKGPDIYKGVYQFKSVEFD – synthesized on a Prelude Peptide Synthesizer (Protein Technologies)). Tested concentrations ranged from 100μM to 1nM at ten-fold dilutions. Cells were incubated for six hours at 37° C in T cell culture media and 5% CO2 in the presence of 10μg/ml brefeldin A (MP Biomedicals). T cell media contained RPMI 1640 (Mediatech), 10% heat-inactivated FBS (Hyclone), 10 mM HEPES buffer (Mediatech), 2mM L-glutamine (Mediatech), 50μM 2-mercaptoethanol (2ME) (Sigma), and 100μg/ml gentamicin (Mediatech). Samples incubated without peptides were used as baseline control while PMA (20nM; Fisher Biotech) and ionomycin (1μM; Sigma) activation served as a positive control. Cells were washed and stained with surface

antibodies for 30 minutes on ice in FACS staining buffer containing phosphate buffered saline (PBS) (Mediatech), 0.1% bovine serum albumin (BSA) (Fisher Scientific), and 0.05% sodium azide (Sigma). Staining antibodies included anti-CD4 FITC (RM4-5; Tonbo biosciences/eBioscience), anti-CD11b PerCP Cy5.5 (M1/70; BD), anti-CD11c PerCP Cy5.5 (HL3; BD), anti-CD19 PerCP Cy5.5 (ID3; BD), anti-CD3ε PECF594 (145-2C11; BD), anti-CD44 AF700 (IM7; LifeTechnologies), anti-CD27 V450 (LG3.A10; BD), Viability Ghost Dye Violet (Tonbo/eBiosciences), anti-PD-1 BV605 (29F.1A12; Biolegend), and anti-CD8 BV785 (53-6.7; Biolegend). Using Invitrogen FIX and PERM or BD Cytofix/Cytoperm kits, cells were fixed and permeabilized in accordance with manufacturer's protocols. Intracellular antibody staining was performed for 30 min on ice using the manufacturers' permeabilization solution and anti-IFNγ APC Cy7 (XMG1.2; BD), anti-TNFα PE Cy7 (MP6-XT22; Biolegend), anti-IL-2 APC (JES6-5H4; BD) antibodies. Aliquots of unstained splenocytes were used to obtain total cell and different population counts using AccuCheck microbeads (Invitrogen). Cells were washed and kept on ice until flow cytometry was carried out using a FACSVerse or LSR II (Beckton Dickson). Data analysis was performed using FlowJo software (Tree Star). To generate avidity curves and derive EC_{50}, the frequency of cytokine-positive cells (with frequency of unstimulated control subtracted) at the 100μM concentration was used as the maximal cytokine producer frequency and equated to a 100% with the remaining frequencies at lower peptide doses normalized to this maximal response as previously described (86, 179). Normalized values were graphed against log-transformed peptide concentrations and the data fitted to a nonlinear regression (log (agonist) vs normalized response) using GraphPad Prism 7 analysis software.

TCR staining

TCR expression differences were quantified using the anti-TCRβ clone H57-597 PE antibody (eBioscience). Briefly, a few million splenocytes from infected mice were surface stained on ice for 30 minutes with anti-CD11b PerCP Cy5.5 (M1/70; BD), anti-CD11c PerCP Cy5.5 (HL3; BD), anti-CD19 PerCP Cy5.5 (ID3; BD), 7AAD (BD), anti-CD3ε PE CF594 (145-2C11; BD), anti-CD44 PE Cy7 (IM7; Biolegend), anti-CD62L APC Cy7 (MEL-14; BD), anti-CD27 V450 (LG3.A10; BD), anti-CD4 BV510 (RM4-5; Biolegend), anti-PD-1 BV605 (29F.1A12; Biolegend), and anti-CD8 BV785 (53-6.7; Biolegend) antibodies along with the anti-TCRβ antibody. Cells were washed and kept on ice until flow cytometry was carried out using an LSR II (Beckton Dickson). Using the FlowJo software (Tree Star), TCR, CD4 and forward scatter (FSC-A) mean fluorescence intensities (MFIs) of CD4+CD44^{hi} (antigen-experienced) and CD4+CD44^{lo}CD62+ (naïve) cells were quantified and compared between the two infections per experiment. Quantibrite PE quantification beads (BD Biosciences) were used per manufacturer instructions to determine the number of TCRs per cell. For further comparison between infections and across different time points, MFI of antigen-experienced cells was normalized to the naïve population within the same sample and quantified as % of naïve ((antigen-experienced MFI/naïve MFI) x 100) (131).

Tetramer avidity

Tetramer staining was performed with splenocytes at a density of 2x10^6 cells (100µl volume) per tested concentration (10µg/ml – 0.01µg/ml at 10 fold dilutions, 5-0.05µg/ml at 10 fold dilutions, 2.5µg/ml, 0.25µg/ml) of the PE-conjugated IA^b GP$_{66-77}$ tetramer

acquired from the NIH Tetramer Core Facility at Emory University, Atlanta, GA. Labeling was done in T cell media at room temperature for 1 hour. As a control, IA^b $hCLIP_{103-117}$ tetramer (NIH Tetramer Core) was used to stain the samples at 10μg/ml. Cells were washed with cold staining buffer and surface stained on ice for 30 minutes prior to sample acquisition on a FACSVerse or an LSRII flow cytometer. Aliquots of unstained splenocytes were used to obtain total cell and different population counts using AccuCheck microbeads (Invitrogen). Antibodies used for surface staining included anti-CD11b PerCP Cy5.5 (M1/70; BD), anti-CD11c PerCP Cy5.5 (HL3; BD), anti-CD19 PerCP Cy5.5 (ID3; BD), 7AAD (BD), anti-CD3ε PE CF594 (145-2C11; BD), anti-CD44 PE Cy7 (IM7; Biolegend), anti-CD62L APC Cy7 (MEL-14; BD), anti-CD27 V450 (LG3.A10; BD), anti-CD4 BV510 (RM4-5; Biolegend), anti-PD-1 BV605 (29F.1A12; Biolegend), and anti-CD8 BV785 (53-6.7; Biolegend). Data analysis was performed using FlowJo software (Tree Star). To generate dose-response curves and derive EC_{50}, the frequency of tetramer stained cells at 10μg/ml concentration was used as the maximal response and equated to a 100% with the remaining frequencies at lower tetramer doses normalized to this maximal frequency as previously described (86, 179, 185). Normalized values were graphed against log-transformed tetramer concentrations and the data fitted to a nonlinear regression (log (agonist) vs normalized response) using GraphPad Prism 7 analysis software.

Tetramer decay

Splenocytes were stained with tetramer at 10μg/ml for 1hr at room temperature at a cell density of $20x10^6$ cells in 1ml of FACS staining buffer (0.05% sodium azide). Cells were washed with ice-cold buffer to remove excess tetramer and kept on ice until an aliquot

($2x10^6$ splenocytes in FACS buffer) was incubated with 100μg/ml of the anti-IA/IE (M5/114.15.2: eBioscience) blocking antibody at room temperature. Decay was measured at 3hrs, 2hrs, 1.5hrs, 1hr, 40mins, 20mins, and 10mins post antibody addition. The tetramer stained sample without blocking antibody addition was used for the 0min time point. Incubation was done in a staggered manner starting with the 3hrs and decreasing to the last time point with all incubations ending concurrently and all samples completed at the same time (begin the 3hrs incubation, 1hr later start the 2hr incubation and so on). Cells were then washed with ice-cold staining buffer to remove excess blocking antibody and kept cold during all washes. Staining for surface markers was performed on ice with anti-CD11b PerCP Cy5.5 (M1/70; BD), anti-CD11c PerCP Cy5.5 (HL3; BD), anti-CD19 PerCP Cy5.5 (ID3; BD), 7AAD (BD), anti-CD3ε PE CF594 (145-2C11; BD), anti-CD44 PE Cy7 (IM7; Biolegend), anti-CD62L APC Cy7 (MEL-14; BD), anti-CD27 V450 (LG3.A10; BD), anti-CD4 BV510 (RM4-5; Biolegend), anti-PD-1 BV605 (29F.1A12; Biolegend), and anti-CD8 BV785 (53-6.7; Biolegend) antibodies. Cells were kept on ice until sample acquisition was done on an LSRII flow cytometer. Mean fluorescence intensity of tetramer-positive cells (control IA^b $hCLIP_{103-117}$ staining used to draw positive gate) was normalized to tetramer staining intensity at time zero ((MFI at time (y)/MFI at zero) x 100) and the normalized MFI was graphed against time. The data were fitted to a one-phase exponential decay curve using Prism 7 analysis software (GraphPad) and the half-life was determined accordingly (64, 225).

2D micropipette adhesion frequency assay (2D-MP)

The relative 2D affinity of polyclonal IA^b GP_{66-77} specific cells was measured using the previously characterized 2-dimensional micropipette adhesion frequency assay (10, 41). In this 2D assessment, the frequency of adhesion between ligand (pMHC on human red blood cell (hRBC)) and receptor (TCR on T cell) carrying cells held on opposing micropipettes was observed using an inverted Zeiss microscope. The presence of adhesion was denoted by the interaction induced stretching of the highly flexible RBC membrane as the two cells were separated after an equilibrium contact time of two seconds. To serve as a surrogate APC, the RBC was first biotinylated (Biotin-x-NHS; Calbiochem) then incubated with streptavidin (ThermoFisher) followed by the addition of biotinylated pMHC monomers (IA^b GP_{66-77} or a control monomer (IA^b $hCLIP_{103-117}$, MTB IA^b $Ag85B_{280-294}$ and IA^b $ESAT\text{-}6_{1-19}$ and Influenza IA^b $NP_{311-325}$). T cell samples were prepared from splenocytes by $CD4+CD44^{hi}$ cell enrichment through CD4 T cell purification using EasySep mouse CD4 T cell negative selection kit (STEM CELL Technologies) and the simultaneous depletion of CD62L+ cells through the addition of biotinylated anti-CD62L antibody (MEL-14: eBioscience at 10ug/ml per $1x10^8$ cells) to the manufacturer recommended volume of the isolation cocktail. For 2D affinity measurements of tetramer-positive cells, CD4+CD62- enriched samples were stained with tetramer (described in tetramer avidity methods) and sorted on a FACSAriaII (BD Biosciences). To determine relative 2D affinity, 30 independent 2-second contacts were tested per T cell to generate an adhesion frequency value (Pa(2s)). Cells showing an adhesion frequency above 10% at the highest pMHC coating densities (>1000/μm^2) were considered antigen reactive (previously identified cutoff (10, 76)). Cells exhibiting 100%

adhesion were further resolved using lower pMHC densities until frequency values below 90% were obtained (79). The adhesion frequency was used to derive the relative 2D affinity of the cell with the following equation. $AcKa = -\ln(1-Pa(2s)) / m_r m_l$ where m_r and m_l represent receptor (TCR) and ligand (pMHC) density per area (μm^2), Pa(2s) is the adhesion frequency at the 2s equilibrium contact time, Ac is the contact area (kept constant) and AcKa is the 2D affinity (in μm^4) (67). TCR and pMHC density per cell were determined using Quantibrite PE quantification beads (BD Biosciences) per manufacturer instructions and staining of TCR with anti-mouse TCRβ PE antibody (H57-597; BD Biosciences) and MHC staining with anti-IA/IE antibody (M5/114/15/2; eBioscience) both at saturating concentrations. Calculations of molecules per area were done by dividing the number of TCR and pMHC per cell by the respective surface areas (hRBC 140 μm^2, T cell – during-assay measured diameter of an individual T cell and the surface area equation of a sphere) (41). A total of 70-400 cells were tested per sample with 20-70 binders/antigen-specific cells used to derive the geometric mean affinity for a given population.

Statistical analysis

Statistical significance of measured values was determined with Ordinary-One Way ANOVA, Turkey's multiple comparisons, Sidak's multiple comparisons, and two-tailed parametric Student's t-tests with ROUT outlier test (Q=1%) used to eliminate outliers all using the Prism 7 Software (GraphPad). Statistical significance indicated as ns = no significance, * $P > 0.05$, ** $P > 0.01$, *** $P > 0.001$, and **** $P > 0.0001$.

Results

Chronic antigen stimulation leads to T cell dysfunction but maintains tetramer-positive cells at a number comparable to the acute response

In the LCMV B6 model, the Armstrong virus causes an acute infection that lasts 8-10 days whereas CL13 persists 40-80 days in serum and spleen but remains in tissues like the brain and kidney (207, 208, 215). Chronic antigen exposure leads to CD4 T cell dysfunction early in CL13 infection and results in a faulty memory pool that is unable to mount a secondary response (167, 169). To compare and contrast how the duration of antigen exposure alters the frequency and number of IA^b restricted GP_{61-80} specific CD4 T cells, we assessed the T_H1 cytokine response and the overall prevalence of pMHCII tetramer-positive cells (i.e higher affinity cells) at time points that corresponded to prior and post viral antigen clearance. CL13 infection led to the increased and sustained expression of the inhibitory and recent antigen experience marker PD-1 on GP_{61-80} specific IFNγ producing T_H1 (Fig. 1A) and pMHCII tetramer-positive cells early in the infection (Fig. 1B). PD-1 expression was upregulated at the early effector (day 8 post-infection (d8)) and chronic stage (d35) of the CL13 response confirming continuous antigen exposure as compared to the acute infection. A marked decrease in PD-1 expression was noted at d120 indicating viral clearance from serum and spleen at this late time point (Fig. 1A, 1B). As is the hallmark of the chronic infection, the dysfunction in the T_H1 response was observed with a significant reduction in the frequency and number of IFNγ positive (Fig. 1C) and polyfunctional IFNγ, TNFα, and IL-2 co-producing CD4 T cells (Supplemental Fig. 1A-C) as compared to the more robust acute response (166, 169). However, the two responses had an equal prevalence of epitope-specific tetramer-

positive CD4 T cells at the later time points (d35 and d120) and only differed in the number of expanded effectors at d8 (Fig. 1D) (167, 169). Although this suggested the inhibitory environment in CL13 infection limited early CD4 T cell expansion, the decay in this population occurred relatively slower with a similar number of tetramer-positive T cells maintained between d8 and d35 and a significant contraction occurring at d120 with antigen clearance (Fig. 1D). In contrast, a continuous decline in tetramer-positive cells was observed as the acute response progressed from the expansion of peak d8 effectors to the formation and maintenance of early (d35) and late (d120) memory cells. Hence, more contraction and culling of antigen-specific cells occurred throughout memory long after clearance of viral antigen. The decay pattern in the T_H1 population (Fig. 1C) mirrored the observed decrease in tetramer-positive cell numbers (Fig. 1D) in both acute and chronic infection and confirmed previous observations of time-dependent memory CD4 T cell decline in acute infections (86, 179, 226). As pMHCII tetramers are partial to high-affinity cell detection, these data suggested high-affinity CD4 T cells are retained in the presence of antigen with chronic infection (185) and that their decline in the absence of antigen was not unique to chronic antigen stimulation but occurred in response to acute infection as well.

CD4 T cell affinity peaks at effector phase and declines equally with memory in acute and chronic infection

As low-affinity cells are expected to participate in the immune response and potentially dominate (78, 185) our observation of a decline in the high-affinity (tetramer-positive) antigen-specific CD4 T cell population in both acute and chronic infection alluded to a

possible decrease in the overall affinity of the response in the progression towards viral clearance. To evaluate if affinity declines in the total antigen-specific population, inclusive of tetramer-positive and negative CD4 T cells, we used the 2D-MP to measure single cell CD4 TCR affinity. In the 2D-MP assay, the adhesion between TCR and pMHC on micropipette anchored CD4 T cells and pMHC coated human red blood cells (hRBCs) was visually assessed using an inverted microscope (10, 41, 67, 79). Adhesion or binding was evidenced as the elongation of the flexible RBC membrane as the two cells were brought in contact and separated sequentially (Supplemental Fig. 2A). These adhesion or binding events along with the surface density of TCR and pMHC were used to generate a relative 2D affinity for individual T cells and the geometric mean affinity was used to compare different populations. To perform these measurements, we enriched for CD4+CD62L- T cells to maximize the frequency of antigen-experienced CD4+CD44^{hi} cells within the sample (Supplemental Fig. 2B). Determining the adhesion frequency to the IA^{b} GP$_{66-77}$ monomer as compared to a control none-LCMV monomer tested the LCMV specificity of individual T cells within each sample (Supplemental Fig. 2C). Using this method, high and low-affinity cells were detected in both the acute and chronic infection at all the time points tested with a >1000-fold affinities represented in each response. However, the peak TCR affinity of the polyclonal response occurred at d8 with both infections showing an increased prevalence of higher affinity CD4 T cells before a decline occurred in the transition to memory time points (Fig. 2A, B). Of interest, at both the d8 peak effector and d120 memory time points the acute (ARM Fig. 2A) and chronic (CL13 Fig. 2B) infections generated an antigen-specific population with equivalent average affinities (ARM;CL13 d8 - $1x10^{-4}$ μm^4; $2x10^{-4}$ μm^4 and d120 - $8x10^{-6}$

μm^4; $3x10^{-6}$ μm^4). While the Armstrong population affinity steadily declined to the d120 time point, the CL13 responders maintained the same high-affinity effector levels between d8 and d35 and only declined in the transition between d35 and d120 (Fig. 2C). Therefore, in the acute and chronic infections, the CD4 T cell population affinity was highest during the effector response with antigen presence maintaining a larger frequency of higher affinity T cells as observed with tetramer staining frequency and numbers. Viral clearance in both infections resulted in a lower affinity memory CD4 T cell population concurrent with a decline in tetramer-positive T cells.

Identification of virus-specific CD4 T cells by 2D-MP revealed a greater frequency of responding T cells than determined using pMHCII tetramer, as previously noted (10, 78). Employing an in vivo limiting dilution assay along with the Nur77GFP reporter mice with peptide antigen delivered in CFA, we had reported the number and affinity of naïve antigen-specific precursors inclusive of lower affinity T cells for several antigens (78). Lower affinity, tetramer-negative precursors were found to dominate the naïve population for all the tested epitopes including the LCMV epitope studied in this work. In the naïve repertoire, tetramer-negative IA^b GP_{66-77} specific lower affinity T cells outnumbered tetramer-positive high-affinity precursors by >3 fold and similarly dominated during Armstrong and CL13 infections reaching a seven-fold difference at d120 (Fig. 2D, E). To validate that tetramer preferentially stains higher affinity CD4 T cells, we sorted pMHCII tetramer-positive cells from d7 Armstrong infected mice to greater than 99% enrichment (Supplemental Fig. 2D) using fluorescence activated cell sorting (FACS) and measured their 2D affinity. Compared to the total antigen-specific CD4 T cell population, the sorted tetramer-positive T cells had a ten-fold higher affinity and demonstrated a narrowed

affinity range (Fig. 2F). Based on this and previous observations from LCMV and myelin oligodendrocyte glycoprotein (MOG) specific tetramer-positive cells (10), $1x10^{-4}$ μm^4 was used as the threshold 2D affinity cutoff for tetramer binding, with higher and lower affinity TCRs falling above and below this line, respectively. As the population affinity decreased below this threshold during memory (Fig. 2A-C), the increasing disparity between the antigen-specific cell frequencies detected by 2D-MP and tetramer largely occurred from pMHCII tetramer missing lower-affinity TCRs.

In a Friend virus protracted infection model, antigen presentation by activated B-cells was necessary for the expansion and over-representation of lower affinity T cell clonotypes and the decay in high-affinity T cells late in the infection (185). To determine if the affinity decline in the LCMV model can also be attributed to a B-cell role and thus abolished in an environment devoid of B-cells, we measured the 2D affinity of IA^b GP_{66-77} specific CD4 T cells in Armstrong infected B-cell deficient mice (Ighm -/-). Similar to the infection of wild-type (WT) B6 mice, Ighm-/- mice demonstrated a decrease in average TCR affinity between effector (d8) and memory (d85) T cells (Fig. 2G – trending significance $p = 0.0522$). 2D-MP identified more antigen-specific cells than pMHCII tetramer during both the effector and memory stages of the response with the transition from the d8 five-fold frequency difference to the twenty-four-fold change by d85 confirming the increased prevalence of low-affinity cells at the later time point (Figure 2h). The increased frequency of low-affinity cells at memory coupled with the drop in 2D affinity demonstrated the skewing to lower affinity cells can occur in the absence of B-cells. While this does not rule out a possible role for B-cells in the B6 model it suggested other mechanisms also contribute to the observed decay in affinity.

Tetramer avidity changes in chronic infection in the absence of TCR affinity differences

Overall, the skewing to lower affinity T cells in the acute response was in opposition to other findings of affinity maturation or selective enrichment of higher affinity cells at memory (56, 58, 92, 142). As these observations were made using pMHC tetramers as surrogate readouts for TCR affinity, we assessed tetramer avidity in the two infections for a comparison to these previous studies and our 2D affinity data. As measures of TCR affinity, 2D-MP and pMHCII tetramer avidity analysis require an accounting of TCR density and the total number of receptors per cell (29, 41, 140). Accordingly, we monitored TCR expression levels in acute and chronic infection with the TCR specific anti-TCRβ (clone H57-597) monoclonal antibody. As performed with our 2D-MP protocols we used quantification beads to determine the number of TCRs on $CD44^{hi}$ cells. CD4 T cells in chronic infection had a higher TCR expression at d35 whereas d8 and d120 numbers remained equivalent to Armstrong responders (Fig. 3A). A lack of TCR downregulation between d8 and d35 in CL13 infection contributed to this observed difference. Of note, TCR numbers decreased past antigen clearance time points within each infection indicating TCR downregulation can occur independently of antigen presence. This finding was analogous to a study that revealed TCR downregulation as a programmed event set early during antigen encounter but manifesting later in the response despite the absence of antigen (131). Although the contribution of the CD4 co-receptor was found to be minimal in binding to pMHCII (28, 29, 141, 227), we next assessed CD4 expression levels on $CD44^{hi}$ cells relative to the naïve population (Fig. 3B.) The difference was limited to d8 effectors with identical expression patterns observed

between acute and chronic infections at d35 and d120 (Fig. 3C). Flow cytometry analysis of forward scatter (FSC-A) was also used to assess T cell size and identify TCR and CD4 density differences. In both infections, activated T cells were larger at the peak of the response and reduced in size towards memory (Fig. 3D). CL13 specific cells at d8 were larger than their Armstrong counterparts while d35 and d120 cells were of equivalent size. Although in CL13 infection exhausted CD8 T cells were previously found to be smaller in size compared to late memory cells (168), CD4 T cell size at d120 was not significantly different between exhausted and memory cells despite showing a similar trend. The cell size data together with the TCR expression changes suggested potential TCR density differences between early and late time points in both the acute and chronic infection. While normalized in our 2D-MP measurements, these differences can affect tetramer avidity (29, 131).

To measure pMHCII tetramer avidity, we stained splenocytes with decreasing concentrations of IA^b GP_{66-77} tetramer and used IA^b $CLIP_{103-117}$ control tetramer to determine the frequency of cells with specific staining. The frequency at the highest tetramer concentration was defined as the maximal frequency (100%), the data normalized accordingly and fitted to a dose-response curve (Fig. 4A, C) for quantification of tetramer EC_{50} concentrations (Fig. 4B, D). Tetramer avidity remained unchanged between effector and memory cells in the Armstrong response (Fig. 4A, B) whereas, in contrast, avidity changes were noted in the chronic infection with d35 CD4 T cells showing increased tetramer avidity (Fig. 4C, D). A comparison of acute and chronic responders showed CD4 T cells in the CL13 response had significantly higher tetramer avidity at all the time points tested (Fig. 4E). Given that the TCR expression difference

across the two infections was only limited to d35, the d8 and d120 increased avidity in CL13 suggested a CD4 and TCR number independent effect thus we next assessed 2D affinity. For a fair comparison between 2D affinity and tetramer avidity, we excluded tetramer-negative T cells from our 2D-MP analysis using the tetramer binding threshold affinity ($1x10^{-4}$ μm^4) to group single cell measurements into high-affinity tetramer binders and tetramer-negative cells. In both acute and chronic infection, the average 2D affinity of antigen-specific cells falling above this threshold remained unchanged throughout each infection and across the two responses (Fig. 4F-G). In the Armstrong infection, this relative 2D affinity mimicked the observed static tetramer avidity, while in the CL13 response, tetramer avidity changes occurred despite the equivalent 2D affinities measured at each time point. The lack of TCR number and 2D affinity differences at d8 and d120 suggested the two responses generate a CD4 T cell population with comparable affinities while other affinity and TCR number independent factors influenced tetramer avidity (EC_{50}). CD4 co-receptor's role in binding pMHCII has previously been shown to be negligible (28, 29, 141, 227) and does not explain differences in avidity and affinity measurements identified here.

Tetramer half-life similar between memory and exhausted CD4 T cells

A direct correlation between TCR affinity and TCR:pMHC interaction half-life have previously been observed, where high-affinity T cells had a longer interaction duration with pMHC displaying antigen presenting cells (8, 108). To determine if pMHCII tetramer interaction half-life correlated to avidity or 2D affinity measurements, we next performed tetramer decay assays. After pMHCII staining of samples from acutely or

chronically infected mice, tetramer labeled cells were incubated with an anti-MHC II antibody that binds dissociated tetramer and prevents rebinding to TCR (56, 60, 131). The decay in tetramer staining intensity was measured over time and normalized to the signal detected at time 0. The data were fitted to a one-phase exponential decay non-linear regression and half-life determined accordingly (Fig. 5A, B) (64, 225). To avoid the inadvertent early skewing to a negative signal (MFI) that occurs with grouping tetramer-positive and negative polyclonal populations together, decay in tetramer staining intensity was measured for T cells falling in the tetramer-positive gate established using the control tetramer. To validate our analysis, we compared the frequency of tetramer-positive cells detected at every decay time point. The frequency of tetramer-positive cells detected at time 0 was similar to the frequency at all other time points during the assay, indicating the decay in tetramer MFI does not lead to a loss in detection of antigen-specific T cells (Supplemental Fig. 3A-C, data not shown). Using this analysis method, tetramer decay measurements in both the Armstrong and CL13 response showed a similar interaction half-life across all infection time points (Fig. 5A, B, Supplemental Fig.3D-E). Equivalent pMHCII tetramer half-lives were also noted between acute and chronic infection at all points of comparison (Fig. 5C) aligning half-life measurements with 2D affinity but not pMHCII tetramer avidity.

Exhausted CD4 T cells have a lower functional avidity compared to memory cells

Functional avidity is often used to infer the affinity of a polyclonal T cell response with a high functional avidity generally predicting the presence of TCRs with a greater affinity for pMHC (4). Furthermore, this ex-vivo testing of a virus-specific CD4 T cell

populations' ability to respond to decreasing doses of cognate antigen allows for a comparison of their sensitivity and potential to generate a functional response in-vivo (228). In this dose-response assay, the frequency of cytokine-producing CD4 T cells at each dose of cognate antigen was normalized to the frequency observed at the highest peptide concentration (100uM), and the data fitted to a nonlinear curve for deriving half-maximal effective concentration (EC_{50}) values. With acute infection (Fig. 6A), IFNγ producing GP_{61-80} specific CD4 T cells showed increased functional avidity in the transition from effectors to early memory cells but no further increase was observed at late memory, contrary to previous findings (86). A similar functional avidity increase was also detected in CD4 T cells responding to CL13 infection (Fig.6B). Despite this similar trend, the CD4 T cells in the acute infection had a significantly higher functional avidity compared to the chronic responders as seen with EC_{50} measurements of IFNγ (Fig. 6C). Within each infection, the antigen sensitivity seen with IFNγ producers was recapitulated with IL-2 (Fig. 6D) and TNFα (data not shown) producers. However, between acute and chronic responders, unlike the IFNγ avidity difference seen at all time points, IL-2 (Fig. 6D) and TNFα (data not shown) avidity equalized at the d120 time point. Collectively, the data demonstrated that virus-specific CD4 T cells increase sensitivity to antigen in response to acute and chronic infection, but initial activation conditions set the degree of sensitivity. Furthermore, this increased sensitivity can occur without an accompanying increase in 2D affinity or pMHCII tetramer avidity.

Discussion

In an infection setting, a T cell's potential for activation, expansion, cytokine production and survival as a memory cell is dependent on TCR affinity as well as other inflammatory environment incited selective pressures (60, 86, 172, 180). In this study, using the 2D-MP assay, we sought to further our understanding of how the antigen-specific CD4 T cell population's average TCR affinity changes under the pressures of acute and chronic infection in the well-studied LCMV model. In LCMV and other infections, CD4 T cells adept at controlling acute infections demonstrate robust cytokine production and form long-lived memory that protects the host against subsequent infections. However, in chronic infections as seen with the LCMV mouse model as well as the human pathogens HIV and HCV, continuous exposure to high antigen levels render CD4 T cells functionally exhausted and with altered T helper and memory differentiation outcomes (166, 167, 170, 205, 216, 229, 230). While the efficacy of the CD4 response in acute infections has previously been correlated with the enrichment of high-affinity/avidity T cells (56, 86, 142, 179), recent observations in retroviral infection models have demonstrated the chronic response to be enriched in lower affinity/avidity clones late in the infection (185, 221).

Our data highlight under acute and chronic infection CD4 T cell affinity diversity is equally maintained. Both responses expanded peak effector CD4 T cells of equivalent 2D affinities and the average affinity of the antigen-specific population similarly declined with antigen clearance. Although both high and low-affinity T cells expanded to infection and later contracted, the relative abundance of each population changed depending on the stage of the immune response. At the peak of the effector response and in the presence of antigen high-affinity cells were more prevalent (185) in both acute and chronic infection. However

with antigen clearance increased contraction of high-affinity T cells (tetramer-positive) (231) and a potential outgrowth of lower affinity (73, 185) clones gave way to a lower affinity T cell dominated memory population in both Armstrong and CL13 infection. As previously noted (10, 78), the 2D-MP detected more antigen-specific cells (2-7 fold higher) in both acute and chronic infection compared to pMHCII tetramer which selectively identified higher affinity cells. In evidence of this affinity bias, we found pMHCII tetramer-positive cells had a ten-fold higher average 2D affinity and spanned a narrower affinity range compared to the tetramer-positive and negative inclusive sample. As the CD4 T cell population affinity declined with memory, more antigen-specific cells were identified using 2D-MP than pMHCII tetramer. At the naïve precursor level, a similar skewing to lower affinity cells was previously observed for GP_{61-80} specific CD4 T cells which showed a 3:1 bias (78) before settling into the observed 7:1 ratio at memory. This would suggest the immune system maintains and resets the ratio of low to higher affinity T cells back to this similar pre-infection hierarchy that existed prior to infection.

Active mechanisms that promote affinity diversity and maintain lower affinity cells in the immune system have previously been proposed (92, 93, 185). In the CD4 T cell response to Friend virus protracted infection model, a similar decrease in affinity and enrichment for lower affinity cells was observed late in the infection (185). While showing this similar skewing to lower affinity cells occurred in the chronic LCMV CL13 model, we also observed this phenomenon was not unique to chronic infection as the acute response shared this progression from a peak affinity at effector time points before a decrease in overall affinity at memory. Of interest, the decline in overall T cell affinity was dependent on B-cell antigen presentation in the Friend virus infection model. In our 2D affinity

measurements of Armstrong infected B-cell deficient Ighm-/- mice a similar affinity decline between effector and memory cells suggested other T cell intrinsic and extrinsic factors regulated CD4 T cell population affinity. Of note, in a previous characterization of Armstrong infection in Ighm-/- mice, CD4 T cell memory numbers and cytokine production were found significantly reduced when compared to the WT response (182). While the poor secondary lymphoid architecture in Ighm-/- mice also contributed towards the deficit in CD4 memory, transient depletion of B-cells in WT mice identified a clear B-cell role in sustaining CD4 T cell memory numbers during the T cell contraction phase (183). These findings together with our observed affinity decline both in the presence and absence of B-cells suggest these cells maintain memory CD4 T cell numbers as a whole and likely without partiality towards higher or lower affinity clones in the LCMV model. Redirection of CD4 T helper differentiation and prevention of immune pathology in Friend virus infection was also dependent on B-cells unlike the LCMV chronic response (170, 230) hence confirming the potential role of other mechanisms in the enrichment of lower affinity cells in the LCMV model. However, further investigation is needed to identify said mechanisms and the contribution of B-cells towards this event without the confounding factors present in Ighm-/- mice. Of interest, the lack of affinity differences between acute and chronic LCMV infection suggested the shift towards a T_{FH} response in CL13 also occurred independently of a differential TCR affinity skewing. In agreement with our observations, the potential for differentiation into T_{FH} cells has been noted for high to low TCR affinity interactions with antigen dose playing a significant role in driving monoclonal T cells down a T_{FH} or alternative differentiation path (170-172).

The CD27/CD70 co-stimulatory pathway has previously been reported as a mechanism that ensures memory T cell survival and TCR affinity diversity through maintenance of lower affinity T cells in the antigen-specific repertoire (92, 93, 232). Characterization of co-stimulatory molecules on pMHCII tetramer-positive memory and exhausted T cells in the same LCMV models of acute and chronic infection has shown increased CD27 expression on exhausted CD4 T cells (169). Although we also noted CL13 specific early effectors had increased CD27 expression compared to Armstrong responders, tetramer-positive and total $CD44^{hi}$ cells did not sustain high CD27 expression levels in the progression to lower affinity memory time points (data not shown). Despite the early difference in CD27 expression, acute and chronic responders demonstrated identical 2D affinities in the high-affinity T cell population (tetramer-positive) at all time points tested. The total population also equally shifted to a lower affinity population at late memory making CD27 expression an unlikely mechanism leading to low-affinity T cell enrichment. However, direct approaches that abrogate CD27/CD70 interaction may further clarify if this pathway plays a role in the observed decline in CD4 T cell affinity.

Contrary to our 2D affinity observations, selection into the memory pool has previously been correlated with increased population affinity as measured by avidity for pMHCII tetramer, longer tetramer binding half-lives and a higher functional avidity (56, 86, 142, 179). Given the correlation between these measurements and monomeric TCR:pMHC affinity, memory is thought to enrich for higher affinity/avidity T cells resulting in T cell affinity maturation (58, 87, 137, 220). Our tetramer avidity measurements in acute and chronic infection revealed neither population enriched for higher avidity cells in the progression to memory time points. In fact, pMHCII tetramer avidity remained identical in

the transition from peak effectors to memory cells in the Armstrong infection while a higher avidity was measured at d35 in the CL13 response. However, TCR expression difference can be a confounding factor when comparing avidity within each infection. Between Armstrong and CL13 responders, the similar TCR expression in d8 and d120 samples allowed for a direct comparison of avidity with the data demonstrating increased avidity in the CL13 response. Our reanalysis of average 2D affinities for T cell populations falling above the $1x10^{-4}$ 2D affinity cutoff for tetramer binding showed affinity to be static in each high-affinity (tetramer-positive) response and equivalent between acute and chronic infection. This suggested TCR affinity independent mechanisms might be playing a role in the observed tetramer avidity differences. CD4 has no contribution toward binding pMHCII tetramer (28, 29, 227) and expression differences were limited to d8 samples thus co-receptor did not explain the increased avidity. Tetramer staining relies on the binding of multiple TCRs to the same pMHCII tetramer complex with one interaction increasing the likelihood of a second TCR:pMHC binding, hence the avidity (9, 64). T cell activation-induced changes in TCR clustering, membrane lipid raft organization and decreased membrane stiffness or enhanced fluidity can lead to altered tetramer binding capabilities at the T cell surface and could be factors different in the inflammatory environment with continuous antigen stimulation (63, 233, 234). Memory T cell population skewing based on increased pMHCII tetramer interaction half-life and in the absence of a tetramer avidity-based enrichment has previously been noted (60). In our comparisons, tetramer half-life measurements remained equivalent over the course of each response and between acute and chronic responders showing a correlation to 2D affinity measurements of the high-affinity CD4 T cell population.

As antigen-specific peak T_H1 effectors progressed down the differentiation path to early and late memory cells, a stepwise increase in functional avidity was noted in Armstrong infection (86, 179). Although functional avidity remained similar between early and late memory cells, our data also demonstrated a shift towards increased antigen sensitivity in the transition from peak effectors to early memory cells. The increased antigen sensitivity occurred in the absence of comparable 2D affinity, tetramer avidity, and half-life changes. Other studies of monoclonal and polyclonal responses have also reported a similar disassociation between TCR affinity and functional avidity (69, 86, 87). Under continuous antigen exposure, exhausted T_H1 cells also increased functional avidity as the immune response progressed towards antigen clearance but the degree of sensitivity was significantly reduced as compared to the robust IFNγ response in Armstrong infection. Antigen dose, the inflammatory environment and the upregulation of inhibitory receptors in the CL13 response can dampen T cell activation and functional responses (180, 228).

Overall, our 2D affinity findings highlight CD4 TCR affinity diversity in the antigen-specific polyclonal population is equally maintained under the pressures of acute and chronic infection with both systems expanding CD4 T cell populations of identical 2D affinities. High-affinity T cells dominated peak effector populations, whereas the increased prevalence of lower affinity cells coincided with antigen clearance. A correlation between functional and tetramer avidity measurements and 2D micropipette based affinity analysis was not consistent, confirming the influence of TCR affinity independent mechanisms on these assays. The dentification of parameters that predict and correlate with the efficacy of a CD4 T cell's response is critical in tailoring therapies and vaccines towards effectively combating acute and chronic infections. While our 2D TCR affinity, pMHCII tetramer

avidity, and half-life analysis did not differentiate CD4 memory cells from their exhausted counterparts, our data confirmed increased functional avidity better correlated to the T cell response difference between acute and chronic infection and the generation of functional memory. We now show in chronic infection, the immune response can maintain a population with an intact TCR affinity distribution that can be targeted by therapies that restore antigen sensitivity and boost CD4 T cell functionality. Future studies are required to identify immune mechanisms that are in place for maintaining this affinity diversity and to further elucidate the role of high and low-affinity cells within the immune response. Comparisons of as yet unmeasured TCR:pMHC kinetic and biophysical parameters can explain the response difference in the two infections and provide better correlates to protection and futures targets for immunotherapies.

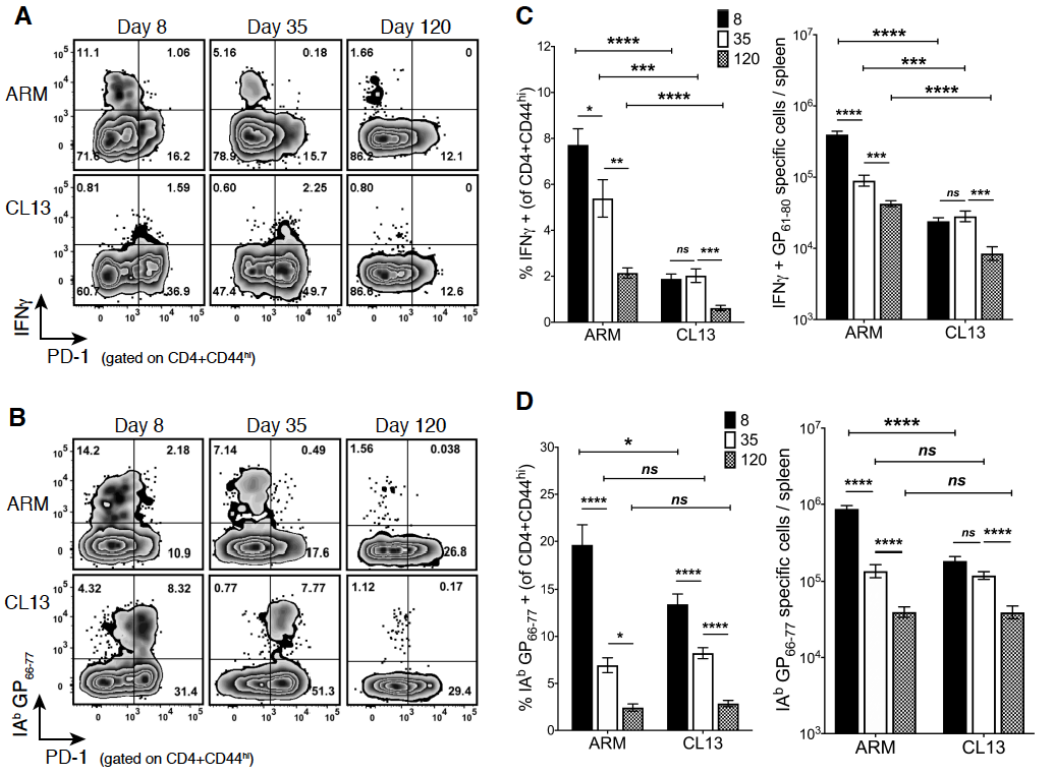

Figure 1. Chronic antigen stimulation leads to T cell dysfunction but maintains tetramer-positive cells at a number comparable to the acute response. (A) A representative flow plot with the frequency of IFNγ and PD-1 expressing cells in ARM and CL13 at the indicated days post infection (dpi) gated on CD4+CD44^{hi} splenocytes. **(B)** A representative flow plot with the frequency of IA^{b} GP$_{66-77}$ tetramer+ and PD-1 expressing cells under the conditions mentioned in (A). **(C)** Frequency (left) and log-transformed absolute numbers (right) of IFNγ producing cells at the time points and infections represented in the flow plot in (A). **(D)** Frequency (left) and log-transformed absolute numbers (right) of IA^{b} GP$_{66-77}$ tetramer+ T cells represented in (B). (C, D) Cumulative data with 3-5 independent experiments and a total n = 7-19 mice/group at n=2-5 mice/experiment/group. Bar graphs with Mean ± SEM. Statistical significance, ns

= no significance, * P > 0.05, ** P > 0.01, *** P > 0.001, **** P > 0.0001, Student t-test (ARM vs CL13), Ordinary one-way ANOVA Tukey's multiple comparison test (between dpi - individual infections).

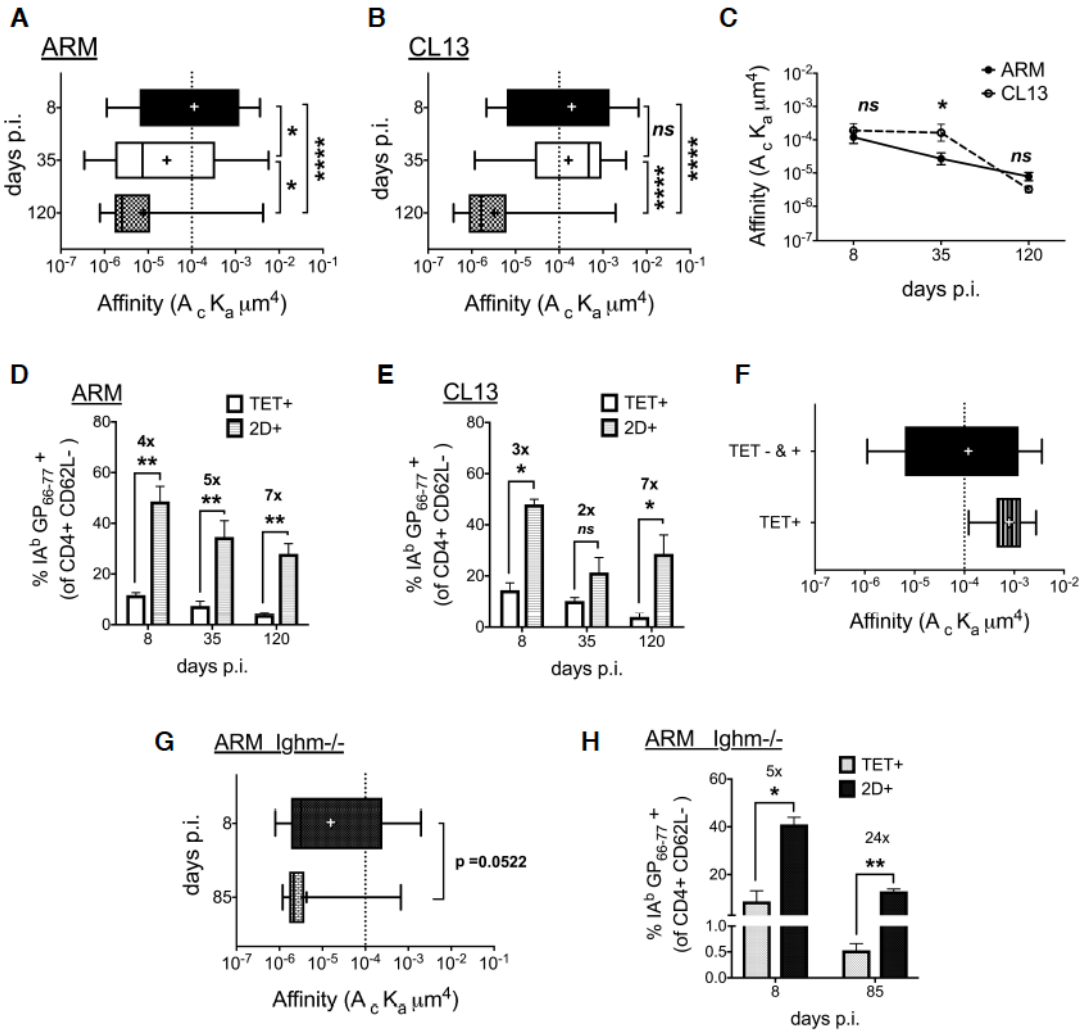

Figure 2. CD4 T cell affinity peaks at effector phase and declines equally with memory in acute and chronic infection. (A, B) 2D affinity of IA^b GP_{66-77} specific cells in CD4+CD62L- enriched samples from ARM **(A)** and CL13 **(B)** infected splenocytes and a comparison of the two infections **(C)** at the designated days. **(D, E)** A comparison of tetramer and 2D detected frequency of IA^b GP_{66-77} specific cells in above-mentioned samples from **(D)** ARM and **(E)** CL13. **(F)** 2D affinity of sorted tetramer+ and total (tet+ and tet-) CD4+CD62L- cells from d7 ARM infected splenocytes. **(G)** 2D affinity of IA^b GP_{66-77} specific CD4+CD62L- T cells from ARM infected B-cell deficient (Ighm-/-) mice at d8 and d85 dpi with p-value (0.0522). **(H)** Comparison of tetramer and 2D frequency

in samples from (G). All data representative of 2-3 independent experiments with splenocytes from 2-3 mice pooled pre-CD4+CD62L- enrichment per time point and per infection. Affinity data log-transformed with (+) sign depicting mean affinity in box and whisker graphs with min to max range of measured single cell affinities. Tetramer + high-affinity cell cutoff as a dotted line at 1×10^{-4}. Mean + SEM in bar graphs. Statistical significance, ns = no significance, * P > 0.05, ** P > 0.01, *** P > 0.001, **** P > 0.0001, (A, B) Ordinary one-way ANOVA Tukey's multiple comparison test, (C) Sidak's multiple comparison test, (D, E, G, H) Student t-test.

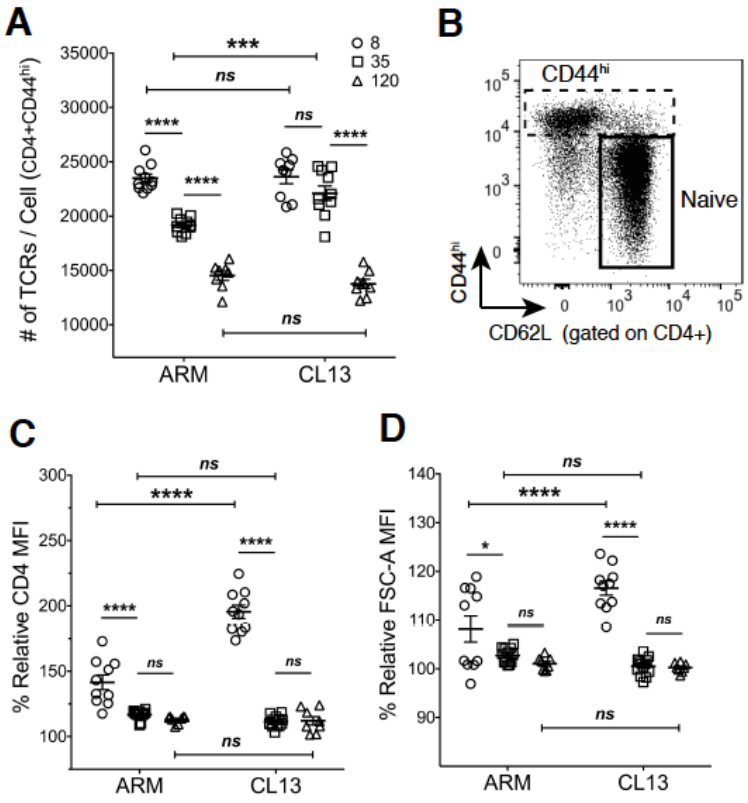

Figure 3. TCR expression higher in CL13 infection. (A) TCRβ per cell numbers for CD44^{hi} CD4 T cells from ARM and CL13 infected splenocytes at the designated days using PE quantification beads. **(B)** A representative flow plot showing the gating strategy for naïve (CD44^{lo}CD62L+) and antigen experienced (CD44^{hi}) cells from total CD4 T cells. **(C)** % CD4 MFI and **(D)** % FSC-A MFI of CD44^{hi} cells normalized to naïve MFIs. (A, C, D) Points representing individual mice (n=7-10 mice with n=2-5 mice/experiment/group). MFI of CD44^{hi} cells divided by MFI of naïve cells and multiplied by hundred to get % relative MFI. Mean ± SEM. Statistical significance, ns = no significance, ** P > 0.01, *** P > 0.001, **** P > 0.0001, Ordinary one-way ANOVA Tukey's multiple comparison test (between dpi - individual infections), Sidak's multiple comparison test (ARM vs CL13).

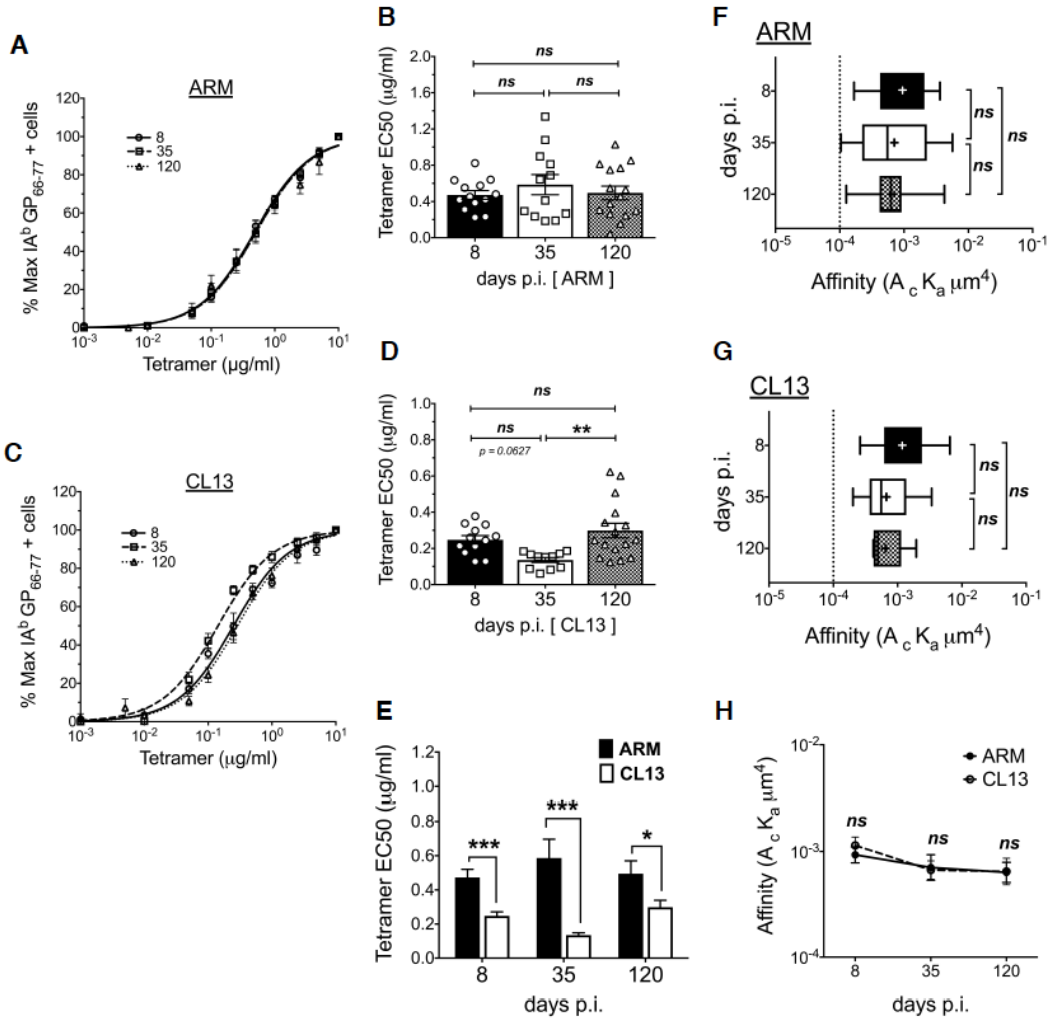

Figure 4. Tetramer avidity changes in chronic infection in the absence of TCR affinity differences. Tetramer avidity curves showing % maximum tetramer+ cells at the different tetramer concentrations used to stain splenocytes from **(A)** ARM and **(C)** CL13 infected mice at the different dpi. The frequency of tetramer+ cells at the different doses was divided by the frequency at the highest concentration (10ug/ml) to calculate % maximum tetramer binders. Curves fitted to a non-linear regression (normalized frequency x log concentration - dose response curve with a variable slope). EC_{50} tetramer concentrations obtained from the dose response curves for individual mice from **(B)** ARM and **(D)** CL13 infections. **(E)** Comparison of EC_{50} values between ARM and CL13

at the different dpi. 2D affinity of antigen-specific cells that fall above the tetramer staining affinity cutoff **(F)** ARM and **(G)** CL13 infection and **(H)** a comparison of the two responses. (A, C) Curves represent the Mean ± SEM of n = 12-16 mice. (B, D, E) Mean ± SEM in bar graphs with n=8-12 mice with each symbol representing individual mice. (F, G, H) pooled sample from 2-3 mice, affinity data log-transformed with (+) sign depicting mean affinity in box and whisker graphs with min to max range of measured single cell affinities. Tetramer + high-affinity cell cutoff as a dotted line at 1×10^{-4}. All data representative of 3-5 independent experiments at n=2-5 mice/experiment/group. Statistical significance, ns = no significance, * P > 0.05, ** P > 0.01, *** P > 0.001, **** P > 0.0001, (B, D, F, G) Ordinary one-way ANOVA Tukey's multiple comparison test (between dpi - individual infections), (E) Student t-test, (H) Sidak's multiple comparison test (ARM vs CL13).

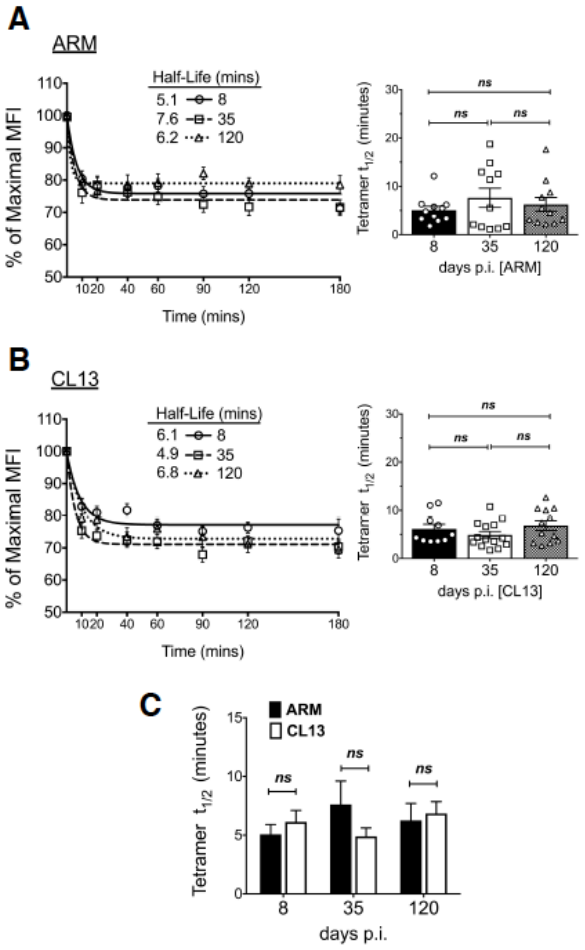

Figure 5. Tetramer half-life similar between memory and exhausted CD4 T cells. Tetramer decay curves (left) and bar graphs of half-lives (right) for CD4 T cells from **(A)** ARM and **(B)** CL13 infected splenocytes and **(C**) a comparison of the two shown for the different dpi. (A, B left) Tetramer MFI at decay time points was normalized to time 0 MFI and the % MFI fitted to a one-phase exponential decay curve. (A, B right) Half-lives derived from curves for individual mice in bar graphs with symbols representing each mouse. Mean ± SEM representative of n = 13-14 mice, 3-5 independent experiments at n=3-5 mice/experiment/group. Statistical significance, ns = no significance. (A, B) Ordinary one-way ANOVA Tukey's multiple comparison test (between dpi - individual infections), (C) Student t-test (ARM vs CL13).

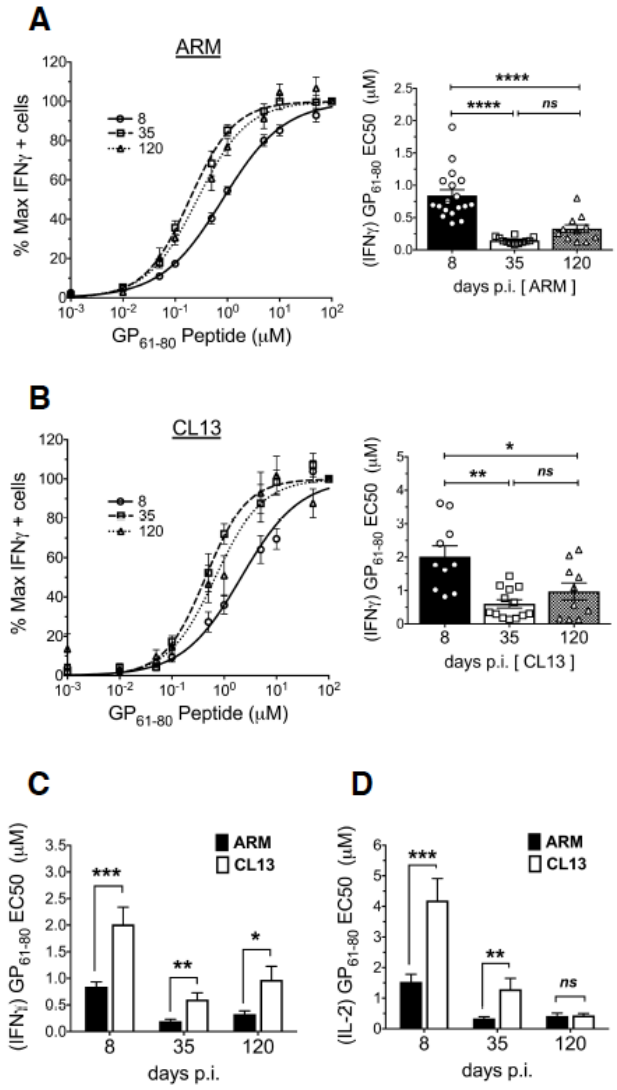

Figure 6. Exhausted CD4 T cells have a lower functional avidity compared to memory cells. Functional avidity dose response curves showing % of maximal IFNγ producers at the different doses of GP_{61-80} peptide used for ex-vivo stimulation of splenocytes from **(A,** left**)** ARM and **(B,** left**)** CL13 infected mice at the different dpi. The frequency of IFNγ producers at the different doses was divided by the frequency of producers at the highest peptide dose (100uM) to calculate % maximal producers. Curves fitted to a non-linear regression (normalized frequency x log concentration - dose

response curve with a variable slope). EC_{50} peptide concentrations derived from the dose response curves for individual mice represented in bar graphs with each symbol representing a mouse for **(A,** right**)** ARM and **(B,** right**)** CL13. **(C)** Comparison of IFNγ and **(D)** IL-2 EC_{50} values between ARM and CL13 at the different dpi. Mean ± SEM (A, B, C) representative of n = 9-18 mice and (D) n=7-10 mice. 3-5 independent experiments at n=2-5 mice/experiment/group. Statistical significance, ns = no significance, * P > 0.05, ** P > 0.01, *** P > 0.001, **** P > 0.0001, (A, B right) Ordinary one-way ANOVA Tukey's multiple comparison test (between dpi - individual infections), (C, D) Student t-test (ARM vs CL13).

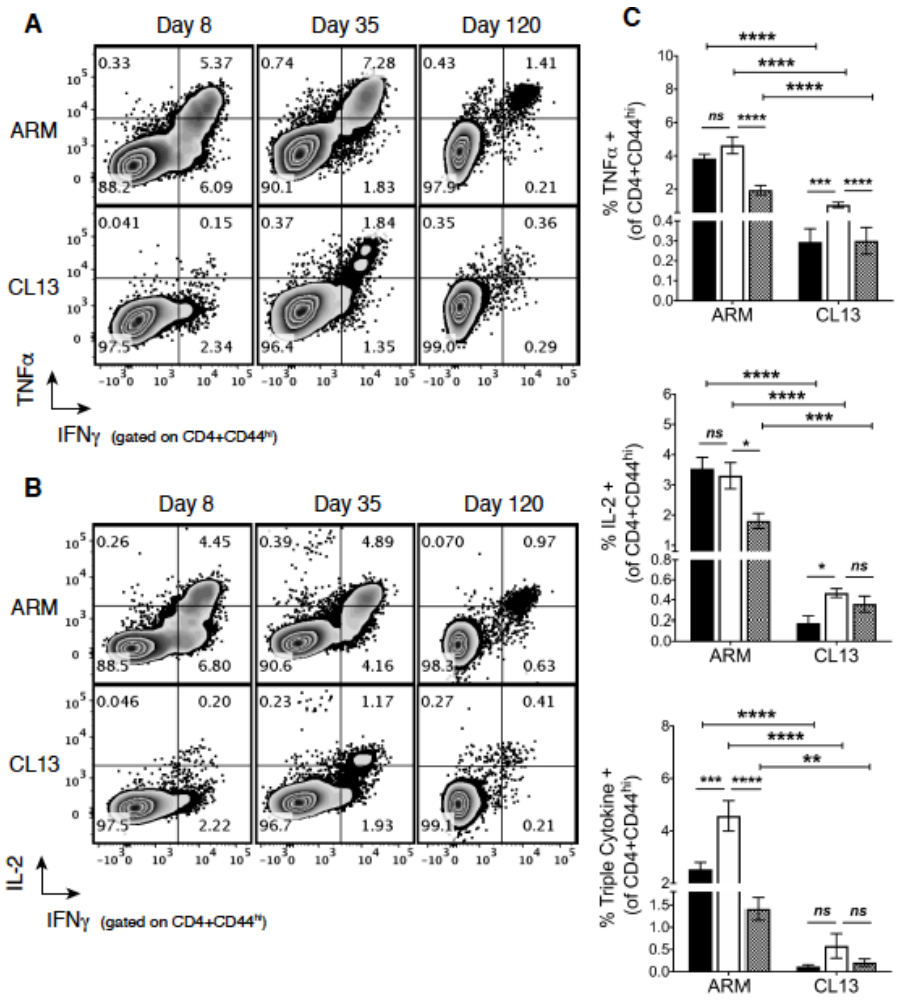

Supplemental Figure 1. Decreased polyfunctionality in chronic infection. Representative flow plots with the frequency of (A) IFNγ and TNFα (B) IFNγ and IL-2 co-expressing cells in ARM and CL13 at the indicated dpi gated on CD4+CD44hi splenocytes. (C) Frequency of TNFα (top), IL-2 (middle)and triple cytokine (bottom) producing cells at the time points and infections represented in the flow plots. Cumulative data with 3-5 independent experiments and a total n=6-17 mice/group at n=2-5 mice/experiment/group. Bar graphs with Mean ± SEM. Statistical significance, ns = no significance, * P > 0.05, ** P > 0.01, *** P > 0.001, **** P > 0.0001, Student t-test (ARM vs CL13), Ordinary one-way ANOVA Tukey's multiple comparison test (between dpi - individual infections).

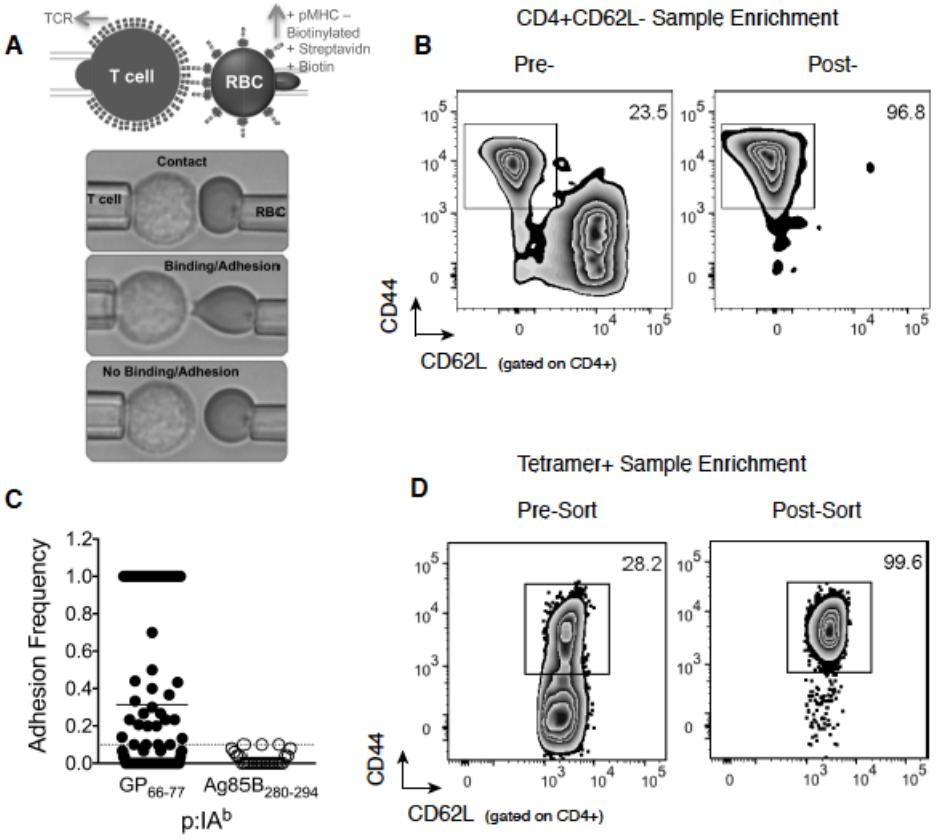

Supplemental Figure 2. 2D micropipette adhesion frequency assay and T cell sample enrichment. (A) Top, drawing of micropipette held T cell with surface TCR in contact with pMHC coated on human RBC through streptavidin – biotin interaction, and below, (first) a microscope bright-field image at 100x magnification showing the two cells held in contact, (second) a binding event when TCR is specific for the coated pMHC evidenced in the stretching of the RBC membrane as the T cell is retracted away from the RBC, (last) the lack of RBC shape change in the absence of specific binding between TCR and pMHC. (B) Representative flow plot of splenocyte enrichment for CD4+CD62L- cells with staining for CD44 and CD62L shown before and after enrichment (shown for day 8 ARM infection). (C) ARM d8 sample tested against the LCMV monomer IA^b GP_{66-77} and the

control non-LCMV monomer IA^b $Ag85B_{280-294}$ from MTB. Individual points represent a single CD4+CD62L- T cell with cells showing adhesion frequencies between 10-100% (0.1-1.0 y-axis) considered specific to the test antigen. (D) Representative flow plot showing IA^b GP_{66-77} tetramer staining of CD4+CD62L- enriched splenocytes from d7 ARM infection before and after sorting (FACS) on tetramer+ cells.

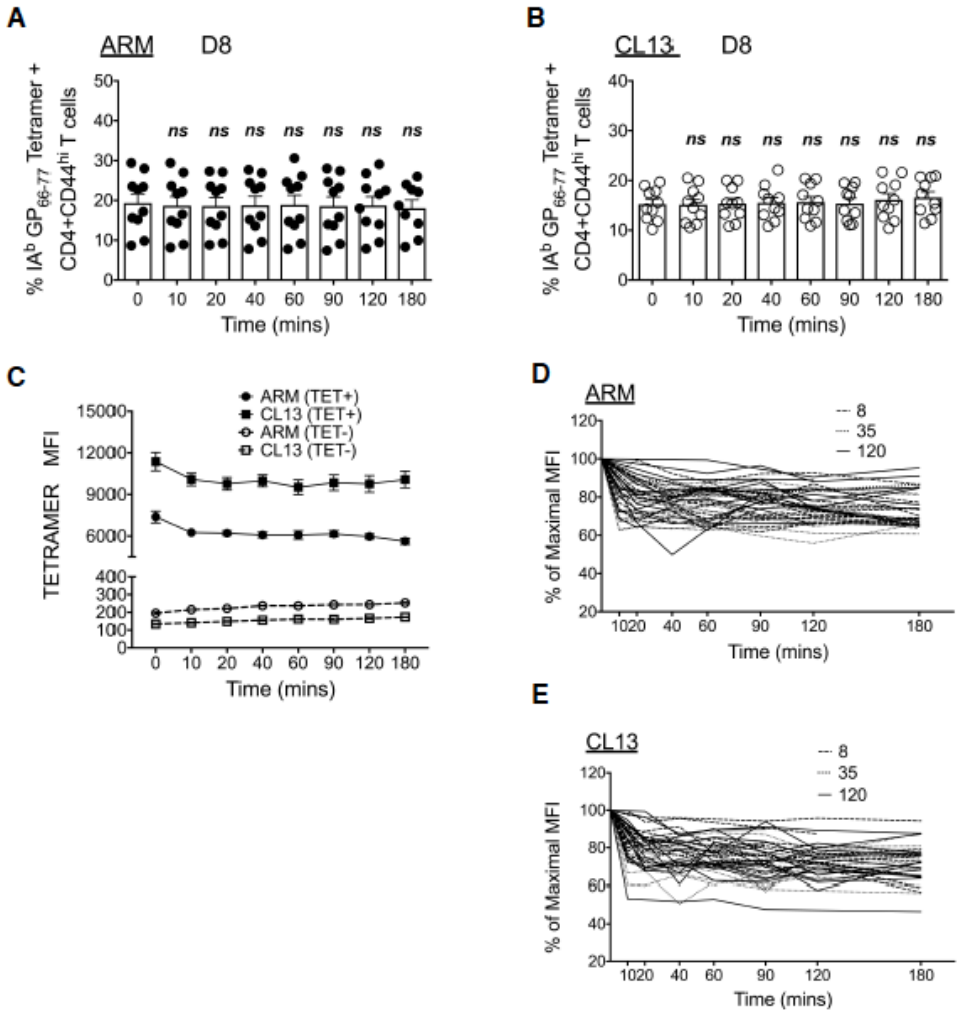

Supplemental Figure 3. Frequency of tetramer+ cells during tetramer decay assay remains unchanged. Frequency of tetramer+ cells at time 0 compared to other decay time points for (A) ARM and (B) CL13 d8 samples and (C) the associated decay in tetramer MFI for tetramer+/- cells in the samples. Data representative of one of three replicates. Tetramer MFI at designated time points was normalized to time 0 MFI and the % MFI plotted for individual mice at the different dpi with (D) ARM and (E) CL13 infection. Representative of n=13-14 mice, 3-5 independent experiments at n= 4-5 mice/experiment/group. Statistical significance, ns = no significance, Sidak's multiple comparison test (A, B).

Chapter 3. Activation induced decrease and recovery of TCR 2D affinity and bond lifetime

Rakieb Andargachew, Elizabeth M. Kolawole , Brian D. Evavold

Abstract

Shortly after encountering antigen, T cells are considered transiently unresponsive or refractory to subsequent simulation. To determine whether antigen stimulation also changes the cell surface biophysical interaction between TCR and pMHC, we assessed the 2D TCR affinity and bond lifetime under force between this receptor-ligand pair. Virus (LCMV) specific SMARTA transgenic CD4+ T cells were stimulated with peptide in vitro and 2D TCR affinity and bond lifetime determined at various time points after stimulation using the 2D micropipette adhesion frequency assay and the biomembrane force probe (BFP) respectively. We found activated T cells downregulated 2D affinity at twelve and twenty-four hours after seeing antigen with affinity recovering to naïve levels by forty-eight hours. Unlike pMHC tetramer staining which was dependent on TCR expression levels, the decrease in affinity was independent of antigen dose and degree of TCR downregulation. TCR:pMHC bond lifetime under force was also reduced early after antigen encounter with a steady recovery observed with time. Our data demonstrate a decrease in the bond lifetime and relative 2D affinity of TCR and pMHC result from early T cell activation events followed by a recovery phase with both changes occurring independently of activation-induced modulation of TCR expression. Thus, TCR affinity for pMHC is dynamic in the 2D T cell membrane context with cellular events allowing the T cell to fine-tune the ability of TCR to interact with antigen.

Introduction

T cells that encounter their cognate antigen travel through a series of events that culminate in cell surface and intracellular changes that fine-tune their functional characteristics. The dynamic event begins with TCR:pMHC binding at the cellular junction between a T cell and an APC preceded by engagement of adhesion mediators and followed by costimulatory receptor binding across the two cells (235). During the early priming phase, the quantity and quality of this interaction is transmitted from the cell surface to the intracellular components leading to signaling events, synapse formation, TCR downregulation, upregulation of T cell activation markers, the initiation of IL-2 production, and T cell proliferation within the first 24-48 hours of antigen experience (101, 106, 107). The T cells are unresponsive and refractory to further antigenic stimulation following these early activation events (131, 236-239). As shown in several of these in vitro studies, this refractory period is mainly associated with TCR downregulation with increased receptor internalization and possible changes in the immediate signaling components maintaining this transient state. It is unclear if these cellular changes are also reflected in the cell surface interaction between TCR and pMHC.

In the context of the T cell, TCR exists anchored to the cellular membrane, associated with the CD3-complex, the co-receptor, other membrane proteins within close proximity and the underlying cell cytoskeleton modulating cell stiffness and polarization (23, 235). Upon TCR:pMHC binding, several biophysical changes occur in this 2D context. One proposed model of TCR triggering indicates possible conformational changes in the TCR and CD3 which allow a physical transmission of this binding signal

to manifest in CD3 ITAM phosphorylation (37, 81, 109, 117, 120, 240). Associated intracellular changes lead to cell cytoskeleton mobilization that leads to the formation of a signaling scaffold allowing synapse formation, altering membrane fluidity and cell polarization (234, 235). The kinetic-segregation model attributes TCR triggering to the shuffling of the receptor away from the phosphatase activity of CD45 and its localization and clustering in lipid rafts enriched with the kinase activity of Lck (115). Further cellular changes that can affect the receptor activity can also occur with metabolic reprogramming, IL-2 signaling and the cell cycle changes that promote cell division (210, 241, 242).

Methods that allow 2D characterization of the TCR:pMHC interaction within the relevant membrane-associated environment have shifted our understanding of the binding kinetics for this receptor-ligand pair (42, 70-72). Such methods include the 2D-MP which measures 2D affinity and binding kinetics between TCR on a T cell and pMHC anchored on a human red blood cell (hRBC) (40, 67). A related method possessing a higher spatial and temporal resolution of binding kinetics and force measurements is the BFP which instead has pMHC coated on glass bead that is attached to a hRBC (72, 80). Previous in solution 3D SPR analysis of recombinant TCR and pMHC interaction contrasted with the 2D cell junction measured binding kinetics using these and other 2D methods which demonstrated the interaction as high-affinity and with faster on and off rates (39, 41, 42, 72). The 2D analysis incorporated the role of cytoskeletal and cell motility precipitated tensile force on bond lifetime and cell signaling, further identifying T cell mechanisms that allow discrimination of ligand quality by the TCR (72, 80-82, 124, 234, 240). Such 2D analysis methods have shown a better correlation between receptor binding

characteristics and the associated functional outcomes measured through cytokine production, proliferation or cytotoxic activity (39, 41, 42, 70, 72).

Such 2D methods have also identified possible TCR triggering related cellular changes that can alter 2D TCR:pMHC binding and reflect functional capabilities. For instance, T cell incubation with cholesterol depletion agents such as cholesterol oxidase and methyl-β-cyclodextrin which disrupt lipid raft integrity, result in reduced 2D TCR affinity (41, 42). Similarly, cytochalasin D and latrunculin treatments which inhibit actin depolymerization altering cell cytoskeleton also result in decreased 2D affinity and interaction kinetic rates (41, 42). Other observations of 2D affinity changes in TCR transgenic monoclonal T cells indicate cellular regulation of TCR:pMHC binding through these possible mechanisms (41, 70). In vitro activated OT-I T cells have for instance demonstrated a higher 2D affinity compared to naïve cells after 5 days in culture (41, 70). Similarly, an in vivo study has identified 2D affinity changes that correlated with specific tissue localization and T cell differentiation status (70). In this study, splenic red pulp residing P14 transgenic CD8 T cells specific for the LCMV glycoprotein (GP33) had a higher affinity than naïve cells and white pulp localized T cells. Effector T cells within the red pulp compartment contributed towards this increased 2D affinity which correlated with an increased cytotoxic capability and an accelerated viral clearance.

Given that the initial stages of T cell activation result in a refractory unresponsiveness state, we set out to determine if TCR:pMHC binding at the T cell surface also reflects this altered cellular status. Following a reductionist approach, we tracked 2D affinity and bond lifetime alterations in SMARTA TCR transgenic CD4 T cells specific to the LCMV GP_{66-77} epitope. 2D-MP affinity measurements of in vitro

peptide stimulated SMARTA revealed a significant decrease in 2D affinity between 12-24 hours post T cell activation. The reduction in affinity was independent of antigen dose and TCR downregulation. A similar decrease in the bond lifetime was observed within this time frame and recovery in 2D affinity and interaction lifetime occurred at 48 hours post-activation, coinciding with T cell proliferation and 2D affinity returning to naïve levels. These findings highlight TCR:pMHC 2D affinity and bond lifetime as dynamic events regulated by T cell activation and differentiation condition underscoring the necessity of evaluating this interaction in the natural 2D context.

Materials and Methods

Mice

C57BL/6 (B6) mice were purchased from the National Cancer Institute (NCI) and Charles River. Lymphocytic choriomeningitis virus GP_{61-80} (IA^b) specific TCR transgenic Thy1.1 SMARTA mice were bred in-house (243). All animals were housed at the Emory University Department of Animal Resources facility and all experiments were performed in accordance with the guidelines for the Care and Use of Laboratory animals under Emory University Institutional Animal Care and Use Committee approved protocols.

In vitro peptide stimulation

Splenocytes from naïve SMARTA mice were harvested, sorted on (FACS AriaII) or enriched for CD44lo CD62L+CD25- naïve CD4 T cells using the Stem Cell EasySep naïve CD4 T cell enrichment kit as per manufacturers' protocols. Cells were then labeled with cell trace violet (CTV) (Thermofisher Scientific) according to manufacturer's instructions at a more dilute labeling concentration of 1:10,000 (500 nM). As antigen presenting cells, splenocytes from B6 mice were first depleted of CD4 T cells using MACS CD4 T cell positive selection kit and plated with SMARTA T cells at a 1:5 ratio ($1x10^5$ SMARTA and $5x10^5$ CD4 depleted APCs) in a 24-well tissue culture plate. For dose-dependent activation conditions, 10^{-3}, 1, and 10μg/ml peptide and 1μg/ml anti-CD28 antibody (Clone 37.51, ThermoFisher) was used to stimulate cells. For time course experiments 1μg/ml peptide and 1μg/ml anti-CD28 antibody were used to activate the cells. GP_{61-80} peptide (GLKGPDIYKGVYQFKSVEFD) was synthesized on a Prelude Peptide Synthesizer (Protein Technologies)). Cells were cultured for different time points (16hrs or 12, 24, 48, 72 hours) at 37° C in T cell culture media and 5% CO2. T cell media contained RPMI 1640

(Mediatech), 10% heat-inactivated FBS (Hyclone), 10 mM HEPES buffer (Mediatech), 2mM L-glutamine (Mediatech), 50μM 2-mercaptoethanol (2ME) (Sigma), and 100μg/ml gentamicin (Mediatech).

TCR blocking, staining and quantification

TCR blocking on naïve SMARTA CD4 T cells which have a Vα2Vβ8.3 TCR (243) was performed using an anti-Vα2 APC antibody (Clone B20.1, eBioscience) at varying concentrations (0.008, 0.02 μg/ml). Naïve CD4 T cells were first enriched from splenocytes of transgenic SMARTA mice (EasySept CD4 negative selection kit, StemCell) and incubated with the blocking antibody at 37° C for 30 min in T cell media at a cell density of $5x10^5$ cells per 200 μl. Cells were washed and stained with surface antibodies for 30 minutes on ice in FACS staining buffer containing phosphate buffered saline (PBS) (Mediatech), 0.1% bovine serum albumin (BSA) (Fisher Scientific), and 0.05% sodium azide (Sigma). TCR expression (free/unblocked) was quantified using the anti-Vα2 PE antibody (Clone B20.1, eBioscience) and Quantibrite PE quantification beads (BD Biosciences). Surface staining was performed on ice for 30 minutes with anti-CD11b PerCP Cy5.5 (M1/70; BD), anti-CD11c PerCP Cy5.5 (HL3; BD), anti-CD19 PerCP Cy5.5 (ID3; BD), 7AAD (BD), anti-CD3ε FITC (145-2C11; BD), anti-CD4 BV500 (RM4-5; Biolegend), and anti-CD8 V450 (53-6.7; Biolegend) antibodies along with the anti-Vα2 PE antibody. Cells were washed and kept on ice until flow cytometry was carried out using an LSR II (Beckton Dickson). Using the FlowJo software (Tree Star), TCR MFI and Quantibrite PE quantification bead MFI were used per manufacturer instructions to determine the number of TCRs per cell.

Tetramer Staining

CD4 enriched samples post TCR blocking or in vitro activation were stained with 4 μg/ml PE (blocking experiment) or APC (activation experiment) conjugated control IA^b $hCLIP_{103-117}$ or IA^b GP_{66-77} tetramers acquired from the NIH Tetramer Core Facility at Emory University, Atlanta, GA. Labeling was done in T cell media at room temperature for 1 hour at a cell density of 1-2 $x10^5$ cells per 100 μl. Cells were washed with cold buffer and surface stained on ice for 30 minutes prior to sample acquisition on a FACSVerse or LSRII flow cytometer. Antibodies used for surface staining included anti-CD25 FITC, anti-CD28 PE, anti-CD11b PerCP Cy5.5 (M1/70; BD), anti-CD11c PerCP Cy5.5 (HL3; BD), anti-CD19 PerCP Cy5.5 (ID3; BD), 7AAD (BD), anti-CD3ε PE CF594 (145-2C11; BD), anti-PD-1 PE CY7 (29F.1A12; Biolegend), anti-CD44 AF700 (IM7; Biolegend), anti-CD62L APC Cy7 (MEL-14; BD), cell trace violet (ThermoFisher), anti-CD4 BV510 (RM4-5; Biolegend), anti-CD69 BV605 (H1.2F3; Biolegend), and anti-CD8 BV785 (53-6.7; Biolegend). Data analysis was performed using FlowJo software (Tree Star).

2D micropipette adhesion frequency assay (2D-MP)

The relative 2D affinity of naïve and activated SMARTA cells was measured using the previously characterized 2-dimensional micropipette adhesion frequency assay (10, 41). In this 2D assessment, the frequency of adhesion between ligand (pMHC on human red blood cell (hRBC)) and receptor (TCR on T cell) carrying cells held on opposing micropipettes was observed using an inverted Zeiss microscope. The presence of adhesion was denoted by the interaction induced stretching of the highly flexible RBC membrane as the two cells were separated after an equilibrium contact time of two

seconds. To serve as a surrogate APC, the RBC was first biotinylated (Biotin-x-NHS; Calbiochem) then incubated with streptavidin (ThermoFisher) followed by the addition of biotinylated pMHC monomers (IA^b GP_{66-77}). T cell samples were enriched for CD4 T cell cells using EasySep mouse CD4 T cell negative selection kit (STEM CELL Technologies) per manufacturer recommendations whereas sorting was done on a FACSAriaII (BD Biosciences). To determine relative 2D affinity, 30 independent 2 second contacts were tested per T cell to generate an adhesion frequency value (Pa(2s)). Cells exhibiting 100% adhesion were further resolved using lower pMHC densities until frequency values below 90% were obtained (79). The adhesion frequency was used to derive the relative 2D affinity of the cell with the following equation. $AcKa = -\ln(1-Pa(2s)) / m_r m_l$ where m_r and m_l represent receptor (TCR) and ligand (pMHC) density per area (μm^2), Pa(2s) is the adhesion frequency at the 2s equilibrium contact time, Ac is the contact area (kept constant) and AcKa is the 2D affinity (in μm^4) (67). TCR and pMHC density per cell were determined using Quantibrite PE quantification beads (BD Biosciences) per manufacturer instructions and staining of TCR with anti-mouse anti-Vα2 APC antibody (Clone B20.1, eBioscience) and MHC staining with anti-IA/IE antibody (M5/114/15/2; eBioscience) both at saturating concentrations. Calculations of molecules per area were done by dividing the number of TCR and pMHC per cell by the respective surface areas (hRBC 140 μm^2, T cell - during assay-measured diameter of an individual T cell and the surface area equation of a sphere) (41). A total of ~20-80 cells were tested per sample with geometric mean affinity used for comparison.

2D Biomembrane force probe (BFP): force clamp

Naïve and activated SMARTA TCR bond lifetime was measured using the previously characterized BFP force clamp assay (66, 72, 80). A variation on the 2D-MP assay, this assay evaluates single bond formation and dissociation events with and without applied force (55, 66). Low density pMHC coated beads attached to a hRBC membrane are used for antigen presentation. Thermal fluctuation, real-time imaging by a high-speed camera and image analysis software were used to track bead activity. These measurements were done with the force clamp assay where the T cell is clamped at a predetermined force until the bond ruptures (72, 80). Bond lifetime was measured as the clamp phase before bond rupture. Multiple bond lifetime measurments are obtained at different clamp forces to generate a force curve.

Statistical analysis

Statistical significance of measured values was determined with Ordinary-One Way ANOVA, Dunett's multiple comparison test, using the Prism 7 Software (GraphPad). Statistical significance indicated as ns = no significance, * $P > 0.05$, ** $P > 0.01$, *** $P > 0.001$, and **** $P > 0.0001$.

Results

T cell activation decreases 2D affinity independent of antigen dose and TCR downregulation.

Early T cell activation events introduce several cellular changes within the naïve CD4 T cell. Post in vitro activation, T cell synapse formation, receptor downregulation, upregulation of activation receptors and initiation of IL-2 production occur within the first 24 hours of antigen encounter (100, 101, 106, 107). Furthermore, TCR signaling and the extent of TCR downregulation and the ensuring functional response is dependent on the antigen dose (96, 100, 152). To determine how a combination of these activation conditions alter 2D affinity, we sorted CD4+CD44^{lo}CD25-CD69- naïve T cells from SMARTA transgenic mice and stimulated the cells in vitro with varying concentrations of GP_{61-80} peptide. CD4 depleted splenocytes (1:5 T cell:APC ratio) were used to present antigen and antibody ligation of CD28 was used for co-stimulation. At 16 hours post-antigen encounter, the frequency of cells expressing the activation markers CD69 and CD25 (IL-2Rα) increased in a dose-dependent manner indicative of the degree of signaling events occurring under the different conditions (Fig. 1A) (126, 236, 244, 245). 2D-MP measurements of T cell diameter confirmed T cell activation given all antigen doses led to an increase in cell size with high dose activation resulting in the largest measurement (Fig. 1B). The SMARTA TCR Vα2 specific antibody was used to quantify TCR downregulation, which followed a similar dose-dependent trend (Fig.1C) with TCR density per surface area varying accordingly (Fig. 1D). Therefore, as previously noted, a higher antigen dose (10μg/ml) led to increased TCR internalization (103, 237, 246). Although low dose (1ng/ml) activation maintained TCR levels that were equivalent to

naïve cells, the activation status of this sample was evident based on CD69 and CD25 expression as well as changes in cell size. Given the high sensitivity of T cells with as low as 1-25 pMHC leading to TCR signaling (111), it is interesting that the signaling required for TCR internalization is higher than what upregulates activation receptors. Previous observations of TCR reserves which work to maximize the effects of low dose antigen or low-affinity interactions indicate TCR downregulation or in this case, maintenance is tuned in response to antigen (247). The 2D-MP adhesion frequency of activated cells to the titrated concentration of pMHC on hRBCs demonstrated a difference between the naïve and activated cells (Fig. 1E). Taking into account TCR:pMHC densities and the resulting adhesion frequency, 2D affinity derivation demonstrated significant differences between naïve and activated cells (Fig. 1F). Of note, all activated samples had similar 2D affinities indicating the affinity change was independent of the activation dose used and the resulting differences in TCR internalization. This suggests the signal perceived with the low dose stimulation was sufficient to induce the decrease in 2D affinity.

In the absence of antigen stimulation 2D affinity unchanged by alterations in TCR levels.

Alterations in TCR expression have direct consequences for binding to pMHC tetramers and measured functional responses (29, 131, 141). To validate the observed decrease in 2D affinity is independent of the degree of TCR downregulation and specific to the activation status of the cells, we set out to determine the effect of TCR density changes in 2D affinity measurements of naïve cells. Naïve SMARTA T cells were incubated with

varying doses of the anti-Vα2 TCR antibody to block the number of TCRs that can interact with pMHC artificially varying the number of free receptors that can bind pMHC (248, 249). The same antibody conjugated to PE was used to quantify free receptors at the cell surface. Compared to untreated cells and CD4 T cells that lack Vα2 expression, the different concentrations of blocking antibody reduced the cell surface expression (Fig. 2A) and density (Fig. 2B) of free receptors to varying degrees. The higher concentration antibody treatment blocked >80% of the receptors with TCR density comparable to what was noted for the high dose peptide stimulation (Fig. 1D) while the lower antibody concentration blocked ~60% of the receptors. Tetramer staining of the different samples demonstrated a TCR density-dependent effect with >80% reduction in TCR numbers leading to a significant decrease in the frequency of tetramer-positive cells (Fig. 2C). However, the 2D affinity of antibody treated and untreated samples was equivalent indicating this assay is less sensitive to TCR density changes (Fig. 2D). Thus, the observed changes in 2D affinity upon T cell activation did not occur as a result of TCR downregulation in the high dose stimulation.

Recovery in 2D affinity coincides with cell division.

To determine how TCR:pMHC affinity changes over the early days of T cell activation, we measured 2D affinity over12 and 24-hour increments for the first 3 days. We activated the cells with the lowest dose that resulted in TCR downregulation (1μg/ml). As TCR upregulation is said to coincide with a return in functional responses, this dose allows for observations of TCR upregulation that might occur within this time-frame. 2D affinity was significantly reduced at 12 and 24 hours post activation with affinity

recovering to naïve levels at the 48-hour mark (Fig. 3A). Although some recovery in TCR cell surface expression occurs at this point (Fig. 3B), an accompanying increase in cell size (Fig. 1C) was also apparent. Thus, the combined effect maintained the initial reduction in TCR density observed at 12 hours post activation (Fig. 3D). This further confirms that 2D affinity changes can occur independently of fluctuations in surface TCR numbers. These data further confirmed the cellular mechanisms that modulate 2D affinity were not linked to signals that regulate TCR levels. Interestingly, tetramer staining of the different samples recovers in a similar manner although TCR density remains reduced and equivalent at all the activation time points (Fig. 3E). Although at the 12 and 24 hour time the observed decrease in tetramer staining could result from the synergistic effects of TCR downregulation and the mechanisms leading to 2D affinity reduction, the recovery in tetramer staining at the 48 and 72 hours likely results from the same events that return 2D affinity to naïve levels. These later time points mark ongoing cell division events as demonstrated by the cell trace violet dilution peaks (Fig. 3F). Hence with the start of cell division which in this case commences sometime between 24 and 48 hours, the associated cellular changes reinstate 2D affinity and for the most part tetramer avidity to naïve levels. Tetramer staining is affected by TCR numbers, cytoskeletal changes, and impaired endocytic pathways while minimal effects were seen with cholesterol depletion (250). Shared factors that affect 2D affinity, as well as tetramer staining, are actin polymerization inhibitors that alter cell cytoskeleton (latrunculin A, cytochalasin D) and cholesterol depletion agents (methyl-β-cyclodextrin and cholesterol oxidase) (41, 42). One or a combination of these factors could drive the observed decrease and recovery in 2D affinity.

TCR:pMHC bond lifetime under force reveals a similar decrease and recovery post antigen stimulation.

The BFP compared to the 2D-MP assay has capabilities that provide a high-resolution kinetic rate and interaction lifetime measurements at the level of single TCR:pMHC bond formation (72, 80). Making use of this sensitivity, we tracked bond lifetime changes with clamp force (Supplemental Fig. 1) under the same conditions that were during the 2D affinity analysis (Fig. 3). Increasing force measurements demonstrated an activation-dependent modulation of peak bond lifetime and the optimal forces that resulted in this longest interaction (Fig. 4A). Naïve SMARTA T cells displayed a typical catch bond formation exhibiting their longest lifetimes at the 10pN force, with the application of lower and higher forces leading to suboptimal lifetimes (80-82, 124). In comparison, the 12 and 24 hour time points demonstrated a reduction in bond lifetimes at all tested forces while recovery occurred at the 48 and 72 hours although the force that corresponded to the peak lifetimes was variable across the samples (Fig. 4A). A direct comparison of interaction times at 10pN force mimicked the observed 2D affinity changes albeit the lack of recovery at 48 hours and the reduced recovery at 72 hours which did not reach naïve levels (Fig. 4B). The 2D affinity changes for this latter phase was better represented in the 20pN force comparison which showed comparable lifetimes between naïve and activated cells (Fig. 2C). Of interest, previous characterization of cytoskeletal (latrunculin) and cholesterol (cholesterol oxidase) perturbations have demonstrated no effect on bond lifetime (71).

Discussion

Analyzing the interplay between TCR and pMHC using methods that mimic the natural interaction context is critical in identifying parameters that modulate T cell function. Here, we used the 2D-MP and BFP assays (39, 41, 42, 66, 190, 200) to measure the 2D affinity and bond lifetime of this receptor-ligand pair in the first few days after antigen encounter. Our findings revealed CD4 T cell activation in the first ~24 hours leads to a decrease in 2D affinity and bond lifetime with a recovery at ~48 hours coinciding with the start of cell division. Interestingly, these changes occurred independent of the antigen dose used for in vitro stimulation of SMARTA CD4 T cells and similarly, the associated TCR downregulation also had no role in the measured affinities and lifetimes. Although previous studies have identified the ability of monoclonal T cells to increase 2D affinity with parallel heightened functional responses (41, 70), our findings demonstrate the reverse can also occur with 2D affinity. This mechanism is possibly part of the "receptor desensitization" phase that allows T cells to undergo the initial rounds of activation-induced changes and the first cycles of T cell division before being receptive to further signaling events.

In the first 24-48 hours, a transient unresponsiveness is said to occur whereby T cell re-stimulation during this time results in diminished proliferation and cytokine production due to TCR downregulation (131, 236-239), Lck inactivity (251, 252) and high dose IL-2 exposure (253). Recovery occurs with the resetting of these mechanisms which transpire upon removal of antigen or TCR upregulation with time. Although our observed decrease in 2D affinity matches this time-frame, TCR affinity remained decreased and unchanged despite varying peptide concentrations and consequently the

degree of TCR downregulation. Furthermore, the recovery in 2D affinity which ensued in the absence of an increase in TCR density and the independence of 2D affinity on decreased TCR numbers all indicated the irrelevance of TCR downregulation on affinity changes. Previous analysis of Lck and its effects on 2D affinity have demonstrated blocking Lck activity had no effect on TCR:pMHC 2D binding affinity (30). CD8 role in the trimolecular interaction with TCR:pMHC was affected by Lck inhibition. However, given the minimal to undetectable contribution of CD4 to pMHC binding (28, 29), changes in Lck likely does not result in the measured SMARTA affinities. This suggested the decrease in affinity was likely precipitated by other cellular changes and not linked to previous observations of TCR desensitization mechanisms.

Known factors that alter 2D affinity have been observed with cholesterol-depleting agents that result in cell surface membrane composition changes (41, 70). Upon activation and in preparation for cell division, T cells synthesize cholesterol and several lipids (241) while shutting down cholesterol catabolism and fatty acid oxidation in favor of glycolysis (242, 254, 255). Furthermore, an increase in lipid rafts and TCR organization into microdomains is among the cell surface changes that also accompanies T cell activation (256). A combination of these effects generally enhances T cell activation and functional responses thus leading to increased TCR affinity (70). While these changes can explain how 2D affinity is restored at 48 hours, it is unclear what precipitates the decreased 2D affinity in these similar settings. Certain lipids are also associated with the cell cytoskeleton which has a role in synapse formation, cell polarization and motility (241). Inhibition of actin polymerization using agents like latrunculin also leads to a reduction in 2D affinity as previously noted (41). However, as

T cell activation leads to synapse and signaling scaffold formation inhibition of actin activity is not expected during the early events. Furthermore, comparison of 2D-MP and BFP analysis has demonstrated actin and cholesterol inhibitors affect 2D-MP analysis but not BFP lifetime measurements (71). As 2D affinity and bond lifetime exhibit a similar decrease and recovery with time, mechanisms controlling the observed changes likely affect both measurements. Cell membrane composition and cytoskeletal changes encompass and integrate multiple synthesis and regulatory pathways. A comparison of these events between samples at < 24 and > 48 hours after activation should further clarify existing synergistic effects or any contribution cytoskeletal and lipid composition have on 2D affinity and bond lifetime.

The above-mentioned possibilities account for changes in the cellular environment and their effect on TCR:pMHC interaction. However, transformations in the TCR and the associated CD3-complex trigger these early activation events. One such aspect is the role of TCR as a mechanosensor which transmits surface interaction quality to the intracellular environment via conformational/allosteric changes (81, 240, 257). Conformational changes in the AB loop of TCR Cα transmit this binding signal while as a secondary event (22, 116, 117), this same region leads to TCR clustering (118). The rigidness in the TCR:CD3 complex as a whole makes it amenable to transducing the force generated by TCR Cβ FG loop pushing on the CD3 complex as a result of TCR:pMHC binding (24, 25). On the cytoplasmic end, CD3ε and ζ chains which at steady state are thought to be associated with the acidic phospholipids of the plasma membrane inner leaflet become accessible upon ligand-induced TCR-CD3 conformational change (121, 122). Alterations in the acidic phosphatidylserine

concentration in the plasma membrane free the ITAMs for phosphorylation (123). Although transient, how these events are reset to pre-triggering conditions and their effect on subsequent antigen binding at later time points is unclear.

The decrease in 2D affinity and bond lifetime represents one interesting aspect of the data which can identify possible regulatory mechanisms that can be used to modulate the T cell response. However, another noteworthy characteristic of the TCR:pMHC interaction is the recovery that occurs not only for affinity and lifetime but also for tetramer staining which improves without any significant changes in TCR density. TCR clustering and lipid raft-associated changes can explain the increased binding to tetramer however as TCR numbers are expected to exert a dominant effect, re-examining tetramer binding parameters in these activation conditions can highlight another dimension of this interaction (61).

The ability of cells to tune their functional response has long been characterized in monoclonal as well as the polyclonal responses (87, 137, 179, 258). T cell signaling changes have accounted for these functional maturation events with the cell surface interaction between TCR and pMHC is thought to be invariable. With assays like the 2D-MP and BFP which can identify in situ changes, the dynamic nature and the resulting influence of TCR:pMHC interaction on functional outcomes is gaining increased recognition (70). Our work provides further evidence of cellular changes that fine-tune TCR:pMHC binding in-situ while an additional characterization of activation events and their effects on 2D affinity and bond lifetime will further delineate mechanisms that can be manipulated for future therapeutic purposes.

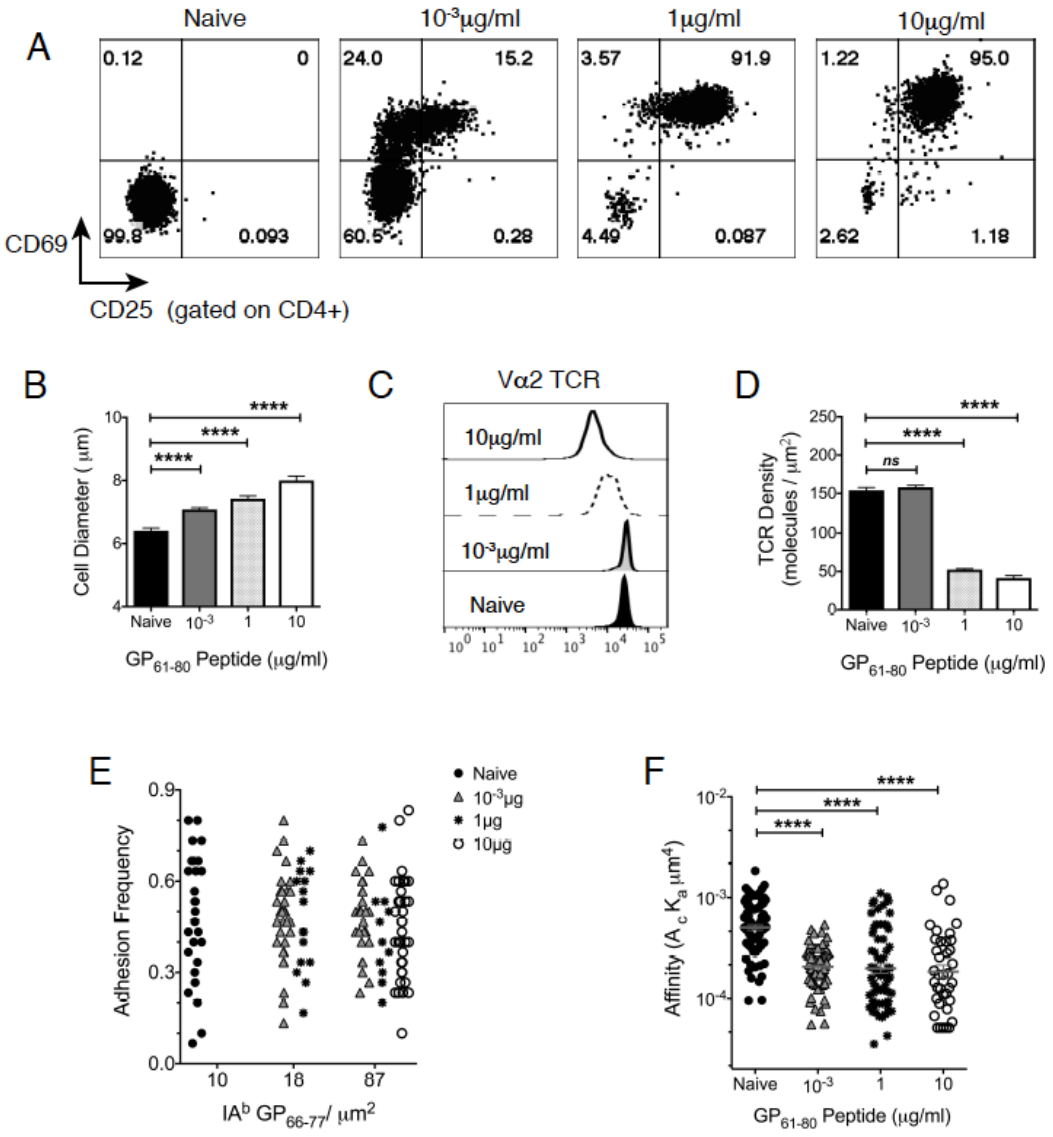

Figure 1. T cell activation decreases 2D affinity independent of antigen dose and TCR downregulation. (A) Representative flow plot showing CD69 and CD25 upregulation on and activated SMARTA CD4 T cells at 16hrs post in vitro peptide stimulation (varying concentrations (µg/ml)) with CD4 depleted splenocytes (1:5 ratio) in the presence of 1µg/ml anti-CD28 antibody. **(B)** Bar graph with Mean + SEM of single cell T cell diameter measurements of activated cells in (A) using 2D-MP microscope

imaging. **(C)** Representative histogram plot depicting TCR downregulation on activated cells in (A). **(D)** Bar graph with Mean + SEM of single cell TCR density measurements of activated cells in (A). TCR numbers per cell calculated using MFI from (B) and divided by single cell surface area derived from cell diameter in (C) to calculate density. **(E)** 2D-MP adhesion frequency plot showing SMARTA single cell adhesion frequency measurements at the designated pMHC densities. **(F)** 2D-affinity of naïve and activated SMARTA from (A). Data representative of 2-3 independent experiments, with cells pooled from 2-3 mice during naïve cell sorting. Mean + SEM representative of 38-84 single cell measurements. Statistical significance, ns = no significance, *** $P > 0.001$, (C, D, F) Ordinary one-way ANOVA Dunnett's multiple comparison.

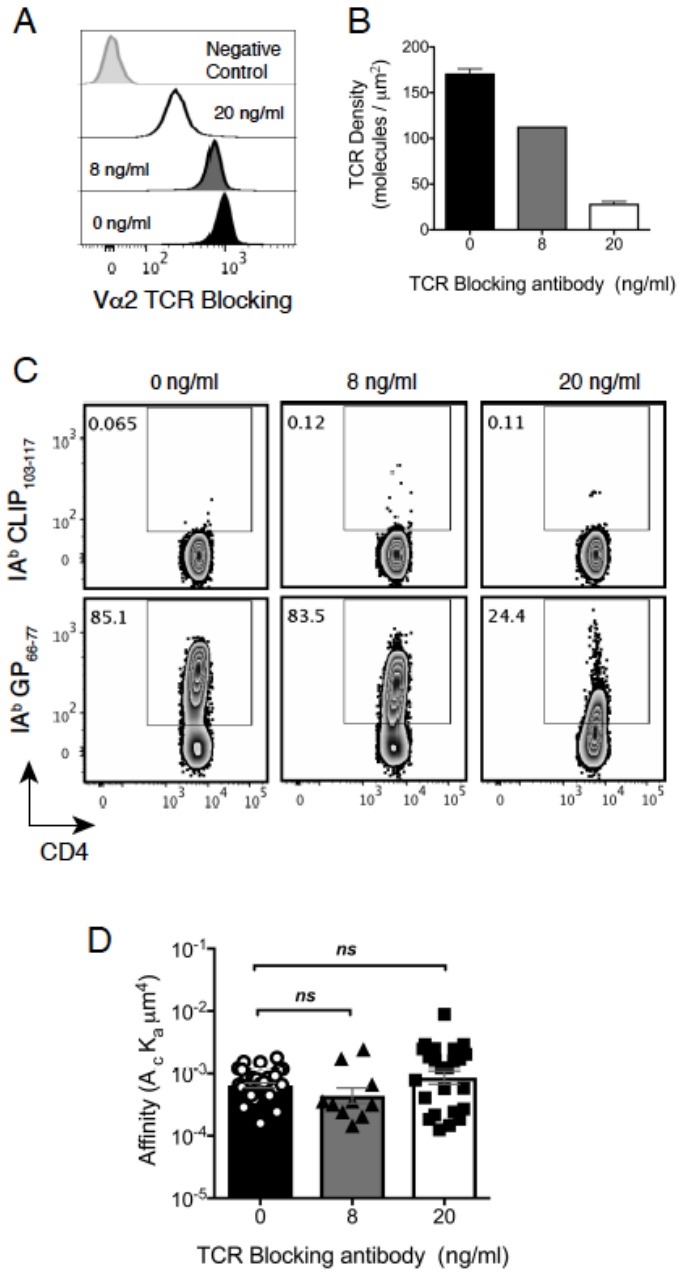

Figure 2. In the absence of antigen stimulation 2D affinity unchanged by alterations in TCR levels. Naïve SMARTA incubated with different concentrations of a blocking antibody targeting the SMARTA Vα2 chain. **(A)** A representative histogram with TCR staining post partial TCR blocking with different concentrations of the antibody. Staining of non- Vα2 cells shown a negative control. **(B)** Changes in the density of free TCR for

treated samples in (A). **(C)** A representative dot plot with tetramer staining of SMARTA T cells from (A-B). **(D)** 2D singe cell affinity of samples from A-C. Bar graph with Mean + SEM of single cell TCR density and affinity measurements post TCR blocking. Data representative of 15-38 single cell measurements, 2-3 mice and 2 independent experiments. Statistical significance, ns = no significance, Ordinary one-way ANOVA Dunnett's multiple comparison.

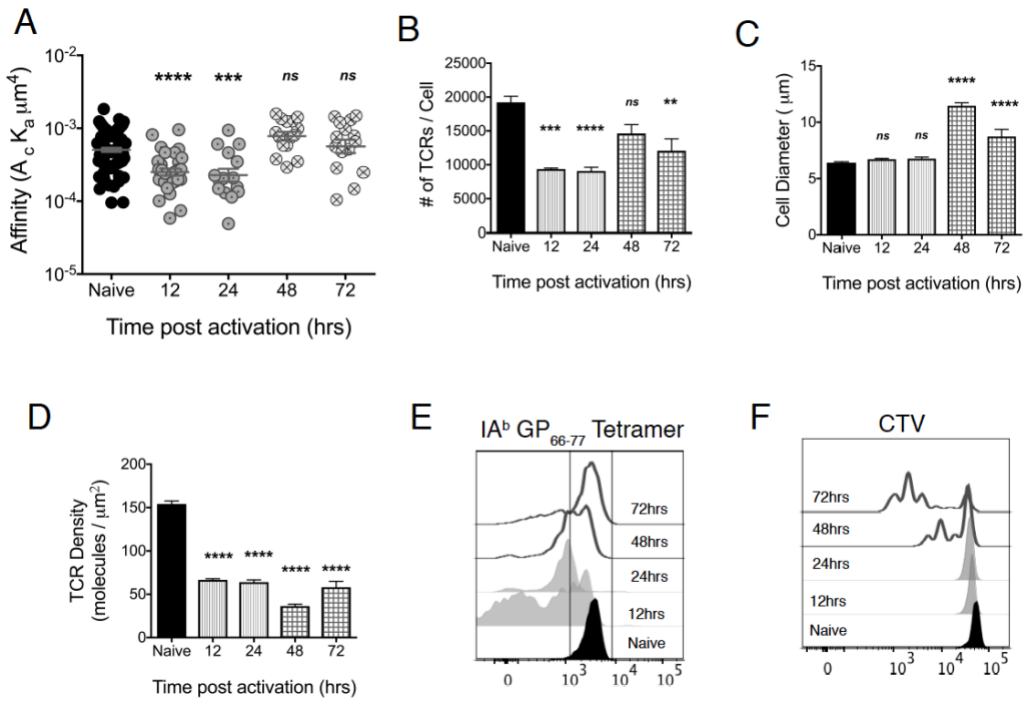

Figure 3. Recovery in 2D affinity coincides with cell division. (A) SMARTA activation time course with associated changes in 2D affinity. Cells activated with CD4 depleted splenocytes (1:5 ratio) in the presence of 1μg/ml GP_{61-80} peptide and 1μg/ml anti-CD28 antibody and affinity measured at different hours post activation. **(B)** TCR numbers per cell calculated for samples in (A) using quantification beads and TCR staining MFI. **(C)** T cell diameter measurements of activated cells in (A) using 2D-MP microscope imaging. **(D)** Bar graph with Mean + SEM of single cell TCR density measurements of activated cells in (A). **(E)** MHC II tetramer staining of activated cells. **(F)** SMARTA T cell proliferation at the different time points tracked using cell trace violet dilution. Mean + SEM representative of 15-84 single cell measurements. Statistical significance, ns = no significance, ** P > 0.01, *** P > 0.001, **** P > 0.0001, (A-C, F) Ordinary one-way ANOVA Dunnett's multiple comparison.

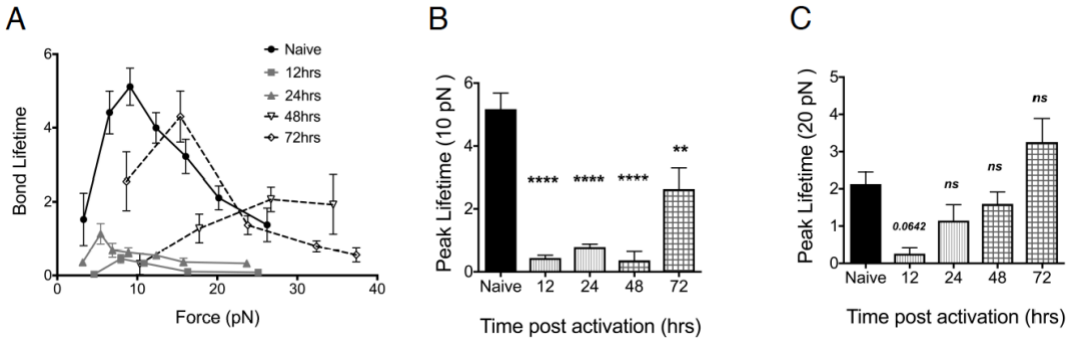

Figure 4. TCR:pMHC bond lifetime under force reveals a similar decrease and recovery post antigen stimulation. SMARTA activation time course with associated changes in 2D bond lifetime. **(A)** Curves depicting changes in bond lifetime with increasing force. A comparison of TCR:pMHC interaction lifetime at **(B)** 10pN and **(C)** 20pN force. Bar graphs with Mean + SEM (B, C) representative of a minimum of 30 independent lifetimes. Statistical significance, ns = no significance, ** P > 0.01, *** P > 0.001, **** P > 0.0001, (B, C) Ordinary one-way ANOVA Dunnett's multiple comparison.

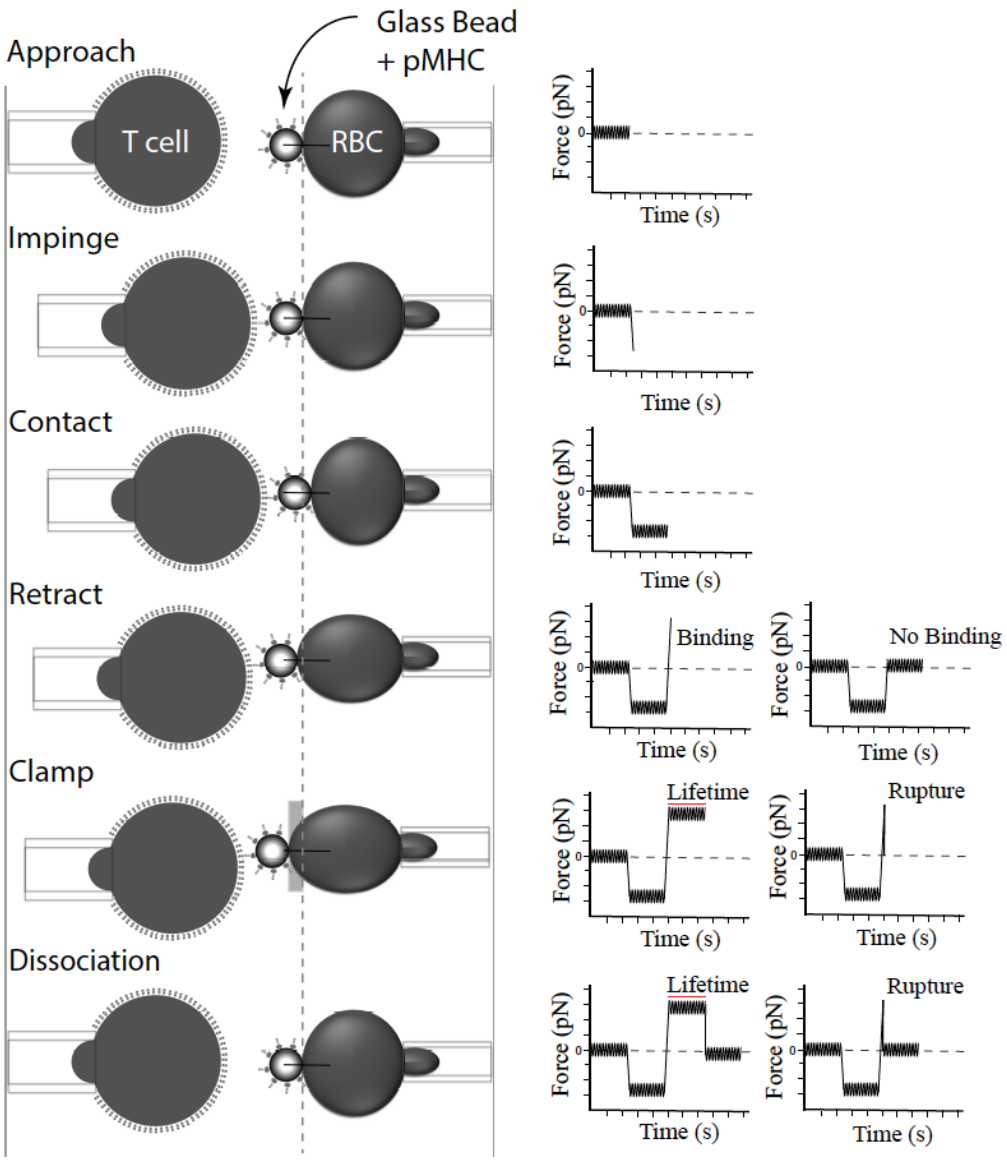

Supplemental Figure 1. The biomembrane force probe assay. The sequence of T cell and bead/RBC interaction (left) that can lead to the recording of bond formation, bond rupture or bond lifetime under force using software analysis of the bead position (through pixel/intensity of the line drawn across the bead and RBC border (black)) during the different events. Gray dotted line showing changes in the bead position during the multiple events (left).

Chapter 4: Discussion

As the gateway into the T cell response, TCR recognition of pMHC and the biophysical and kinetic interaction parameters that predict the collective set of characteristics that define an optimal T cell response have been the target of several decades of work. Multiple avenues of inquiry have culminated in the current outlook which highlights the need for assessing this interaction in situ with TCR on a T cell and pMHC two-dimensionally restricted to an opposing cell membrane (41, 42). The emerging views on TCR as a mechanosensor also underscore the need to evaluate TCR:pMHC binding in 2D and with force simulating conditions (72, 80-82, 234). However, radio-ligand binding assays (3D), SPR (3D), pMHC tetramer/oligomers (3D), and mechanical (2D-MP, BFP) or fluorescence-based (FRET) 2D methods have all been employed to study this interaction over the years with each assay having its strengths and weaknesses and applicability to monoclonal or polyclonal TCR studies. The consensus data from one or more of these assays predominantly identify affinity or half-life/off-rate as the parameters that best correlate to T cell function, memory formation and thus long-term survival (3, 41, 72).

The evaluation of TCR:pMHC affinity and half-life in the polyclonal response to infection have the potential to distinguish these parameters as predictors correlating to an efficacious CD4 T cell response. Of the currently available assays, 2D-MP is the one method that combines the ability to detect frequency, single cell 2D affinity/kinetic rates of varying ranges and can be used with polyclonal T cell samples (10, 41, 72, 75, 78). Previous 2D-MP measurements not only have demonstrated this sensitivity but also a correlation to T cell function (41, 72). These assets made 2D-MP the best candidate for re-examining the decades-old questions of what affinity ranges exist in the pathogen immune

repertoire, how it evolves through the distinct phases of the T cell response, what affinities correlate to sterilizing immunity/protection in acute and chronic infections. Combined with the 2D-MP, the LCMV acute and chronic infection model provided the best setting for making these comparisons.

In the context of current knowledge, our findings highlight and confirm several aspects of TCR affinity and its co-evolution with functional responses under acute and chronic antigen exposure. Based on the work by Martinez and authors, at the naïve state polyclonal LCMV GP_{66-77} specific CD4 T cells at the least start with a 1:3 high (tetramer+) to low (tetramer- (2D+)) affinity frequency bias at the population level (250) (model Fig.1A). As current methods do not allow isolation of both high and low-affinity cells in the naïve state, the single cell affinities represented in this precursor pool is unknown. Upon LCMV infection, both acute and chronic infection antigen-specific CD4 T cells expand and contract resulting in a similar frequency of high and low-affinity antigen-specific cells at peak (day8) (1:3-4 ratio) and post-antigen clearance (day120) (1:7 ratio). At early memory in Armstrong (day 35) (1:5 ratio) and the chronic stage in CL13 (1:2 ratio), low-affinity cell numbers differed between the two responses. The frequency data was reflected in the geometric average of all the measured single cell affinities of each population. Day 8 and day 120 average affinities were equivalent whereas day 35 exhausted cells had a higher affinity than their Armstrong memory counterparts. However, single cell affinity measurements showed a similar >1000-fold affinity range across all samples and time points.

One notable finding that is contrary to popular notion, but supported by other studies (259), is the lack of affinity maturation or high-affinity cell enrichment at memory.

Affinity peaks with the T cell response and contracts with memory. This trend is also true for chronic infection although the kinetics differ in parallel with the antigen load. Earlier observations with tetramer and functional avidity assays have indicated that memory and secondary challenge confers affinity maturation, enriching for high-affinity cells (56, 86, 142, 143, 179). Antigen confers the presence of a larger high-affinity cell population relative to naïve and memory (185). Based on monoclonal TCR studies, a spectrum of high to low-affinity interactions can expand to antigen, form memory and respond to re-challenge indicating the immune response accommodates multiple affinities (4, 52). However, expansion size differences indicate high-affinity interaction accumulates a larger number of cells and by this virtue, memory should be dominated by higher affinity cells. Unlike the polyclonal system where all affinity interactions are represented within the same host and multiple TCR species tracked, mechanisms that confer advantages to a lower affinity cell over a high-affinity clone may be missed in such monoclonal TCR models. Two reported mechanisms that work to ensure low-affinity representation are antigen presentation by B-cells (185) and co-stimulatory receptors such as the CD27-CD70 pathway (93, 143, 232). Our analysis of these two mechanisms did not show a clear correlation to low-affinity maintenance but further investigation is needed.

The idea of chronic infection maintaining a similar affinity diversity as an acute response is also one novel aspect of our findings. Although observations in the Friend virus model also suggested a similar antigen-dependent peak and decline in affinity, it was unclear if the phenomenon was specific to a protracted infection setting (185). The reduced functional avidity and frequency of polyfunctional T cells in the CL13 environment do not reflect the intact acute infection equivalent 2D affinity of the repertoire. Profiling of

antigen-specific (tetramer +) exhausted cells as compared to naive and memory cells has demonstrated under chronic conditions, CD4 T cells undergo genetic reprogramming with alterations to multiple pathways (168, 169). Some of these include cytokine production, inhibitory molecules, regulation of cell proliferation, apoptosis and metabolism. Assuming these observations also extend to tetramer-negative cells, these profiles indicate the immune response enforces functional regulation and creates similar transcriptional profiles in high and low-affinity cells formulating adaptability to the chronic environment. The emergence of more T_{FH} like cells (170) and the shift towards more IL-21 production (260) providing aid to humoral and CD8 T cell responses is one such aspect of this reprogramming. Despite the presence of antigen, the expansion and contraction kinetics that are similar to the acute environment also depict the regulation on cell cycle and proliferation which limits antigen-specific cell numbers (168, 169). The advantages of maintaining a diverse affinity repertoire have previously been highlighted with regards to providing protection against viral variants (93, 150). In the clinical setting, the programming of exhausted cells and their redirected functions still confer protection in HIV and HCV infections targeting viral variants. The absence of such cells leads to increased viremia indicating that these cells serve a purpose despite their exhausted phenotype (210). Our data confirm the immune response maintains TCR affinity diversity in a chronic infection similar to what exists during an acute response likely to provide protection against viral variants.

The emerging model from other previous findings and our observations here indicates an affinity independent recruitment of antigen-specific cells during infection. More specifically, high-affinity T cells do not have an advantage over the lower affinity

TCRs in the population. Based on the methods used to identify naïve precursors (tetramer and LDA isolated cells with their affinity measured using the 2D-MP) the starting population affinity for this epitope likely falls at or above the 2D-MP lower detection limit of 10^{-7} and the upper limit of 10^{-2} based on up-to-date measured affinities of tetramer-positive T cells (model Fig. 1A). Given the similar range observed in the expanded population in both the acute and chronic infection setting, it follows that all cells are recruited into the immune response regardless of affinity. However, it is unclear if precursors with affinities below this range are missing from these assessments due to the detection limit of the employed assays. Affinities that confer thymic positive selection fall within this detection range while self-antigens that provide tonic signaling for T cell homeostatic survival in the periphery have yet to be measured, but are also thought to be similar to the positive selecting ligands (2). Hence, as proposed in some studies an affinity threshold could exist (143) with T cells exhibiting 2D affinity of 10^{-7} and above possessing the ability to expand with antigen. Upon expansion, the initial hierarchy of the low-affinity dominated naïve population shifts to a high-affinity peak T cell response regardless of acute (model Fig. 1B) or chronic (model Fig. 1C) antigen exposure. However, the difference in two environments leads to differential regulation of overall cell numbers independent of affinity. This indicates the presence and absence of inhibitory receptors and other regulatory mechanisms does not alter TCR affinity distribution and solely works to limit other aspects of the T cell response. Hence, at the chronic stage, T cell numbers contract despite antigen being present (day 35) and interestingly antigen clearance leads to a similar affinity ending point for both responses (model Fig. 1D) returning the population to the similar low-affinity favored population observed in the naïve repertoire. This is achieved

either through the increased expansion of high-affinity T cells at the peak of the response followed by they increased contraction (226) relative to the low-affinity population which at the same time might exhibit decreased contraction or a favored late expansion (185). Our previous published and unpublished data with CD4 T cells in Friend virus infection (185) and CD8 T cell responses in Influenza X31 and LCMV infection (unpublished) demonstrate a similar decline in T cell affinity at memory highlighting this environment independent differential behavior of high and low-affinity T cells. This suggests potential T cell inherent and extrinsic regulation that modulates antigen-specific T cell frequency independently or in cooperation with TCR affinity.

Tetramer half-life measurements did not show a difference between the two populations confirming the population similarity identified with 2D-MP. Tetramer avidity analysis did not complement half-life nor 2D affinity measurements likely due to confounding factors related to T cell activation changes which included TCR downregulation, cell surface and cytoskeletal changes (41, 42). Interestingly, gene profiling has identified the latter two elements as potential points of differences between memory and exhausted cells (169). In both the acute and chronic infection, the overall or high only polyclonal affinity data did not reflect the functional avidity maturation observed in both responses and the increased functionality (EC_{50}) of memory cells over exhausted cells. As several mechanisms including changes in TCR signaling machinery and antigen dose have been implicated in manipulating functional avidity independent of TCR affinity our findings are in line with such observations (87, 89, 90, 179, 180, 228).

The lack of correlation between 2D affinity/tetramer half-life and T cell function in both infections suggested other TCR:pMHC interaction behaviors known to predict T cell

behavior might be at play. Although the overall immunosuppressive environment (inhibitory receptors, regulatory cells) could explain the dissociation between 2D affinity and T cell function in the chronic response, CD4 memory T cells in an Armstrong infection also show a similar lack of correlation between affinity and function. Although tetramer half-life has previously been correlated to T cell function for monoclonal T cells in this same model (60), our polyclonal data does not demonstrate this parameter as the selection factor that correlates with memory formation and increased functional avidity. The emerging views that demonstrate the TCR as a mechanosensor that discriminates ligands in a tensile force-dependent manner introduce the need to assess this interaction under such conditions (72, 80-82, 240). BFP analysis of bond lifetime under force is the next potential parameter that can differentiate acute and chronic infection responding T cells and better correlate to T cell function.

The average 2D affinities measured over the course of each LCMV infection reflects affinity changes at the population level but it is unclear if longitudinal tracking of the same TCR/monoclonal population would show variation. The stable affinity range observed across time points indicates T cell frequency changes and less likely altered single cell affinity lead to the measured decline in 2D affinity. The time point dependent increase in the 2D detected frequency over tetramer supports this observation. In monoclonal T cells that express a fixed TCR, 2D affinity increases have been reported (41, 70) indicating the activation status and anatomical location of the T cell can confer an enhanced recognition of cognate pMHC. SMARTA CD4 T cells (10K) transferred into B6 hosts that were later infected with Armstrong or CL13 showed a similar affinity when comparing peak effectors in the two infections and were also equivalent to their starting naïve 2D affinity

measurements (data not shown). This suggested 2D affinity was fixed in this model although a comparison of antigen clearance time points is needed for definitive conclusions. However, a 2D affinity decline was yet to be identified.

To characterize how activation alters 2D affinity and bond lifetime at the monoclonal/single TCR level, we tracked in vitro activated SMARTA transgenic T cells in the first few days of antigen encounter, a refractory time-frame in which TCR re-stimulation results in a diminished functional response. SMARTA 2D affinity and bond lifetime demonstrated a significant decrease at 12-24 hours post activation whereas 48-72 hours returned 2D affinity to naïve levels. Bond lifetime recovered with a similar trend although not to naïve levels. These changes were independent of TCR downregulation and peptide dose with recovery occurring with the onset of cell division. Previous observations have revealed alterations in cholesterol and actin polymerization as the cellular changes that affect 2D affinity (41, 42). Conversely, using the same inhibitors had no effect on bond lifetime measurements under force (71). The lack of agreement between these findings but the similarity in the decline and recovery trend in both measurements suggested the role of a novel contributor.

Upon TCR stimulation, T cells undergo several changes with notable modifications made to proximal and distal signaling modules (261) and more interestingly, the possible effects of TCR triggering which takes into account all the proposed models of TCR clustering, kinetic segregation, and conformational changes (109). Other modifications include the upregulation and downregulation of costimulatory and regulatory receptors, the changes in metabolic (123, 130, 242, 254) pathways, and alterations in protein and lipid synthesis (241). Combinations of these changes which alter T cell membrane, cytoskeleton

and TCR proximal proteins like the CD3 and Lck, can lead to changes in 2D affinity and bond lifetime. A systematic approach that identifies the cause of this decrease in TCR:pMHC should identify possible regulatory mechanisms that can be employed to alter the interaction as necessary towards beneficial outcomes.

Our findings both in the polyclonal and monoclonal study address questions regarding the fundamental nature of TCR:pMHC interaction and its influence on a T cell's biological response. Although affinity and bond lifetime can predict the functional behavior of T cells in general, context-dependent alterations within the T cell and extrinsic regulation that can alter this interaction can modulate T cell function. Further understanding of the singular and synergistic effects of intrinsic and extrinsic regulators and TCR:pMHC interaction will inform context dependent therapeutic avenues.

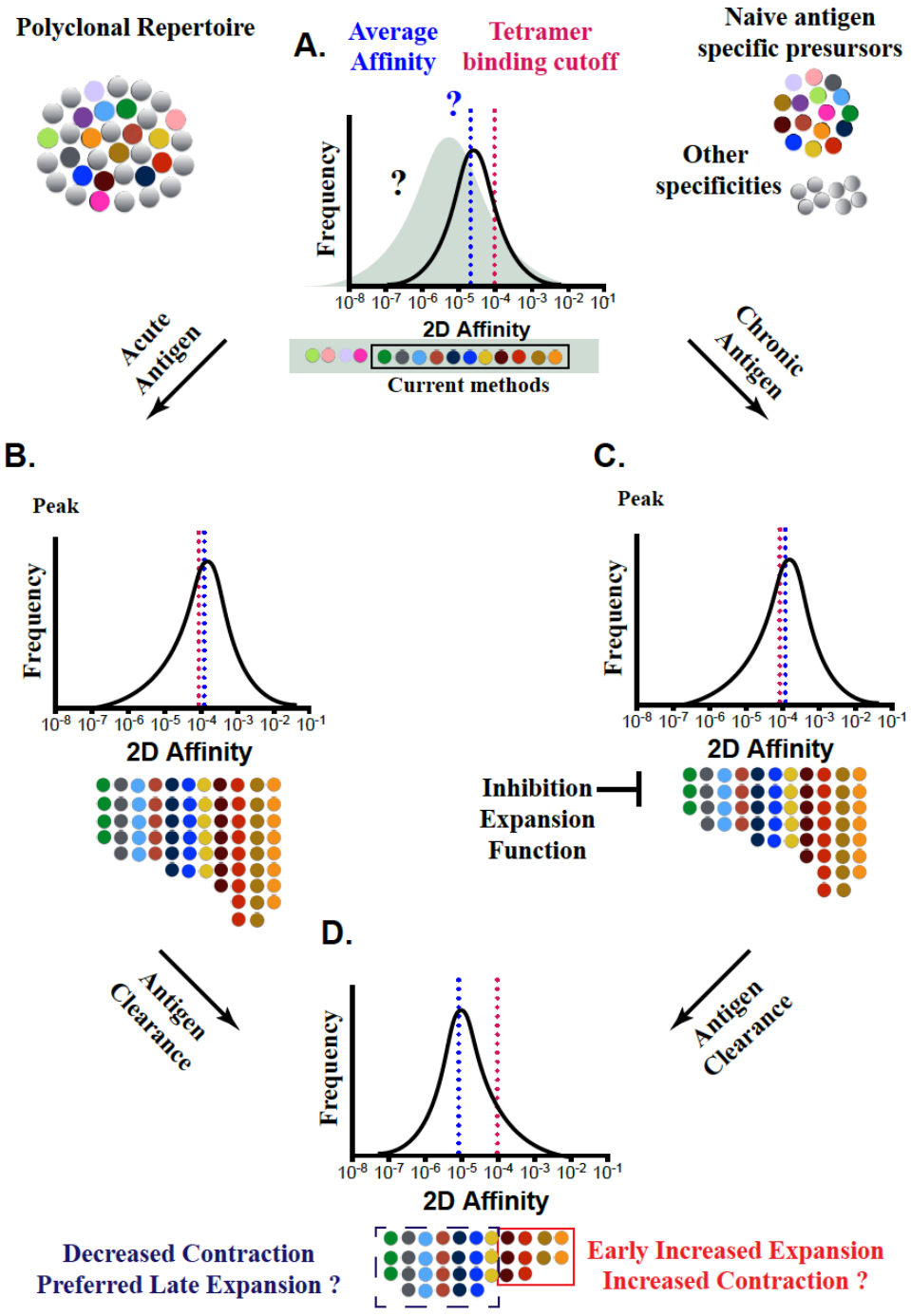

Figure 1. Polyclonal CD4 T cell 2D affinity evolution. **(A)** Estimated affinity distribution of naïve antigen precursor T cells detected by current methods (black histogram -Tetramer and LDA) and the possible method independent full repertoire (green shaded histogram). Relative frequency of high (tetramer+) and low (LDA+ tetramer-) affinity T cells separated

by the 2D affinity cutoff for tetramer binding (red line). Average population affinity (blue line) and distribution unknown. **(B)** Measured average 2D affinity of the antigen expanded population and observed frequency distribution of high and low-affinity cells at peak T cell response in acute and (**C)** chronic infection. Below, depiction of frequency/number indicated relative expansion of antigen-specific T cells, with expansion numbers limited in the inhibitory chronic stimulation environment. **(D)** A similar average affinity and distribution in acute and chronic infection after antigen clearance.

References

1. Davis, M. M., and P. J. Bjorkman. 1988. T-cell antigen receptor genes and T-cell recognition. *Nature* 334: 395-402.

2. Morris, G. P., and P. M. Allen. 2012. How the TCR balances sensitivity and specificity for the recognition of self and pathogens. *Nat. Immunol.* 13: 121-128.

3. Stone, J. D., A. S. Chervin, and D. M. Kranz. 2009. T-cell receptor binding affinities and kinetics: impact on T-cell activity and specificity. *Immunology* 126: 165-176.

4. Zehn, D., S. Y. Lee, and M. J. Bevan. 2009. Complete but curtailed T-cell response to very low-affinity antigen. *Nature* 458: 211-214.

5. Kersh, G. J., E. N. Kersh, D. H. Fremont, and P. M. Allen. 1998. High- and low-potency ligands with similar affinities for the TCR: the importance of kinetics in TCR signaling. *Immunity* 9: 817-826.

6. Alam, S. M., P. J. Travers, J. L. Wung, W. Nasholds, S. Redpath, S. C. Jameson, and N. R. Gascoigne. 1996. T-cell-receptor affinity and thymocyte positive selection. *Nature* 381: 616-620.

7. Holmberg, K., S. Mariathasan, T. Ohteki, P. S. Ohashi, and N. R. Gascoigne. 2003. TCR binding kinetics measured with MHC class I tetramers reveal a positive selecting peptide with relatively high affinity for TCR. *J. Immunol.* 171: 2427-2434.

8. Daniels, M. A., E. Teixeiro, J. Gill, B. Hausmann, D. Roubaty, K. Holmberg, G. Werlen, G. A. Holländer, N. R. Gascoigne, and E. Palmer. 2006. Thymic

selection threshold defined by compartmentalization of Ras/MAPK signalling. *Nature* 444: 724-729.

9. Altman, J. D., P. A. H. Moss, P. J. R. Goulder, D. H. Barouch, M. G. McHeyzer-Williams, J. I. Bell, A. J. McMichael, and M. M. Davis. 1996. Phenotypic Analysis of Antigen-Specific T Lymphocytes. *Science* 274: 94-96.

10. Sabatino, J. J., J. Huang, C. Zhu, and B. D. Evavold. 2011. High prevalence of low affinity peptide-MHC II tetramer-negative effectors during polyclonal CD4+ T cell responses. *J. Exp. Med.* 208: 81-90.

11. Kamphorst, A. O., and R. Ahmed. 2013. CD4 T-cell immunotherapy for chronic viral infections and cancer. *Immunotherapy* 5: 975-987.

12. Patel, S., B. R. Jones, D. F. Nixon, and C. M. Bollard. 2016. T-cell therapies for HIV: Preclinical successes and current clinical strategies. *Cytotherapy* 18: 931-942.

13. Schmitt, A., T. Tonn, D. H. Busch, G. U. Grigoleit, H. Einsele, M. Odendahl, L. Germeroth, M. Ringhoffer, S. Ringhoffer, M. Wiesneth, J. Greiner, D. Michel, T. Mertens, M. Rojewski, M. Marx, S. von Harsdorf, H. Döhner, E. Seifried, D. Bunjes, and M. Schmitt. 2011. Adoptive transfer and selective reconstitution of streptamer-selected cytomegalovirus-specific CD8+ T cells leads to virus clearance in patients after allogeneic peripheral blood stem cell transplantation. *Transfusion (Paris)* 51: 591-599.

14. Shi Zhong, K. M., Laura A. Johnson, Zhiya Yu, Eleazar Vega-Saenz de Miera, Farbod Darvishian, Katelyn McGary, Kevin Huang, Josh Boyer, Emily Corse, Yongzhao Shao, Steven A. Rosenberg, Nicholas P. Restifo, Iman Osman,

Michelle Krogsgaard. 2013. T-cell receptor affinity and avidity defines antitumor response and autoimmunity in T-cell immunotherapy. *Proceedings of the National Academy of Sciences* 110: 6973-6978.

15. Miles, J. J., D. C. Douek, and D. A. Price. 2011. Bias in the αβ T-cell repertoire: implications for disease pathogenesis and vaccination. *Immunol. Cell Biol.* 89: 375-387.

16. Davis, M. M. 1990. T Cell Receptor Gene Diversity and Selection. *Annu. Rev. Biochem.* 59: 475-496.

17. Garcia, C. K., M. Degano, R. L. Stanfield, A. Brunmark, M. R. Jackson, P. A. Peterson, L. Teyton, and I. A. Wilson. 1996. An αβ T Cell Receptor Structure at 2.5 Å and Its Orientation in the TCR-MHC Complex. *Science* 274: 209-219.

18. Garcia, C. K. 2012. Reconciling views on T cell receptor germline bias for MHC. *Trends Immunol.* 33: 429-436.

19. Feng, D., C. J. Bond, L. K. Ely, J. Maynard, and K. C. Garcia. 2007. Structural evidence for a germline-encoded T cell receptor-major histocompatibility complex interaction 'codon'. *Nat. Immunol.* 8: 975-983.

20. Marrack, P., K. Rubtsova, J. Scott-Browne, and J. W. Kappler. 2008. T cell receptor specificity for major histocompatibility complex proteins. *Curr. Opin. Immunol.* 20: 203-207.

21. Kersh, G. J., and P. M. Allen. 1996. Essential flexibility in the T-cell recognition of antigen. *Nature* 380: 495-498.

22. Rudolph, M. G., R. L. Stanfield, and I. A. Wilson. 2006. How TCRs bind MHCs, peptides, and coreceptors. *Annu. Rev. Immunol.* 24: 419-466.

23. Wang, J.-h. H., and E. L. Reinherz. 2012. The structural basis of αβ T-lineage immune recognition: TCR docking topologies, mechanotransduction, and co-receptor function. *Immunol. Rev.* 250: 102-119.

24. Kuhns, M. S., and H. B. Badgandi. 2012. Piecing together the family portrait of TCR-CD3 complexes. *Immunol. Rev.* 250: 120-143.

25. Sun, Z. Y. J., K. S. Kim, G. Wagner, and E. L. Reinherz. 2001. Mechanisms contributing to T cell receptor signaling and assembly revealed by the solution structure of an ectodomain fragment of the CD3εγ heterodimer. *Cell* 105: 913-923.

26. Call, M. E., J. R. Schnell, C. Xu, R. A. Lutz, J. J. Chou, and K. W. Wucherpfennig. 2006. The structure of the zetazeta transmembrane dimer reveals features essential for its assembly with the T cell receptor. *Cell* 127: 355-368.

27. Call, M. E., J. Pyrdol, M. Wiedmann, and K. W. Wucherpfennig. 2002. The organizing principle in the formation of the T cell receptor-CD3 complex. *Cell* 111: 967-979.

28. Xiong, Y., P. Kern, H. Chang, and E. Reinherz. 2001. T Cell Receptor Binding to a pMHCII Ligand Is Kinetically Distinct from and Independent of CD4. *J. Biol. Chem.* 276: 5659-5667.

29. Crawford, F., H. Kozono, J. White, P. Marrack, and J. Kappler. 1998. Detection of antigen-specific T cells with multivalent soluble class II MHC covalent peptide complexes. *Immunity* 8: 675-682.

30. Jiang, N., J. Huang, L. J. Edwards, B. Liu, Y. Zhang, C. D. Beal, B. D. Evavold, and C. Zhu. 2011. Two-stage cooperative T cell receptor-peptide major

histocompatibility complex-CD8 trimolecular interactions amplify antigen discrimination. *Immunity* 34: 13-23.

31. Kim, P. W., Z.-Y. J. Y. Sun, S. C. Blacklow, G. Wagner, and M. J. Eck. 2003. A zinc clasp structure tethers Lck to T cell coreceptors CD4 and CD8. *Science (New York, N.Y.)* 301: 1725-1728.

32. Van Laethem, F., S. D. Sarafova, J.-H. H. Park, X. Tai, L. Pobezinsky, T. I. Guinter, S. Adoro, A. Adams, S. O. Sharrow, L. Feigenbaum, and A. Singer. 2007. Deletion of CD4 and CD8 coreceptors permits generation of alphabetaT cells that recognize antigens independently of the MHC. *Immunity* 27: 735-750.

33. Van Laethem, F., A. N. Tikhonova, and A. Singer. 2012. MHC restriction is imposed on a diverse T cell receptor repertoire by CD4 and CD8 co-receptors during thymic selection. *Trends Immunol.* 33: 437-441.

34. Beringer, D. X., F. S. Kleijwegt, F. Wiede, A. R. Slik, K. Loh, J. Petersen, N. L. Dudek, G. Duinkerken, S. Laban, and A. Joosten. 2015. T cell receptor reversed polarity recognition of a self-antigen major histocompatibility complex. *Nat. Immunol.* 16: 1153.

35. Adams, J. J., S. Narayanan, B. Liu, M. E. Birnbaum, A. C. Kruse, N. A. Bowerman, W. Chen, A. M. Levin, J. M. Connolly, C. Zhu, D. M. Kranz, and K. C. Garcia. 2011. T cell receptor signaling is limited by docking geometry to peptide-major histocompatibility complex. *Immunity* 35: 681-693.

36. Krogsgaard, M., and M. M. Davis. 2005. How T cells 'see' antigen. *Nat. Immunol.* 6: 239-245.

37. Krogsgaard, M., N. Prado, E. J. Adams, X.-l. L. He, D.-C. C. Chow, D. B. Wilson, K. C. Garcia, and M. M. Davis. 2003. Evidence that structural rearrangements and/or flexibility during TCR binding can contribute to T cell activation. *Mol. Cell* 12: 1367-1378.

38. Kuhns, M. S., and M. M. Davis. 2012. TCR Signaling Emerges from the Sum of Many Parts. *Front. Immunol.* 3: 159.

39. Zhu, C., N. Jiang, J. Huang, V. I. Zarnitsyna, and B. D. Evavold. 2013. Insights from in situ analysis of TCR-pMHC recognition: response of an interaction network. *Immunol. Rev.* 251: 49-64.

40. Zhu, C. 2000. Kinetics and mechanics of cell adhesion. *J. Biomech.* 33: 23-33.

41. Huang, J., V. I. Zarnitsyna, B. Liu, L. J. Edwards, N. Jiang, B. D. Evavold, and C. Zhu. 2010. The kinetics of two-dimensional TCR and pMHC interactions determine T-cell responsiveness. *Nature* 464: 932-936.

42. Huppa, J. B., M. Axmann, M. A. Mörtelmaier, B. F. Lillemeier, E. W. Newell, M. Brameshuber, L. O. Klein, G. J. Schütz, and M. M. Davis. 2010. TCR-peptide-MHC interactions in situ show accelerated kinetics and increased affinity. *Nature* 463: 963-967.

43. Fägerstam, L. G., Å. Frostell, R. Karlsson, M. Kullman, A. Larsson, M. Malmqvist, and H. Butt. 1990. Detection of antigen—antibody interactions by surface plasmon resonance. Application to Epitope Mapping. *J. Mol. Recognit.* 3: 208-214.

44. Margulies, D. H., D. Plaksin, S. N. Khilko, and M. T. Jelonek. 1996. Studying interactions involving the T-cell antigen receptor by surface plasmon resonance. *Curr. Opin. Immunol.* 8: 262-270.

45. Malmqvist, M. 1993. Surface plasmon resonance for detection and measurement of antibody-antigen affinity and kinetics. *Curr. Opin. Immunol.* 5: 282-286.

46. Martinez, R. J., and B. D. Evavold. 2015. Lower affinity T cells are critical components and active participants of the immune response. *Front. Immunol.* 6: 468.

47. Matsui K, B. J., Steffner P, Reay PA, Davis MM. 1994. Kinetics of T-cell receptor binding to peptide/I-Ek complexes: correlation of the dissociation rate with T-cell responsiveness. *Proc. Natl. Acad. Sci. U. S. A.* 91: 12862-12866.

48. Corr, M., A. E. Slanetz, L. F. Boyd, M. T. Jelonek, S. Khilko, B. K. al-Ramadi, Y. S. Kim, S. E. Maher, A. L. Bothwell, and D. H. Margulies. 1994. T cell receptor-MHC class I peptide interactions: affinity, kinetics, and specificity. *Science* 265: 946-949.

49. Matsui, K., J. J. Boniface, P. A. Reay, H. Schild, F. B. de Groth, and M. M. Davis. 1991. Low affinity interaction of peptide-MHC complexes with T cell receptors. *Science* 254: 1788-1791.

50. Sykulev, Y., A. Brunmark, M. Jackson, R. J. Cohen, P. A. Peterson, and H. N. Eisen. 1994. Kinetics and affinity of reactions between an antigen-specific T cell receptor and peptide-MHC complexes. *Immunity* 1: 15-22.

51. Wassaf, D., G. Kuang, K. Kopacz, Q.-L. L. Wu, Q. Nguyen, M. Toews, J. Cosic, J. Jacques, S. Wiltshire, J. Lambert, C. C. Pazmany, S. Hogan, R. C. Ladner, A.

E. Nixon, and D. J. Sexton. 2006. High-throughput affinity ranking of antibodies using surface plasmon resonance microarrays. *Anal. Biochem.* 351: 241-253.

52. Corse, E., R. A. Gottschalk, M. Krogsgaard, and J. P. Allison. 2010. Attenuated T cell responses to a high-potency ligand in vivo. *PLoS Biol.* 8.

53. Alam, S. M., G. M. Davies, C. M. Lin, T. Zal, W. Nasholds, S. C. Jameson, K. A. Hogquist, N. R. Gascoigne, and P. J. Travers. 1999. Qualitative and quantitative differences in T cell receptor binding of agonist and antagonist ligands. *Immunity* 10: 227-237.

54. Boulter, J. M., N. Schmitz, A. K. Sewell, A. J. Godkin, M. F. Bachmann, and A. M. Gallimore. 2007. Potent T cell agonism mediated by a very rapid TCR/pMHC interaction. *Eur. J. Immunol.* 37: 798-806.

55. Zarnitsyna, V., and C. Zhu. 2012. T cell triggering: insights from 2D kinetics analysis of molecular interactions. *Phys. Biol.* 9: 45005.

56. Savage, P. A., J. J. Boniface, and M. M. Davis. 1999. A kinetic basis for T cell receptor repertoire selection during an immune response. *Immunity* 10: 485-492.

57. Davis, M. M., J. D. Altman, and E. W. Newell. 2011. Interrogating the repertoire: broadening the scope of peptide-MHC multimer analysis. *Nature reviews. Immunology* 11: 551-558.

58. Busch, D. H., and E. G. Pamer. 1999. T cell affinity maturation by selective expansion during infection. *J. Exp. Med.* 189: 701-710.

59. Nauerth, M., B. Weißbrich, R. Knall, T. Franz, G. Dössinger, J. Bet, P. J. Paszkiewicz, L. Pfeifer, M. Bunse, W. Uckert, R. Holtappels, D. Gillert-Marien, M. Neuenhahn, A. Krackhardt, M. J. Reddehase, S. R. Riddell, and D. H. Busch.

2013. TCR-ligand koff rate correlates with the protective capacity of antigen-specific CD8+ T cells for adoptive transfer. *Sci. Transl. Med.* 5: 192ra187.

60. Kim, C., T. Wilson, K. F. Fischer, and M. A. Williams. 2013. Sustained interactions between T cell receptors and antigens promote the differentiation of $CD4^+$ memory T cells. *Immunity* 39: 508-520.

61. Cameron, T. O., J. R. Cochran, B. Yassine-Diab, R. P. Sékaly, and L. J. Stern. 2001. Cutting edge: detection of antigen-specific CD4+ T cells by HLA-DR1 oligomers is dependent on the T cell activation state. *J. Immunol.* 166: 741-745.

62. Fahmy, T. M., J. G. Bieler, M. Edidin, and J. P. Schneck. 2001. Increased TCR avidity after T cell activation: a mechanism for sensing low-density antigen. *Immunity* 14: 135-143.

63. Drake, D. R., and T. J. Braciale. 2001. Cutting edge: lipid raft integrity affects the efficiency of MHC class I tetramer binding and cell surface TCR arrangement on CD8+ T cells. *J. Immunol.* 166: 7009-7013.

64. Stone, J. D., M. N. Artyomov, A. S. Chervin, A. K. Chakraborty, H. N. Eisen, and D. M. Kranz. 2011. Interaction of streptavidin-based peptide-MHC oligomers (tetramers) with cell-surface TCRs. *J. Immunol.* 187: 6281-6290.

65. Derby, M. A., J. Wang, D. H. Margulies, and J. A. Berzofsky. 2001. Two intermediate-avidity cytotoxic T lymphocyte clones with a disparity between functional avidity and MHC tetramer staining. *Int. Immunol.* 13: 817-824.

66. Chen, W., V. I. Zarnitsyna, K. K. Sarangapani, J. Huang, and C. Zhu. 2008. Measuring Receptor-Ligand Binding Kinetics on Cell Surfaces: From Adhesion Frequency to Thermal Fluctuation Methods. *Cell. Mol. Bioeng.* 1: 276-288.

67. Chesla, S. E., P. Selvaraj, and C. Zhu. 1998. Measuring two-dimensional receptor-ligand binding kinetics by micropipette. *Biophys. J.* 75: 1553-1572.

68. Krummey, S. M., R. J. Martinez, R. Andargachew, D. Liu, M. Wagener, J. E. Kohlmeier, B. D. Evavold, C. P. Larsen, and M. L. Ford. 2016. Low-affinity memory CD8+ T cells mediate robust heterologous immunity. *J. Immunol.* 196: 2838-2846.

69. Shorter, S. K., F. J. Schnell, S. R. McMaster, D. F. Pinelli, R. Andargachew, and B. D. Evavold. 2016. Viral escape mutant epitope maintains TCR affinity for antigen yet curtails CD8 T cell responses. *PLoS One* 11: e0149582.

70. Seo, Y.-J., P. Jothikumar, M. S. Suthar, C. Zhu, and A. Grakoui. 2016. Local Cellular and Cytokine Cues in the Spleen Regulate In Situ T Cell Receptor Affinity, Function, and Fate of CD8+ T Cells. *Immunity* 45: 988-998.

71. Liu, B., W. Chen, K. Natarajan, and L.-Z. journal of …. 2015. The cellular environment regulates in situ kinetics of T-cell receptor interaction with peptide major histocompatibility complex. *Eur. J. Immunol.* 45: 2099-2110.

72. Hong, J., S. P. Persaud, S. Horvath, P. M. Allen, B. D. Evavold, and C. Zhu. 2015. Force-Regulated In Situ TCR-Peptide-Bound MHC Class II Kinetics Determine Functions of CD4+ T Cells. *J. Immunol.* 195: 3557-3564.

73. Rosenthal, K. M., L. J. Edwards, J. J. Sabatino, J. D. Hood, H. A. Wasserman, C. Zhu, and B. D. Evavold. 2012. Low 2-dimensional CD4 T cell receptor affinity for myelin sets in motion delayed response kinetics. *PLoS One* 7.

74. Williams, C. M., A. A. Schonnesen, S.-Q. Zhang, K.-Y. Ma, C. He, T. Yamamoto, G. S. Eckhardt, C. A. Klebanoff, and N. Jiang. 2017. Normalized

Synergy Predicts That CD8 Co-Receptor Contribution to T Cell Receptor (TCR) and pMHC Binding Decreases As TCR Affinity Increases in Human Viral-Specific T Cells. *Front. Immunol.* 8: 894.

75. Frost, E. L., A. E. Kersh, B. D. Evavold, and A. E. Lukacher. 2015. Cutting Edge: Resident Memory CD8 T Cells Express High-Affinity TCRs. *J. Immunol.* 195: 3520-3524.

76. Hood, J. D., V. I. Zarnitsyna, C. Zhu, and B. D. Evavold. 2015. Regulatory and T effector cells have overlapping low to high ranges in TCR affinities for self during demyelinating disease. *J. Immunol.* 195: 4162-4170.

77. Kersh, A. E., L. J. Edwards, and B. D. Evavold. 2014. Progression of relapsing-remitting demyelinating disease does not require increased TCR affinity or epitope spread. *J. Immunol.* 193: 4429-4438.

78. Martinez, R. J., R. Andargachew, H. A. Martinez, and B. D. Evavold. 2016. Low-affinity CD4+ T cells are major responders in the primary immune response. *Nature communications* 7: 1-10.

79. Zhang, S.-Q., P. Parker, K.-Y. Ma, C. He, Q. Shi, Z. Cui, C. M. Williams, B. S. Wendel, A. I. Meriwether, M. Salazar, and N. Jiang. 2016. Direct measurement of T cell receptor affinity and sequence from naïve antiviral T cells. *Sci. Transl. Med.* 8: 341ra377.

80. Liu, B., W. Chen, B. D. Evavold, and C. Zhu. 2014. Accumulation of dynamic catch bonds between TCR and agonist peptide-MHC triggers T cell signaling. *Cell* 157: 357-368.

81. Kim, S., K. Takeuchi, Z.-Y. J. Sun, M. Touma, C. E. Castro, A. Fahmy, M. J. Lang, G. Wagner, and E. L. Reinherz. 2009. The αβ T Cell Receptor Is an Anisotropic Mechanosensor. *J. Biol. Chem.* 284: 31028-31037.

82. Liu, Y., L. Blanchfield, V. P. Ma, R. Andargachew, K. Galior, Z. Liu, B. Evavold, and K. Salaita. 2016. DNA-based nanoparticle tension sensors reveal that T-cell receptors transmit defined pN forces to their antigens for enhanced fidelity. *Proc. Natl. Acad. Sci. U. S. A.* 113: 5610-5615.

83. Evavold, B. D., J. Sloan-Lancaster, K. J. Wilson, J. B. Rothbard, and P. M. Allen. 1995. Specific T cell recognition of minimally homologous peptides: evidence for multiple endogenous ligands. *Immunity* 2: 655-663.

84. Hogquist, K. A., S. C. Jameson, W. R. Heath, J. L. Howard, M. J. Bevan, and F. R. Carbone. 1994. T cell receptor antagonist peptides induce positive selection. *Cell* 76: 17-27.

85. Viganò, S., D. T. Utzschneider, M. Perreau, G. Pantaleo, D. Zehn, and A. Harari. 2012. Functional avidity: a measure to predict the efficacy of effector T cells? *Clin. Dev. Immunol.* 2012: 153863.

86. Williams, M. A., E. V. Ravkov, and M. J. Bevan. 2008. Rapid culling of the CD4+ T cell repertoire in the transition from effector to memory. *Immunity* 28: 533-545.

87. Slifka, M. K., and J. L. Whitton. 2001. Functional avidity maturation of CD8(+) T cells without selection of higher affinity TCR. *Nat. Immunol.* 2: 711-717.

88. Kroger, C. J., and M. A. Alexander-Miller. 2007. Cutting edge: CD8+ T cell clones possess the potential to differentiate into both high- and low-avidity effector cells. *J. Immunol.* 179: 748-751.

89. Sharma, S. K., and M. A. Alexander-Miller. 2011. Increased sensitivity to antigen in high avidity CD8(+) T cells results from augmented membrane proximal T-cell receptor signal transduction. *Immunology* 133: 307-317.

90. Persaud, S. P., C. R. Parker, W.-L. L. Lo, K. S. Weber, and P. M. Allen. 2014. Intrinsic CD4(+) T cell sensitivity and response to a pathogen are set and sustained by avidity for thymic and peripheral complexes of self peptide and MHC. *Nat. Immunol.* 15: 266-274.

91. Blackburn, S. D., H. Shin, N. W. Haining, T. Zou, C. J. Workman, A. Polley, M. R. Betts, G. J. Freeman, D. A. A. Vignali, and J. E. Wherry. 2009. Coregulation of CD8+ T cell exhaustion by multiple inhibitory receptors during chronic viral infection. *Nat. Immunol.* 10: 29-37.

92. Baumgartner, C. K., H. Yagita, and L. P. Malherbe. 2012. A TCR affinity threshold regulates memory CD4 T cell differentiation following vaccination. *J. Immunol.* 189: 2309-2317.

93. van Gisbergen, K. P., P. L. Klarenbeek, N. A. Kragten, P.-P. A. P. Unger, M. B. B. Nieuwenhuis, F. M. Wensveen, A. ten Brinke, P. P. Tak, E. Eldering, M. A. Nolte, and R. A. van Lier. 2011. The costimulatory molecule CD27 maintains clonally diverse CD8(+) T cell responses of low antigen affinity to protect against viral variants. *Immunity* 35: 97-108.

94. McKeithan, T. W. 1995. Kinetic proofreading in T-cell receptor signal transduction. *Proc. Natl. Acad. Sci. U. S. A.* 92: 5042-5046.

95. Chakraborty, A. K., and A. Weiss. 2014. Insights into the initiation of TCR signaling. *Nat. Immunol.* 15: 798.

96. Rosette, C., G. Werlen, M. A. Daniels, P. O. Holman, S. M. Alam, P. J. Travers, N. R. Gascoigne, E. Palmer, and S. C. Jameson. 2001. The impact of duration versus extent of TCR occupancy on T cell activation: a revision of the kinetic proofreading model. *Immunity* 15: 59-70.

97. Aleksic, M., O. Dushek, H. Zhang, E. Shenderov, J.-L. L. Chen, V. Cerundolo, D. Coombs, and P. A. van der Merwe. 2010. Dependence of T cell antigen recognition on T cell receptor-peptide MHC confinement time. *Immunity* 32: 163-174.

98. Dushek, O., R. Das, and D. Coombs. 2009. A Role for Rebinding in Rapid and Reliable T Cell Responses to Antigen. *PLoS Comput. Biol.* 5.

99. Valitutti, S. 2012. The Serial Engagement Model 17 Years After: From TCR Triggering to Immunotherapy. *Front. Immunol.* 3: 272.

100. Valitutti, S., S. Müller, M. Cella, E. Padovan, and A. Lanzavecchia. 1995. Serial triggering of many T-cell receptors by a few peptide-MHC complexes. *Nature* 375: 148-151.

101. Gottschalk, R. A., M. M. Hathorn, H. Beuneu, E. Corse, M. L. Dustin, G. Altan-Bonnet, and J. P. Allison. 2012. Distinct influences of peptide-MHC quality and quantity on in vivo T-cell responses. *Proc. Natl. Acad. Sci. U. S. A.* 109: 881-886.

102. Liu, C. P., F. Crawford, P. Marrack, and J. Kappler. 1998. T cell positive selection by a high density, low affinity ligand. *Proceedings of the National Academy of Sciences* 95: 4522-4526.

103. San José, E., A. Borroto, F. Niedergang, A. Alcover, and B. Alarcón. 2000. Triggering the TCR complex causes the downregulation of nonengaged receptors by a signal transduction-dependent mechanism. *Immunity* 12: 161-170.

104. Kalergis, A. M., N. Boucheron, M. A. Doucey, E. Palmieri, E. C. Goyarts, Z. Vegh, I. F. Luescher, and S. G. Nathenson. 2001. Efficient T cell activation requires an optimal dwell-time of interaction between the TCR and the pMHC complex. *Nat. Immunol.* 2: 229-234.

105. Friedl, P., and M. Gunzer. 2001. Interaction of T cells with APCs: the serial encounter model. *Trends Immunol.* 22: 187-191.

106. Henrickson, S. E., T. R. Mempel, I. B. Mazo, B. Liu, M. N. Artyomov, H. Zheng, A. Peixoto, M. P. Flynn, B. Senman, T. Junt, H. C. Wong, A. K. Chakraborty, and U. H. von Andrian. 2008. T cell sensing of antigen dose governs interactive behavior with dendritic cells and sets a threshold for T cell activation. *Nat. Immunol.* 9: 282-291.

107. Mempel, T. R., S. E. Henrickson, and U. H. von Andrian. 2004. T-cell priming by dendritic cells in lymph nodes occurs in three distinct phases. *Nature* 427: 154.

108. Moreau, H. D., F. Lemaître, E. Terriac, G. Azar, M. Piel, A.-M. M. Lennon-Dumenil, and P. Bousso. 2012. Dynamic in situ cytometry uncovers T cell receptor signaling during immunological synapses and kinapses in vivo. *Immunity* 37: 351-363.

109. van der Merwe, P. A., and O. Dushek. 2011. Mechanisms for T cell receptor triggering. *Nature reviews. Immunology* 11: 47-55.

110. Krogsgaard, M., Q.-J. J. Li, C. Sumen, J. B. Huppa, M. Huse, and M. M. Davis. 2005. Agonist/endogenous peptide-MHC heterodimers drive T cell activation and sensitivity. *Nature* 434: 238-243.

111. Irvine, D. J., M. A. Purbhoo, M. Krogsgaard, and M. M. Davis. 2002. Direct observation of ligand recognition by T cells. *Nature* 419: 845-849.

112. Krogsgaard, M., J. Juang, and M. M. Davis. 2007. A role for "self" in T-cell activation. *Semin. Immunol.* 19: 236-244.

113. Secrist, J. P., L. A. Burns, L. Karnitz, G. A. Koretzky, and R. T. Abraham. 1993. Stimulatory effects of the protein tyrosine phosphatase inhibitor, pervanadate, on T-cell activation events. *The Journal of biological chemistry* 268: 5886-5893.

114. Nika, K., C. Soldani, M. Salek, W. Paster, A. Gray, R. Etzensperger, L. Fugger, P. Polzella, V. Cerundolo, O. Dushek, T. Höfer, A. Viola, and O. Acuto. 2010. Constitutively active Lck kinase in T cells drives antigen receptor signal transduction. *Immunity* 32: 766-777.

115. Irles, C., A. Symons, F. Michel, and B.-T. R. Nature …. 2003. CD45 ectodomain controls interaction with GEMs and Lck activity for optimal TCR signaling. *Nature Immunology* 4: 189-197.

116. Kjer-Nielsen, L., C. S. Clements, A. W. Purcell, A. G. Brooks, J. C. Whisstock, S. R. Burrows, J. McCluskey, and J. Rossjohn. 2003. A structural basis for the selection of dominant alphabeta T cell receptors in antiviral immunity. *Immunity* 18: 53-64.

117. Beddoe, T., Z. Chen, C. S. Clements, L. K. Ely, S. R. Bushell, J. P. Vivian, L. Kjer-Nielsen, S. S. Pang, M. A. Dunstone, Y. C. Liu, W. A. Macdonald, M. A. Perugini, M. C. Wilce, S. R. Burrows, A. W. Purcell, T. Tiganis, S. P. Bottomley, J. McCluskey, and J. Rossjohn. 2009. Antigen ligation triggers a conformational change within the constant domain of the alphabeta T cell receptor. *Immunity* 30: 777-788.

118. Kuhns, M. S., A. T. Girvin, L. O. Klein, R. Chen, K. D. Jensen, E. W. Newell, J. B. Huppa, B. F. F. Lillemeier, M. Huse, Y.-H. H. Chien, K. C. Garcia, and M. M. Davis. 2010. Evidence for a functional sidedness to the alphabetaTCR. *Proc. Natl. Acad. Sci. U. S. A.* 107: 5094-5099.

119. Sun, Z. J., K. S. Kim, G. Wagner, and E. L. Reinherz. 2001. Mechanisms contributing to T cell receptor signaling and assembly revealed by the solution structure of an ectodomain fragment of the CD3 epsilon gamma heterodimer. *Cell* 105: 913-923.

120. Martínez-Martín, N., R. M. Risueño, A. Morreale, I. Zaldívar, E. Fernández-Arenas, F. Herranz, A. R. Ortiz, and B. Alarcón. 2009. Cooperativity between T cell receptor complexes revealed by conformational mutants of CD3epsilon. *Science Signaling* 2: ra43.

121. Deford-Watts, L. M., T. C. Tassin, A. M. Becker, J. J. Medeiros, J. P. Albanesi, P. E. Love, C. Wülfing, and N. S. van Oers. 2009. The cytoplasmic tail of the T cell receptor CD3 epsilon subunit contains a phospholipid-binding motif that regulates T cell functions. *J. Immunol.* 183: 1055-1064.

122. Xu, C., E. Gagnon, M. E. Call, J. R. Schnell, C. D. Schwieters, C. V. Carman, J. J. Chou, and K. W. Wucherpfennig. 2008. Regulation of T cell receptor activation by dynamic membrane binding of the CD3epsilon cytoplasmic tyrosine-based motif. *Cell* 135: 702-713.

123. Gagnon, E., D. A. Schubert, S. Gordo, H. H. Chu, and K. W. Wucherpfennig. 2012. Local changes in lipid environment of TCR microclusters regulate membrane binding by the CD3ε cytoplasmic domain. *J. Exp. Med.* 209: 2423-2439.

124. Li, Y.-C. C., B.-M. M. Chen, P.-C. C. Wu, T.-L. L. Cheng, L.-S. S. Kao, M.-H. H. Tao, A. Lieber, and S. R. Roffler. 2010. Cutting Edge: mechanical forces acting on T cells immobilized via the TCR complex can trigger TCR signaling. *J. Immunol.* 184: 5959-5963.

125. Yachi, P. P., J. Ampudia, T. Zal, and N. R. Gascoigne. 2006. Altered peptide ligands induce delayed CD8-T cell receptor interaction--a role for CD8 in distinguishing antigen quality. *Immunity* 25: 203-211.

126. Hemmer, B., I. Stefanova, and V.-M. of …. 1998. Relationships among TCR ligand potency, thresholds for effector function elicitation, and the quality of early signaling events in human T cells. *J. Immunol.* 160: 5807-5814.

127. King, C. G., S. Koehli, B. Hausmann, M. Schmaler, D. Zehn, and E. Palmer. 2012. T cell affinity regulates asymmetric division, effector cell differentiation, and tissue pathology. *Immunity* 37: 709-720.

128. Nish, S. A., K. D. Zens, R. Kratchmarov, W.-H. W. Lin, W. C. Adams, Y.-H. Chen, B. Yen, N. J. Rothman, A. Bhandoola, H.-H. Xue, D. L. Farber, and S. L.

Reiner. 2016. CD4+ T cell effector commitment coupled to self-renewal by asymmetric cell divisions. *J. Exp. Med.* 214: 39-47.

129. Mahnke, J., V. Schumacher, S. Ahrens, and K.-N. reports. 2016. Interferon Regulatory Factor 4 controls TH1 cell effector function and metabolism. *Sci. Rep.* 6: 35521.

130. Man, K., M. Miasari, W. Shi, A. Xin, D. C. Henstridge, S. Preston, M. Pellegrini, G. T. Belz, G. K. Smyth, M. A. Febbraio, S. L. Nutt, and A. Kallies. 2013. The transcription factor IRF4 is essential for TCR affinity-mediated metabolic programming and clonal expansion of T cells. *Nat. Immunol.* 14: 1155-1165.

131. Gallegos, A. M., H. Xiong, I. M. Leiner, B. Sušac, M. S. Glickman, E. G. Pamer, and J. W. van Heijst. 2016. Control of T cell antigen reactivity via programmed TCR downregulation. *Nat. Immunol.* 17: 379-386.

132. Weber, K. S., Q.-J. J. Li, S. P. Persaud, J. D. Campbell, M. M. Davis, and P. M. Allen. 2012. Distinct CD4+ helper T cells involved in primary and secondary responses to infection. *Proc. Natl. Acad. Sci. U. S. A.* 109: 9511-9516.

133. Bettini, M., L. Blanchfield, A. Castellaw, Q. Zhang, M. Nakayama, M. P. Smeltzer, H. Zhang, K. A. Hogquist, B. D. Evavold, and D. A. A. Vignali. 2014. TCR affinity and tolerance mechanisms converge to shape T cell diabetogenic potential. *J. Immunol.* 193: 571-579.

134. **Waldmann, H., H Pope, and I Lefkovits**. 1976. Limiting dilution analysis of helper T-cell function. II. An approach to the study of the function of single helper T cells. *Immunology* 31: 343-352.

135. Tubo, N. J., A. J. Pagán, J. J. Taylor, R. W. Nelson, J. L. Linehan, J. M. Ertelt, E. S. Huseby, S. S. Way, and M. K. Jenkins. 2013. Single naive CD4+ T cells from a diverse repertoire produce different effector cell types during infection. *Cell* 153: 785-796.

136. Blattman, J. N., R. Antia, D. J. Sourdive, X. Wang, S. M. Kaech, K. Murali-Krishna, J. D. Altman, and R. Ahmed. 2002. Estimating the precursor frequency of naive antigen-specific CD8 T cells. *J. Exp. Med.* 195: 657-664.

137. Whitmire, J. K., N. Benning, and J. L. Whitton. 2006. Precursor frequency, nonlinear proliferation, and functional maturation of virus-specific CD4+ T cells. *J. Immunol.* 176: 3028-3036.

138. Moon, J. J., H. H. Chu, M. Pepper, S. J. McSorley, S. C. Jameson, R. M. Kedl, and M. K. Jenkins. 2007. Naive CD4(+) T cell frequency varies for different epitopes and predicts repertoire diversity and response magnitude. *Immunity* 27: 203-213.

139. Moon, J. J., H. H. Chu, J. Hataye, A. J. Pagán, M. Pepper, J. B. McLachlan, T. Zell, and M. K. Jenkins. 2009. Tracking epitope-specific T cells. *Nat. Protoc.* 4: 565-581.

140. Wooldridge, L., A. Lissina, D. K. Cole, H. A. van den Berg, D. A. Price, and A. K. Sewell. 2009. Tricks with tetramers: how to get the most from multimeric peptide-MHC. *Immunology* 126: 147-164.

141. Nepom, G. T. 2012. MHC class II tetramers. *J. Immunol.* 188: 2477-2482.

142. Malherbe, L., C. Hausl, L. Teyton, and M. G. McHeyzer-Williams. 2004. Clonal selection of helper T cells is determined by an affinity threshold with no further skewing of TCR binding properties. *Immunity* 21: 669-679.

143. Baumgartner, C. K., H. Yagita, and L. P. Malherbe. 2012. A TCR affinity threshold regulates memory CD4 T cell differentiation following vaccination. *J. Immunol.* 189: 2309-2317.

144. Bachmann, M. F., D. E. Speiser, and P. S. Ohashi. 1997. Functional management of an antiviral cytotoxic T-cell response. *J. Virol.* 71: 5764-5768.

145. Abdel-Hakeem, M. S., M. Boisvert, J. Bruneau, H. Soudeyns, and N. H. Shoukry. 2017. Selective expansion of high functional avidity memory CD8 T cell clonotypes during hepatitis C virus reinfection and clearance. *PLoS Pathog.* 13.

146. McHeyzer-Williams, M. G., and M. M. Davis. 1995. Antigen-specific development of primary and memory T cells in vivo. *Science* 268: 106-111.

147. Cukalac, T., J. Chadderton, A. Handel, P. C. Doherty, S. J. Turner, P. G. Thomas, and N. L. La Gruta. 2014. Reproducible selection of high avidity CD8+ T-cell clones following secondary acute virus infection. *Proc. Natl. Acad. Sci. U. S. A.* 111: 1485-1490.

148. Cukalac, T., Kan, W. , Dash, P. , Guan, J. , Quinn, K. M., Gras, S. , Thomas, P. G. and La Gruta, N. L. 2015. Paired TCRαβ analysis of virus-specific CD8+ T cells exposes diversity in a previously defined 'narrow'repertoire. *Immunol. Cell Biol.* 93: 804-814.

149. Attaf, M., E. Huseby, and A. K. Sewell. 2015. αβ T cell receptors as predictors of health and disease. *Cell. Mol. Immunol.* 12: 391-399.

150. Messaoudi, I., J. A. Guevara Patiño, R. Dyall, J. LeMaoult, and J. Nikolich-Zugich. 2002. Direct link between mhc polymorphism, T cell avidity, and diversity in immune defense. *Science* 298: 1797-1800.

151. Rius, C., M. Attaf, K. Tungatt, V. Bianchi, M. Legut, A. Bovay, M. Donia, P. thor Straten, M. Peakman, I. Svane, S. Ott, T. Connor, B. Szomolay, G. Dolton, and A. K. Sewell. 2018. Peptide–MHC Class I Tetramers Can Fail To Detect Relevant Functional T Cell Clonotypes and Underestimate Antigen-Reactive T Cell Populations. *J. Immunol.* 200: 2263-2279.

152. Demotz, S., H. M. Grey, and A. Sette. 1990. The minimal number of class II MHC-antigen complexes needed for T cell activation. *Science* 249: 1028-1030.

153. Delon, J., N. Bercovici, G. Raposo, R. Liblau, and A. Trautmann. 1998. Antigen-dependent and-independent Ca2+ responses triggered in T cells by dendritic cells compared with B cells. *J. Exp. Med.* 188: 1473-1484.

154. Sykulev, Y., M. Joo, I. Vturina, T. J. Tsomides, and H. N. Eisen. 1996. Evidence that a single peptide–MHC complex on a target cell can elicit a cytolytic T cell response. *Immunity* 4: 565-571.

155. Porgador, A., J. W. Yewdell, Y. Deng, J. R. Bennink, and R. N. Germain. 1997. Localization, quantitation, and in situ detection of specific peptide-MHC class I complexes using a monoclonal antibody. *Immunity* 6: 715-726.

156. Potter, T. A., K. Grebe, B. Freiberg, and A. Kupfer. 2001. Formation of supramolecular activation clusters on fresh ex vivo CD8+ T cells after engagement of the T cell antigen receptor and CD8 by antigen-presenting cells. *Proc. Natl. Acad. Sci. U. S. A.* 98: 12624-12629.

157. Purbhoo, M. A., D. J. Irvine, J. B. Huppa, and M. M. Davis. 2004. T cell killing does not require the formation of a stable mature immunological synapse. *Nat. Immunol.* 5: 524-530.

158. Holler, P. D., and D. M. Kranz. 2003. Quantitative analysis of the contribution of TCR/pepMHC affinity and CD8 to T cell activation. *Immunity* 18: 255-264.

159. Obst, R., H.-M. M. van Santen, D. Mathis, and C. Benoist. 2005. Antigen persistence is required throughout the expansion phase of a CD4(+) T cell response. *J. Exp. Med.* 201: 1555-1565.

160. Kaech, S. M., and R. Ahmed. 2001. Memory CD8+ T cell differentiation: initial antigen encounter triggers a developmental program in naïve cells. *Nat. Immunol.* 2: 415-422.

161. Corbin, G. A., and J. T. Harty. 2004. Duration of infection and antigen display have minimal influence on the kinetics of the CD4+ T cell response to Listeria monocytogenes infection. *J. Immunol.* 173: 5679-5687.

162. Williams, M. A., and M. J. Bevan. 2004. Shortening the infectious period does not alter expansion of CD8 T cells but diminishes their capacity to differentiate into memory cells. *J. Immunol.* 173: 6694-6702.

163. Celli, S., F. Lemaître, and P. Bousso. 2007. Real-time manipulation of T cell-dendritic cell interactions in vivo reveals the importance of prolonged contacts for CD4+ T cell activation. *Immunity* 27: 625-634.

164. Ravkov, E. V., and M. A. Williams. 2009. The magnitude of CD4+ T cell recall responses is controlled by the duration of the secondary stimulus. *J. Immunol.* 183: 2382-2389.

165. Han, S., A. Asoyan, H. Rabenstein, N. Nakano, and R. Obst. 2010. Role of antigen persistence and dose for CD4+ T-cell exhaustion and recovery. *Proc. Natl. Acad. Sci. U. S. A.* 107: 20453-20458.

166. Fuller, M. J., A. Khanolkar, A. E. Tebo, and A. J. Zajac. 2004. Maintenance, loss, and resurgence of T cell responses during acute, protracted, and chronic viral infections. *J. Immunol.* 172: 4204-4214.

167. Brooks, D. G., L. Teyton, M. B. Oldstone, and D. B. McGavern. 2005. Intrinsic functional dysregulation of CD4 T cells occurs rapidly following persistent viral infection. *J. Virol.* 79: 10514-10527.

168. Wherry, J. E., S.-J. Ha, S. M. Kaech, N. W. Haining, S. Sarkar, V. Kalia, S. Subramaniam, J. N. Blattman, D. L. Barber, and R. Ahmed. 2007. Molecular Signature of CD8+ T Cell Exhaustion during Chronic Viral Infection. *Immunity* 27: 670-684.

169. Crawford, A., J. M. Angelosanto, C. Kao, T. A. Doering, P. M. Odorizzi, B. E. Barnett, and E. J. Wherry. 2014. Molecular and transcriptional basis of CD4(+) T cell dysfunction during chronic infection. *Immunity* 40: 289-302.

170. Fahey, L. M., E. B. Wilson, H. Elsaesser, C. D. Fistonich, D. B. McGavern, and D. G. Brooks. 2011. Viral persistence redirects CD4 T cell differentiation toward T follicular helper cells. *J. Exp. Med.* 208: 987-999.

171. Keck, S., M. Schmaler, S. Ganter, L. Wyss, S. Oberle, E. S. Huseby, D. Zehn, and C. G. King. 2014. Antigen affinity and antigen dose exert distinct influences on CD4 T-cell differentiation. *Proc. Natl. Acad. Sci. U. S. A.* 111: 14852-14857.

172. Tubo, N. J., and M. K. Jenkins. 2014. TCR signal quantity and quality in CD4(+) T cell differentiation. *Trends Immunol.* 35: 591-596.

173. Billeskov, R., Y. Wang, S. Solaymani-Mohammadi, B. Frey, S. Kulkarni, P. Andersen, E. Agger, Y. Sui, and J. A. Berzofsky. 2017. Low Antigen Dose in Adjuvant-Based Vaccination Selectively Induces CD4 T Cells with Enhanced Functional Avidity and Protective Efficacy. *J. Immunol.* 198: 3494-3506.

174. Rees, W., J. Bender, T. K. Teague, R. M. Kedl, F. Crawford, P. Marrack, and J. Kappler. 1999. An inverse relationship between T cell receptor affinity and antigen dose during CD4(+) T cell responses in vivo and in vitro. *Proc. Natl. Acad. Sci. U. S. A.* 96: 9781-9786.

175. Malherbe, L., L. Mark, N. Fazilleau, L. J. McHeyzer-Williams, and M. G. McHeyzer-Williams. 2008. Vaccine Adjuvants Alter TCR-Based Selection Thresholds. *Immunity* 28: 698-709.

176. Ugolini, M., J. Gerhard, S. Burkert, K. J. Jensen, P. Georg, F. Ebner, S. M. Volkers, S. Thada, K. Dietert, L. Bauer, A. Schäfer, E. T. Helbig, B. Opitz, F. Kurth, S. Sur, N. Dittrich, S. Gaddam, M. L. Conrad, C. S. Benn, U. Blohm, A. D. Gruber, A. Hutloff, S. Hartmann, M. V. Boekschoten, M. Müller, G. Jungersen, R. R. Schumann, N. Suttorp, and L. E. Sander. 2018. Recognition of microbial viability via TLR8 drives TFH cell differentiation and vaccine responses. *Nat. Immunol.* 19: 386-396.

177. Thorborn, G., M. J. J. Ploquin, U. Eksmond, R. Pike, W. Bayer, U. Dittmer, K. J. Hasenkrug, M. Pepper, and G. Kassiotis. 2014. Clonotypic composition of the

CD4+ T cell response to a vectored retroviral antigen is determined by its speed. *J. Immunol.* 193: 1567-1577.

178. Richer, M. J., J. C. Nolz, and J. T. Harty. 2013. Pathogen-specific inflammatory milieux tune the antigen sensitivity of CD8(+) T cells by enhancing T cell receptor signaling. *Immunity* 38: 140-152.

179. Kim, C., D. C. Jay, and M. A. Williams. 2012. Stability and function of secondary Th1 memory cells are dependent on the nature of the secondary stimulus. *J. Immunol.* 189: 2348-2355.

180. Kim, C., D. C. Jay, and M. A. Williams. 2014. Dynamic functional modulation of CD4+ T cell recall responses is dependent on the inflammatory environment of the secondary stimulus. *PLoS Pathog.* 10.

181. Petra, K., and B. Thomas. 2005. Concerted antigen presentation by dendritic cells and B cells is necessary for optimal CD4 T-cell immunity in vivo. *Immunology* 115: 556-564.

182. Whitmire, J. K., M. S. Asano, and S. M. Kaech. 2009. Requirement of B cells for generating CD4+ T cell memory. *J. Immunol.* 182: 1868-1876.

183. Misumi, I., and J. K. Whitmire. 2014. B cell depletion curtails CD4+ T cell memory and reduces protection against disseminating virus infection. *J. Immunol.* 192: 1597-1608.

184. Lykken, J. M., D. J. DiLillo, E. T. Weimer, S. Roser-Page, M. T. Heise, J. M. Grayson, N. M. Weitzmann, and T. F. Tedder. 2014. Acute and chronic B cell depletion disrupts CD4+ and CD8+ T cell homeostasis and expansion during acute viral infection in mice. *J. Immunol.* 193: 746-756.

185. Merkenschlager, J., M. J. J. Ploquin, U. Eksmond, R. Andargachew, G. Thorborn, A. Filby, M. Pepper, B. Evavold, and G. Kassiotis. 2016. Stepwise B-cell-dependent expansion of T helper clonotypes diversifies the T-cell response. *Nature Communications* 7 (10281): 1-13.

186. Rivera, A., C. C. Chen, N. Ron, J. P. Dougherty, and Y. Ron. 2001. Role of B cells as antigen-presenting cells in vivo revisited: antigen-specific B cells are essential for T cell expansion in lymph nodes and for systemic T cell responses to low antigen concentrations. *Int. Immunol.* 13: 1583-1593.

187. Lund, J. M., L. Hsing, T. T. Pham, and A. Y. Rudensky. 2008. Coordination of early protective immunity to viral infection by regulatory T cells. *Science* 320: 1220-1224.

188. Soerens, A. G., A. Costa, and J. M. Lund. 2016. Regulatory T cells are essential to promote proper CD4 T-cell priming upon mucosal infection. *Mucosal Immunol.* 9: 1395.

189. Laidlaw, B. J., W. Cui, R. A. Amezquita, S. M. Gray, T. Guan, Y. Lu, Y. Kobayashi, R. A. Flavell, S. H. Kleinstein, J. Craft, and S. M. Kaech. 2015. Production of IL-10 by CD4(+) regulatory T cells during the resolution of infection promotes the maturation of memory CD8(+) T cells. *Nat. Immunol.* 16: 871-879.

190. Laidlaw, B. J., J. E. Craft, and S. M. Kaech. 2016. The multifaceted role of CD4(+) T cells in CD8(+) T cell memory. *Nature reviews. Immunology* 16: 102-111.

191. Swain, S. L., K. K. McKinstry, and T. M. Strutt. 2012. Expanding roles for $CD4^+$ T cells in immunity to viruses. *Nature reviews. Immunology* 12: 136-148.

192. Li, S., E. J. Gowans, C. Chougnet, M. Plebanski, and U. Dittmer. 2008. Natural regulatory T cells and persistent viral infection. *J. Virol.* 82: 21-30.

193. Penaloza-MacMaster, P., A. O. Kamphorst, A. Wieland, K. Araki, S. S. Iyer, E. E. West, L. O' Mara, S. Yang, B. T. Konieczny, and A. H. Sharpe. 2014. Interplay between regulatory T cells and PD-1 in modulating T cell exhaustion and viral control during chronic LCMV infection. *J. Exp. Med.* 211: 1905-1918.

194. Tamara, V.-P., S. Sharvan, and R. B. T. 2013. Role of regulatory T cells during virus infection. *Immunol. Rev.* 255: 182-196.

195. MacLeod, M. K., E. T. Clambey, J. W. Kappler, and P. Marrack. 2009. CD4 memory T cells: what are they and what can they do? *Semin. Immunol.* 21: 53-61.

196. Sun, J. C., M. A. Williams, and M. J. Bevan. 2004. CD4+ T cells are required for the maintenance, not programming, of memory CD8+ T cells after acute infection. *Nat. Immunol.* 5: 927-933.

197. Sun, J. C., and M. J. Bevan. 2003. Defective CD8 T cell memory following acute infection without CD4 T cell help. *Science* 300: 339-342.

198. Janssen, E. M., E. E. Lemmens, T. Wolfe, U. Christen, M. G. von Herrath, and S. P. Schoenberger. 2003. CD4+ T cells are required for secondary expansion and memory in CD8+ T lymphocytes. *Nature* 421: 852-856.

199. Williams, M. A., A. J. Tyznik, and M. J. Bevan. 2006. Interleukin-2 signals during priming are required for secondary expansion of CD8+ memory T cells. *Nature* 441: 890-893.

200. Crotty, S., E. N. Kersh, J. Cannons, P. L. Schwartzberg, and R. Ahmed. 2003. SAP is required for generating long-term humoral immunity. *Nature* 421: 282-287.

201. Whitmire, J. K. 2011. Induction and function of virus-specific CD4+ T cell responses. *Virology* 411: 216-228.

202. Walton, S., S. Mandaric, and A. Oxenius. 2013. CD4 T cell responses in latent and chronic viral infections. *Front. Immunol.* 4.

203. Porichis, F., and D. E. Kaufmann. 2011. HIV-specific CD4 T cells and immune control of viral replication. *Curr. Opin. HIV AIDS* 6: 174-180.

204. Klenerman, P., and R. Thimme. 2012. T cell responses in hepatitis C: the good, the bad and the unconventional. *Gut* 61: 1226-1234.

205. Schulze zur Wiesch, J., D. Ciuffreda, L. Lewis-Ximenez, V. Kasprowicz, B. E. Nolan, H. Streeck, J. Aneja, L. L. Reyor, T. M. Allen, A. W. Lohse, B. McGovern, R. T. Chung, W. W. Kwok, A. Y. Kim, and G. M. Lauer. 2012. Broadly directed virus-specific CD4+ T cell responses are primed during acute hepatitis C infection, but rapidly disappear from human blood with viral persistence. *J. Exp. Med.* 209: 61-75.

206. Buchmeier, M. J., R. M. Welsh, F. J. Dutko, and M. B. Oldstone. 1980. The virology and immunobiology of lymphocytic choriomeningitis virus infection. *Adv. Immunol.* 30: 275-331.

207. Ahmed, R., A. Salmi, L. D. Butler, J. M. Chiller, and M. B. Oldstone. 1984. Selection of genetic variants of lymphocytic choriomeningitis virus in spleens of

persistently infected mice. Role in suppression of cytotoxic T lymphocyte response and viral persistence. *J. Exp. Med.* 160: 521-540.

208. Matloubian, M., T. Somasundaram, S. R. Kolhekar, R. Selvakumar, and R. Ahmed. 1990. Genetic basis of viral persistence: single amino acid change in the viral glycoprotein affects ability of lymphocytic choriomeningitis virus to persist in adult mice. *J. Exp. Med.* 172: 1043-1048.

209. Oldstone, M. B., and K. P. Campbell. 2011. Decoding arenavirus pathogenesis: essential roles for alpha-dystroglycan-virus interactions and the immune response. *Virology* 411: 170-179.

210. Zehn, D., and E. J. Wherry. 2015. Immune Memory and Exhaustion: Clinically Relevant Lessons from the LCMV Model. *Adv. Exp. Med. Biol.* 850: 137-152.

211. Zinkernagel, R. M., and P. C. Doherty. 1974. Restriction of in vitro T cell-mediated cytotoxicity in lymphocytic choriomeningitis within a syngeneic or semiallogeneic system. *Nature* 248: 701-702.

212. Butz, E. A., and M. J. Bevan. 1998. Massive expansion of antigen-specific CD8+ T cells during an acute virus infection. *Immunity* 8: 167-175.

213. Murali-Krishna, K., J. D. Altman, M. Suresh, D. J. Sourdive, A. J. Zajac, J. D. Miller, J. Slansky, and R. Ahmed. 1998. Counting antigen-specific CD8 T cells: a reevaluation of bystander activation during viral infection. *Immunity* 8: 177-187.

214. Lau, L. L., B. D. Jamieson, T. Somasundaram, and R. Ahmed. 1994. Cytotoxic T-cell memory without antigen. *Nature* 369: 648-652.

215. Wherry, E. J., J. N. Blattman, K. Murali-Krishna, R. van der Most, and R. Ahmed. 2003. Viral persistence alters CD8 T-cell immunodominance and tissue

distribution and results in distinct stages of functional impairment. *J. Virol.* 77: 4911-4927.

216. Fuller, M. J., and A. J. Zajac. 2003. Ablation of CD8 and CD4 T cell responses by high viral loads. *J. Immunol.* 170: 477-486.

217. Barber, D. L., E. J. Wherry, D. Masopust, B. Zhu, J. P. Allison, A. H. Sharpe, G. J. Freeman, and R. Ahmed. 2006. Restoring function in exhausted CD8 T cells during chronic viral infection. *Nature* 439: 682-687.

218. Matloubian, M., R. J. Concepcion, and R. Ahmed. 1994. CD4+ T cells are required to sustain CD8+ cytotoxic T-cell responses during chronic viral infection. *J. Virol.* 68: 8056-8063.

219. Aubert, R. D., A. O. Kamphorst, S. Sarkar, V. Vezys, S.-J. J. Ha, D. L. Barber, L. Ye, A. H. Sharpe, G. J. Freeman, and R. Ahmed. 2011. Antigen-specific CD4 T-cell help rescues exhausted CD8 T cells during chronic viral infection. *Proc. Natl. Acad. Sci. U. S. A.* 108: 21182-21187.

220. Kedl, R. M., J. W. Kappler, and P. Marrack. 2003. Epitope dominance, competition and T cell affinity maturation. *Curr. Opin. Immunol.* 15: 120-127.

221. Lichterfeld, M., X. G. Yu, S. K. Mui, K. L. Williams, A. Trocha, M. A. Brockman, R. L. Allgaier, M. T. Waring, T. Koibuchi, M. N. Johnston, D. Cohen, T. M. Allen, E. S. Rosenberg, B. D. Walker, and M. Altfeld. 2007. Selective depletion of high-avidity human immunodeficiency virus type 1 (HIV-1)-specific CD8+ T cells after early HIV-1 infection. *J. Virol.* 81: 4199-4214.

222. Penaloza-MacMaster, P., and N. M. Provine. 2015. CD4 T Cell depletion substantially augments the rescue potential of PD-L1 blockade for deeply exhausted CD8 T cells. *J. Immunol.* 195: 1054-1063.

223. Dow, C., C. Oseroff, B. Peters, C. Nance-Sotelo, J. Sidney, M. Buchmeier, A. Sette, and B. R. Mothé. 2008. Lymphocytic choriomeningitis virus infection yields overlapping CD4+ and CD8+ T-cell responses. *J. Virol.* 82: 11734-11741.

224. Kitamura, D., J. Roes, R. Kühn, and K. Rajewsky. 1991. A B cell-deficient mouse by targeted disruption of the membrane exon of the immunoglobulin mu chain gene. *Nature* 350: 423-426.

225. Laugel, B., H. A. van den Berg, E. Gostick, and D. K. W. Cole, L. Boulter, J. Milicic, A. Price, D. Sewell, A. K. 2007. Different T cell receptor affinity thresholds and CD8 coreceptor dependence govern cytotoxic T lymphocyte activation and tetramer binding properties. *J. Biol. Chem.* 282: 23799–23810.

226. Homann, D., L. Teyton, and M. Oldstone. 2001. Differential regulation of antiviral T-cell immunity results in stable CD8+ but declining CD4+ T-cell memory. *Nat. Med.* 7: 913–919.

227. Hamad, A. R., S. M. O'Herrin, M. S. Lebowitz, A. Srikrishnan, J. Bieler, J. Schneck, and D. Pardoll. 1998. Potent T cell activation with dimeric peptide-major histocompatibility complex class II ligand: the role of CD4 coreceptor. *J. Exp. Med.* 188: 1633-1640.

228. Viganò, S., D. T. Utzschneider, M. Perreau, G. Pantaleo, D. Zehn, and A. Harari. 2012. Functional avidity: a measure to predict the efficacy of effector T cells? *Clin. Dev. Immunol.* 2012: 14.

229. Day, C. L., D. E. Kaufmann, P. Kiepiela, J. A. Brown, E. S. Moodley, S. Reddy, E. W. Mackey, J. D. Miller, A. J. Leslie, C. DePierres, Z. Mncube, J. Duraiswamy, B. Zhu, Q. Eichbaum, M. Altfeld, J. E. Wherry, H. M. Coovadia, P. J. R. Goulder, P. Klenerman, R. Ahmed, G. J. Freeman, and B. D. Walker. 2006. PD-1 expression on HIV-specific T cells is associated with T-cell exhaustion and disease progression. *Nature* 443: 350-354.

230. Ploquin, M. J. J., U. Eksmond, and G. Kassiotis. 2011. B cells and TCR avidity determine distinct functions of CD4+ T cells in retroviral infection. *J. Immunol.* 187: 3321-3330.

231. Ertelt, J. M., T. M. Johanns, M. A. Mysz, M. R. Nanton, J. H. Rowe, M. N. Aguilera, and S. S. Way. 2011. Selective culling of high avidity antigen-specific CD4+ T cells after virulent Salmonella infection. *Immunology* 134: 487-497.

232. Hendriks, J., L. A. Gravestein, K. Tesselaar, R. A. van Lier, T. N. Schumacher, and J. Borst. 2000. CD27 is required for generation and long-term maintenance of T cell immunity. *Nat. Immunol.* 1: 433-440.

233. Schamel, W. W., I. Arechaga, R. M. Risueño, H. M. van Santen, P. Cabezas, C. Risco, J. M. Valpuesta, and B. Alarcón. 2005. Coexistence of multivalent and monovalent TCRs explains high sensitivity and wide range of response. *J. Exp. Med.* 202: 493-503.

234. Thauland, T. J., K. H. Hu, M. A. Bruce, and M. J. Butte. 2017. Cytoskeletal adaptivity regulates T cell receptor signaling. *Sci. Signal.* 10.

235. Dustin, M. L., and J. A. Cooper. 2000. The immunological synapse and the actin cytoskeleton: molecular hardware for T cell signaling. *Nat. Immunol.* 1: 23-29.

236. Viola, A., and A. Lanzavecchia. 1996. T cell activation determined by T cell receptor number and tunable thresholds. *Science* 273: 104-106.

237. Utzny, C., D. Coombs, S. Müller, and S. Valitutti. 2006. Analysis of peptide/MHC-induced TCR downregulation. *Cell Biochem. Biophys.* 46: 101-111.

238. Viola, A., and A. Lanzavecchia. 1996. T cell activation determined by T cell receptor number and tunable thresholds. *Science* 273: 104-106.

239. Friedman, R. S., P. Beemiller, and C. M. Sorensen. 2010. Real-time analysis of T cell receptors in naive cells in vitro and in vivo reveals flexibility in synapse and signaling dynamics. *J. Exp. Med.* 207: 2733-2749.

240. Das, D. K., Y. Feng, R. J. Mallis, X. Li, D. B. Keskin, R. E. Hussey, S. K. Brady, J.-H. H. Wang, G. Wagner, E. L. Reinherz, and M. J. Lang. 2015. Force-dependent transition in the T-cell receptor β-subunit allosterically regulates peptide discrimination and pMHC bond lifetime. *Proc. Natl. Acad. Sci. U. S. A.* 112: 1517-1522.

241. Atilla-Gokcumen, G. E., E. Muro, J. Relat-Goberna, S. Sasse, A. Bedigian, M. L. Coughlin, S. Garcia-Manyes, and U. S. Eggert. 2014. Dividing cells regulate their lipid composition and localization. *Cell* 156: 428-439.

242. Robinson, G. A., K. E. Waddington, I. Pineda-Torra, and E. C. Jury. 2017. Transcriptional Regulation of T-Cell Lipid Metabolism: Implications for Plasma Membrane Lipid Rafts and T-Cell Function. *Front. Immunol.* 8: 1636.

243. Oxenius, A., M. F. Bachmann, R. M. Zinkernagel, and H. Hengartner. 1998. Virus specific major MHC class II restricted TCR transgenic mice: effects on

humoral and cellular immune responses after viral infection. *Eur. J. Immunol.* 28: 390-400.

244. Gett, A. V., F. Sallusto, A. Lanzavecchia, and J. Geginat. 2003. T cell fitness determined by signal strength. *Nat. Immunol.* 4: 355-360.

245. Au-Yeung, B. B., G. Smith, J. L. Mueller, C. S. Heyn, R. Jaszczak, A. Weiss, and J. Zikherman. 2017. IL-2 Modulates the TCR Signaling Threshold for CD8 but Not CD4 T Cell Proliferation on a Single-Cell Level. *J. Immunol.* 198: 2445-2456.

246. Bachmann, M. F., A. Oxenius, D. E. Speiser, S. Mariathasan, H. Hengartner, R. M. Zinkernagel, and P. S. Ohashi. 1997. Peptide-induced T cell receptor down-regulation on naive T cells predicts agonist/partial agonist properties and strictly correlates with T cell activation. *Eur. J. Immunol.* 27: 2195-2203.

247. McNeil, L. K., and B. D. Evavold. 2003. TCR reserve: a novel principle of CD4 T cell activation by weak ligands. *J. Immunol.* 170: 1224-1230.

248. McNeil, L. K., and B. D. Evavold. 2003. TCR reserve: a novel principle of CD4 T cell activation by weak ligands. *J. Immunol.* 170: 1224-1230.

249. Jones, D. S., P. Reichardt, M. L. Ford, L. J. Edwards, and B. D. Evavold. 2008. TCR antagonism by peptide requires high TCR expression. *J. Immunol.* 181: 1760-1766.

250. Cameron, T. O., J. R. Cochran, B. Yassine-Diab, R. P. Sékaly, and L. J. Stern. 2001. Cutting edge: detection of antigen-specific CD4+ T cells by HLA-DR1 oligomers is dependent on the T cell activation state. *J. Immunol.* 166: 741-745.

251. Lee, J. E., M. B. Cossoy, L. A. Chau, B. Singh, and J. Madrenas. 1997. Inactivation of lck and loss of TCR-mediated signaling upon persistent engagement with complexes of peptide: MHC molecules. *J. Immunol.* 159: 61-69.

252. Martin, S., and M. J. Bevan. 1998. Transient alteration of T cell fine specificity by a strong primary stimulus correlates with T cell receptor down-regulation. *Eur. J. Immunol.* 28: 2991-3002.

253. Wilde, D. B., and F. W. Fitch. 1984. Antigen-reactive cloned helper T cells. I. Unresponsiveness to antigenic restimulation develops after stimulation of cloned helper T cells. *J. Immunol.* 132: 1632-1638.

254. Bensinger, S. J., M. N. Bradley, S. B. Joseph, N. Zelcer, E. M. Janssen, M. A. Hausner, R. Shih, J. S. Parks, P. A. Edwards, B. D. Jamieson, and P. Tontonoz. 2008. LXR signaling couples sterol metabolism to proliferation in the acquired immune response. *Cell* 134: 97-111.

255. Wang, R., C. P. Dillon, L. Z. Shi, S. Milasta, R. Carter, D. Finkelstein, L. L. McCormick, P. Fitzgerald, H. Chi, J. Munger, and D. R. Green. 2011. The transcription factor Myc controls metabolic reprogramming upon T lymphocyte activation. *Immunity* 35: 871-882.

256. Dinic, J., A. Riehl, J. Adler, and I. Parmryd. 2015. The T cell receptor resides in ordered plasma membrane nanodomains that aggregate upon patching of the receptor. *Sci. Rep.* 5: 10082.

257. Reinherz, E. L. 2015. αβ TCR-mediated recognition: relevance to tumor-antigen discovery and cancer immunotherapy. *Cancer immunology research* 3: 305-312.

258. von Essen, M. R., M. Kongsbak, and C. Geisler. 2012. Mechanisms behind functional avidity maturation in T cells. *Clin. Dev. Immunol.* 2012: 163453.

259. Blattman, J. N., D. J. Sourdive, K. Murali-Krishna, R. Ahmed, and J. D. Altman. 2000. Evolution of the T cell repertoire during primary, memory, and recall responses to viral infection. *J. Immunol.* 165: 6081-6090.

260. Elsaesser, H., K. Sauer, and D. G. Brooks. 2009. IL-21 is required to control chronic viral infection. *Science* 324: 1569-1572.

261. Uhlin, M., M. G. Masucci, and V. Levitsky. 2005. Regulation of lck degradation and refractory state in CD8+ cytotoxic T lymphocytes. *Proc. Natl. Acad. Sci. U. S. A.* 102: 9264-9269.